CR160168

LinCom Corporation

FINAL REPORT

SHUTTLE/TDRSS MODELLING

AND LINK SIMULATION STUDY

PREPARED FOR

NASA LYNDON B. JOHNSON SPACE CENTER
HOUSTON, TX   77058

TECHNICAL MONITORS: W. TEASDALE
S. NOVOSAD

CONTRACT NAS 9-14846

PREPARED BY

W. R. BRAUN
T. M. McKENZIE
L. BIEDERMAN
W. C. LINDSEY

LINCOM CORPORATION
P.O. BOX 2793D
PASADENA, CA   91105

APRIL 20, 1979

LinCom

TABLE OF CONTENTS

LinCom

TABLE OF CONTENTS (Cont'd)

TABLE OF CONTENTS (Cont'd)

1.0 INTRODUCTION

1.1 General

This document presents the final report on the Shuttle/ TDRSS Modelling and Link Simulation Study performed for NASA Johnson Space Center under Contract NAS 9-14846 directed by William Teasdale and Sid Novosad. It represents a portion of the work accomplished during the period June 10, 1976 through April 20, 1979.

The general objectives of the overall contract are the following: (1) to develop Shuttle/TDRSS link simulation models which can predict the performance sensitivity of these links to Shuttle transmitted signal distortions, (2) to exercise the simulation to predict the bit error rate performance as a function of the signal distortion parameters, (3) to present these data in a form suitable to support ESTL hardware tests and (4) to provide ESTL with a quick assessment of the basic differences between the ESTL TDRSS simulator hardware and the actual TDRSS system. This last item was covered in informal briefings to pertinent ESTL personnel and is not further addressed in this final report.

In what follows an overall description of the contractual effort and a brief summary of the results is given. This is followed by backup material which includes simulation data and analyses from which our summary results and recommendations have been drawn.

1.1.1 Final Report Contents

This report addresses and documents LinCom's findings on the task statements detailed in the Statement of Work. All tasks

pertain to the performance prediction of Shuttle forward and return links through the Tracking and Data Relay Satellite System (TDRSS).

Chapter 2 describes in detail the Shuttle/TDRSS S-band and Ku-band link simulation package, called LinCsim, developed for evaluation of link performance for specific Shuttle signal designs. The link models are described in detail and the transmitter distortion parameters, the so-called User Constraints are defined carefully. A complete list of the present values of all parameters used in the simulation is also included in the description.

Chapter 3 contains the results of extensive simulation of the Shuttle/TDRSS S-band return link. The overall link degradation (excluding hardware degradations) relative to an ideal BPSK channel are shown for various sets of user constraint values and the performance sensitivity to each individual user constraint is illustrated. The results can be used by NASA/JSC as a technical base for negotiating interface parameters between the Shuttle and TDRSS.

Chapters 4 and 5 take an indepth look at two specific problems. The effect of excessive Spacelab clock-jitter on the return link BER performance is analyzed in Chapter 4. This investigation accounts for the effects of the clock clean-up system (scrubber) in the Shuttle as well as for the coding and for the high level of data asymmetry expected on this link. Chapter 5 considers the problem of subcarrier recovery for the K-band Shuttle return link signal when one of the channels contains unprocessed digital data from a detached payload. Two different implementations for the payload interrogator are investigated and their performance compared.

1.2 Summary and Recommendations

1.2.1 Shuttle S-band Return Link Performance Summary

The performance degradation of the Shuttle/TDRSS return link due to Shuttle signal imperfections has been evaluated for the expected Shuttle distortion values based on current link budgets and TDRS/ground station hardware data. The results show a loss relative to ideal BPSK of 1.65 dB at the nominal bit error probability of 10^{-4}. The TDRS and ground station contribute .9 dB to this loss and the Shuttle the remaining .75 dB. This is illustrated in Fig. 1.1.

The single biggest contributor to the Shuttle degradation is the phase noise which is specified as 10° rms in the frequency interval 0 to 270 Hz. We recommend to separate the phase noise into components lying inside and outside the carrier tracking loop bandwidth, respectively, since these components affect the bit error rate performance differently. Such a refinement of the specification could greatly improve the accuracy of the predicted performance results. Since our present prediction is based on worst-case assumptions the overall degradation would be reduced.

1.2.2 Attached Spacelab Bit Jitter Performance Summary

The functional model of the Spacelab return link is shown in Fig. 1.2. The data and/or clock transitions from the Spacelab into the Shuttle are subject to severe phase jitter. The clock regenerator (scrubber) removes some of this jitter on the reclocked and convolutionally encoded data. However, the coded data may exhibit up to 10% of data asymmetry.
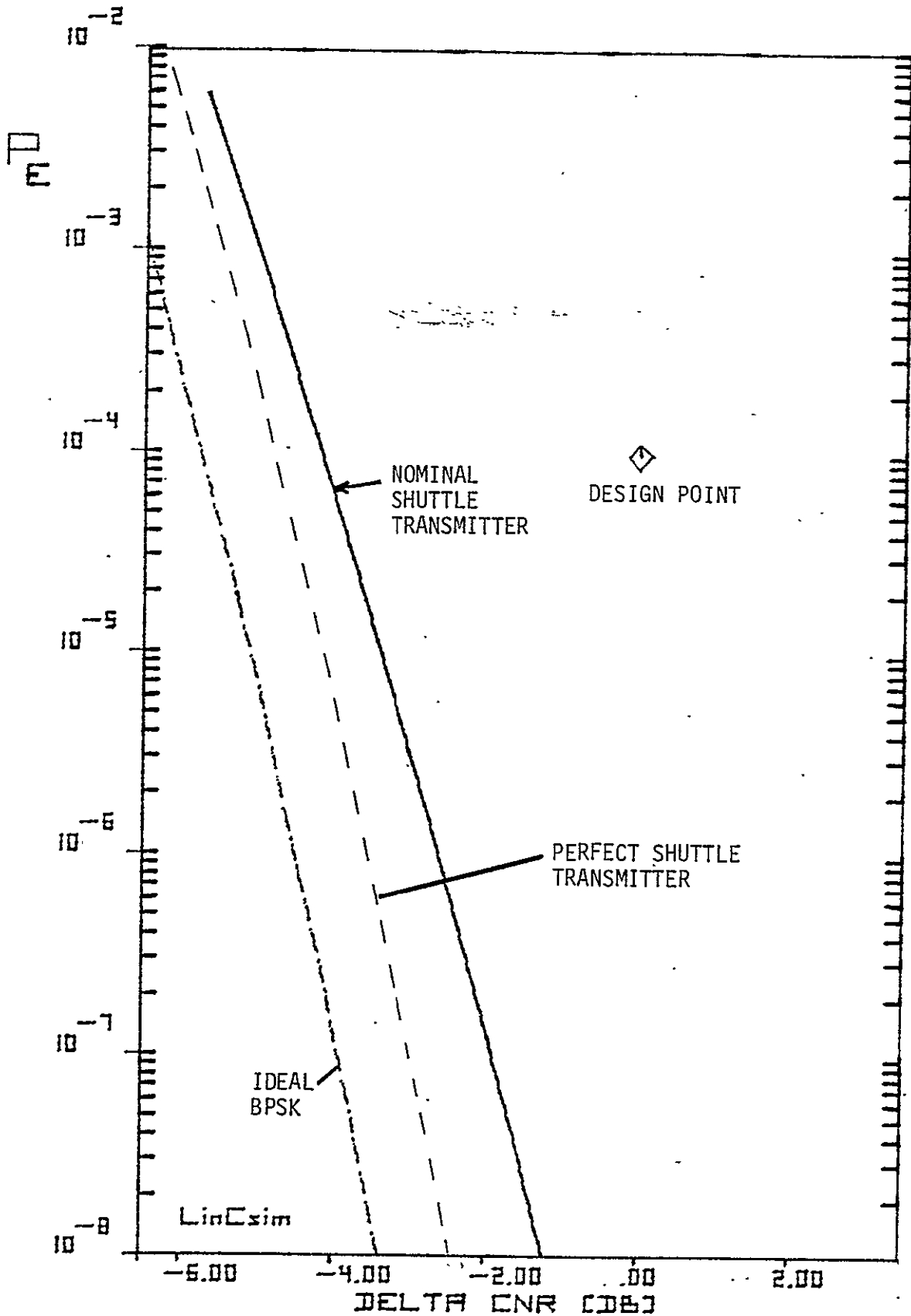
Fig. 1.1. Performance of Shuttle S-Band Return Link.

79 0061
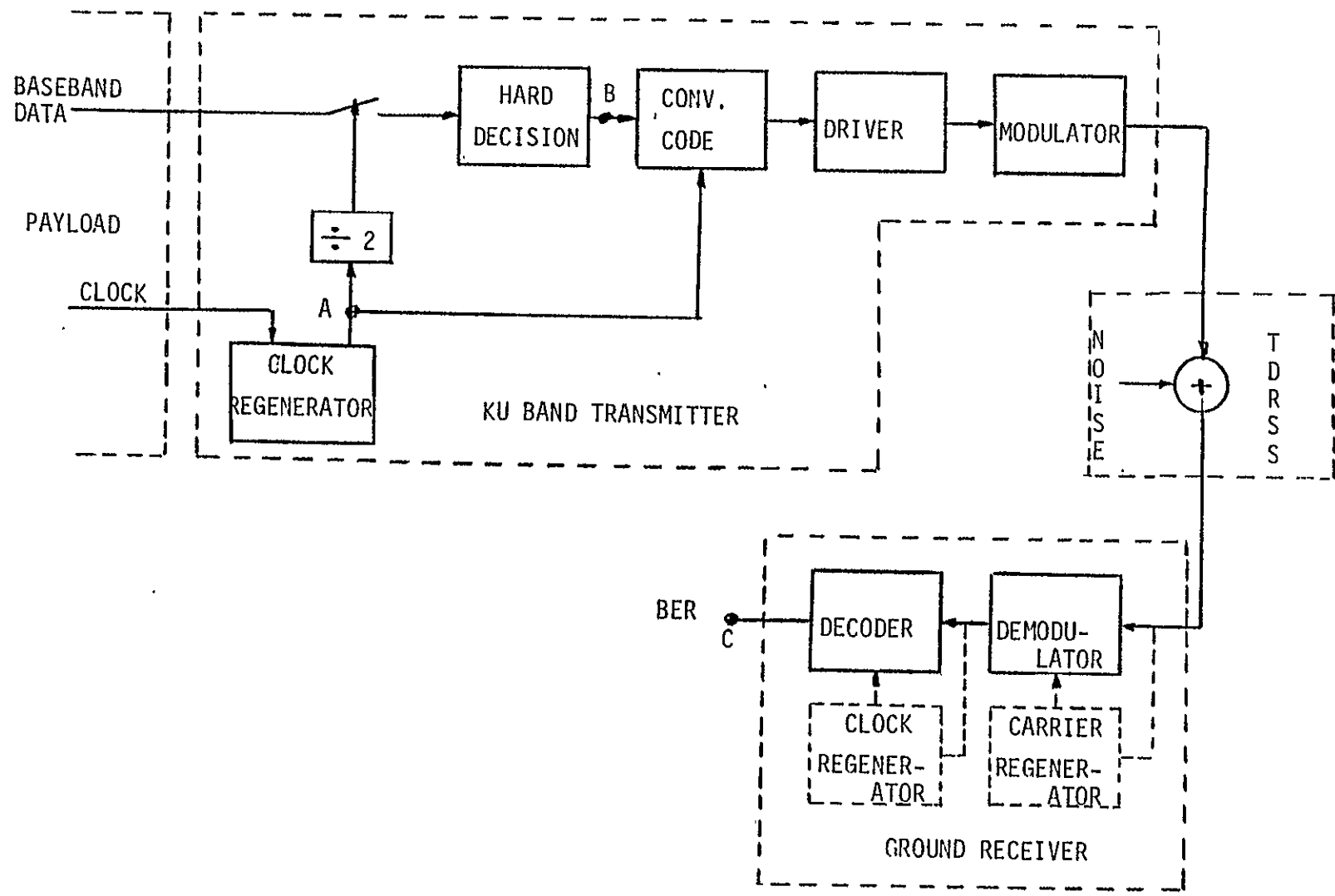
Figure 1.2.   Spacelab Return Link Block Diagram.

78 0391

The effect of bit jitter in the scrubber was analyzed using measured pulse shapes. The results (Fig. 1.3) show that the error rate of the reclocked data is negligible for bit jitter values which can be tolerated on the Shuttle-to-ground link. This holds for the case where the mean sampling instant is in the center of the bit (0% bias in Fig. 1.3) as well as when it is offset by 12.5%, which is the maximum predicted value. It remains then to analyze the effect of the residual bit jitter and of the data asymmetry on the Shuttle-to-ground link performance. The analysis, based on an ideal clock in the ground station receiver, shows that the CNR loss due to 10% data asymmetry amounts to .52 dB for an otherwise perfect signal. The incremental loss due to bit jitter is shown in Table 1.1.

Based on spectral data provided by JSC personnel the clock phase jitter at the scrubber output was estimated to be less than 2%. From Table 1.1 it is then clear that the associated CNR loss is well below .1 dB.

1.2.3 Shuttle Bent-Pipe Mode Subcarrier Performance Summary

A typical functional diagram of a detached payload return link is shown in Fig. 1.4. The payload signal is received by the payload processor, converted to baseband, hard-limited and then modulated onto one quadrature component of the K-band return link subcarrier. The recovery of the subcarrier phase from such a signal was investigated and compared with the performance of a similar system, but without the hard-limiter in the interrogator. The results show that both implementations perform adequately over all data rates. Removing the hard-limited improves the tracking performance slightly, however at the expense of reduced power

Figure 1.3.   BER PERFORMANCE AT KU BÁND ENCODER INPUT (A)

$E_b/N_0 \geq 20$ dB

BIT ERROR RATE

+12.5% BIAS

0% BIAS

CLOCK REGENERATOR OUTPUT PHASE JITTER (%)

78 9198

-7-
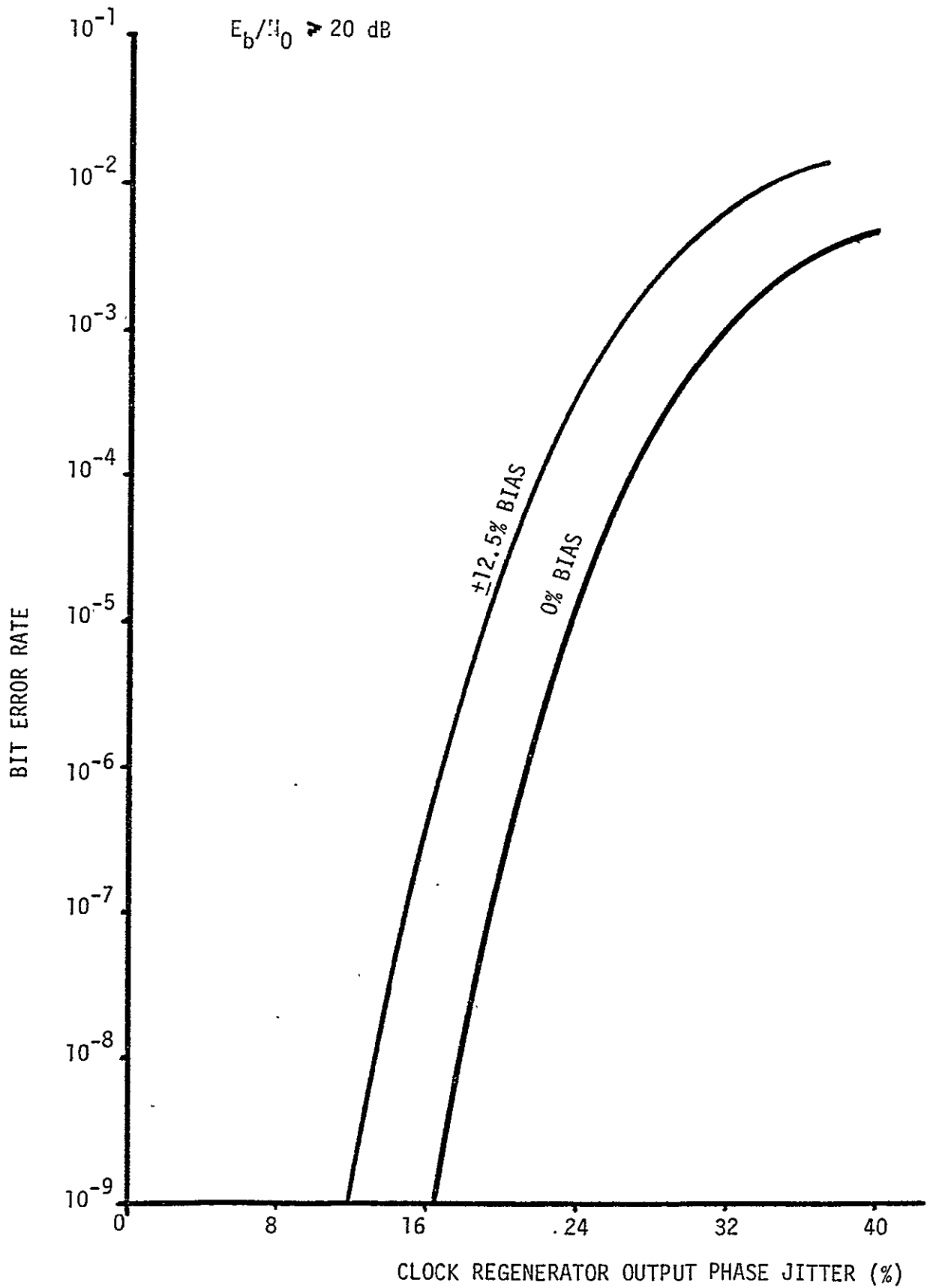
Table 1.1.   CNR Loss Due to Bit Jitter.

ΔCNR	Bit Jitter
dB	%
0.1	5.70
0.2	8.01
0.3	9.75
0.4	11.10
0.5	12.48
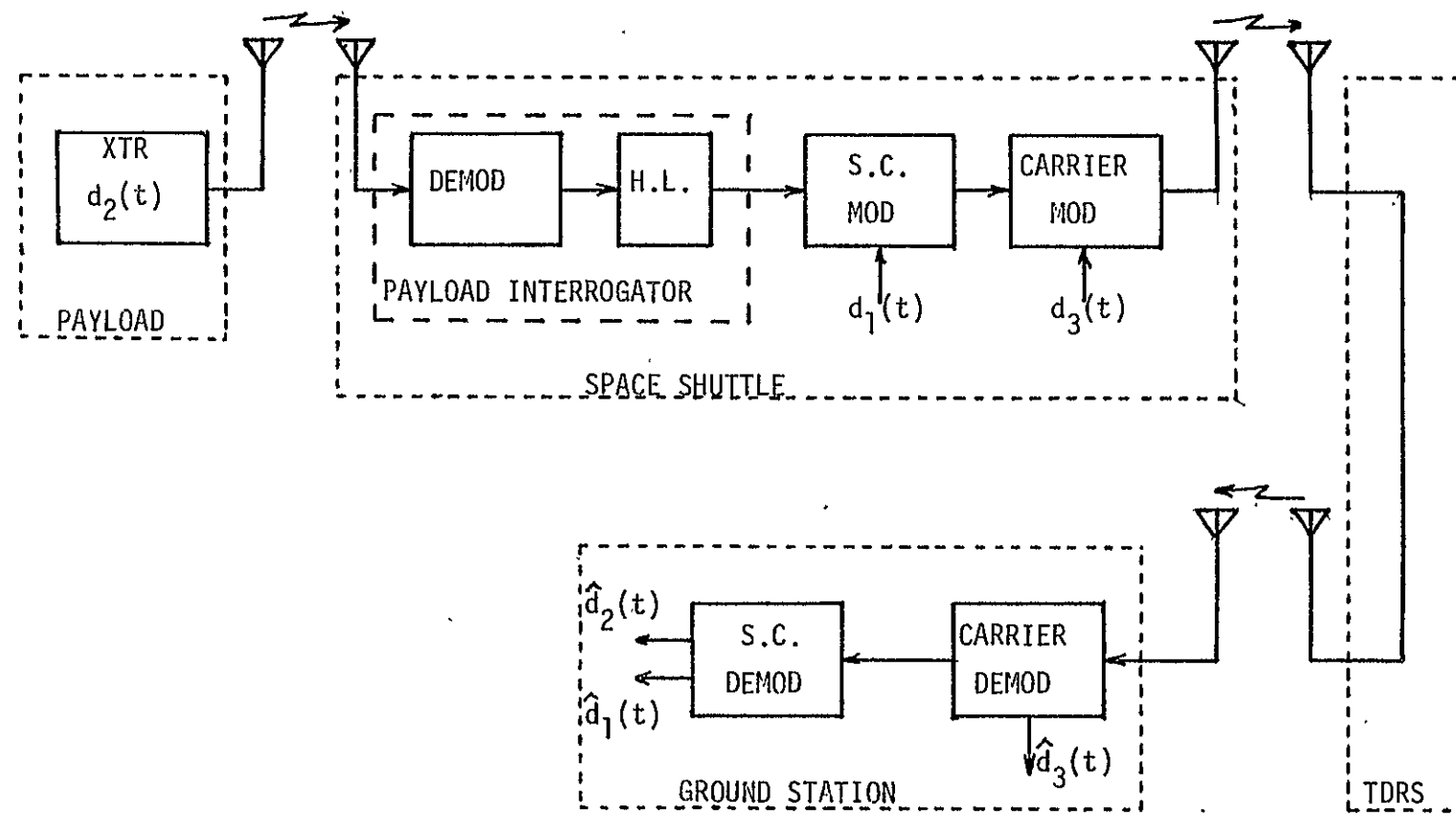
Fig. 1.4. Detached Payload Return Link Block Diagram.

control and hence more crosstalk into the low-rate channel and
is therefore not recommended.

The results of our analysis also allow to predict the effect
of losing the detached payload signal. With the proper choice for
the Costas loop arm filter bandwidths the loop can still track
the subcarrier properly. However, if the arm filter bandwidth is less
than approximately one fourth of the payload interrogator bandwidth
the lock-points of the loop S-curve are shifted by 90 degrees and
the channels are interchanged at the detector output.

2.0 DESCRIPTION OF LinCsim

2.1 Introduction

LinCsim is a software package designed to predict the effect of certain signal distortions in the transmitter (those specified in the TDRSS User's Guide, [1] Table 3-14 as user constraints) on the bit error rate performance of the Shuttle/TDRSS links.

Analytical simulation has been used as the basis for developing a computer simulation model which defines the service performance capability of the TDRSS as a function of the specific subsystem characteristics. The model includes the dynamic effects of the TDRS/ ground terminal links and TDRS/Shuttle links. The analytical char- acterization includes all factors which affect TDRSS services for representative operational conditions. This includes (but is not limited to) the following: channel linear and nonlinear distortions (AM/AM and AM/PM effects, TWT backoff, amplifier limiting), oscillator phase noise sources, additive thermal noise sources, filtering effects in the TDRS and ground station, demodulation and despreading losses for balanced and unbalanced QPSK signals, bit synchronization effects and convolutional coding performance. At present the program has the capability of predicting the bit error rate performance for S-band single access (SSA) and Ku-band single access (KSA) forward and return links. Both coherent and noncoherent turnaround implementations, oper- ating via the hybrid and cross-support tracking modes are available.

The analytical simulation program can be used for several purposes:

(1) To perform a detailed evaluation of several key com- munication features of the Shuttle services in order to

ensure the consistency of TDRSS and Shuttle user space-

craft transponder performance specifications.

(2) To verify that the TDRSS return link and tracking services

are provided without degradation for a Shuttle user with

transmitted signal characteristics within the Shuttle

user constraints of NASA Specifications [1].

(3) To simulate the full range of permissible Shuttle space-

craft characteristics in order to meet the TDRSS achievable

data rate.

(4) As a verification tool of Shuttle spacecraft characteristics

with TDRSS operational.

In order to fulfill these purposes the program must accurately

model the true signal format, filtering, nonlinear channel effects

and any other parameter affecting data transmission or tracking

performance. Input and output must be in terms of parameters relevant

to the design engineer. In the following we will discuss the models

used for the signals and the transmission path and the general set-up

of the program. Typical results obtained from LinCsim will be given

in Chapter 3.

2.2 Link Models

2.2.1 Introduction

This chapter presents the models on which the LinCsim computer

simulation is based. There is a basic channel model which is general

enough to emulate all forward and return services. This generic link

model is presented first, followed by channel descriptions for the

individual services. To complete the channel definition, a list of

the design values of all parameters associated with the link or one

of its subsystems is included. These design values are based on actual system parameter values whenever they are available; other-wise, an estimate was used. The source of each value is indicated.

2.2.2 Channel Model Description

LinCsim is based on a generic channel model which can be modified to fit any particular service (see Sections 2.2.3 and 2.2.4) by specifying the parameters for each subsystem or by bypassing it if necessary. This model is depicted in Figs. 2.1 to 2.3. In Fig. 2.1 d_1 and d_2 are two binary independent data streams (except for the K-band return link where d_2 is a subcarrier with UQPSK modulation). They may be routed through convolutional encoders and NRZ-to-Biphase converters. Then they may be modulated by the independent pseudo-noise sequences PN_1, PN_2 before they modulate the IF carrier in the modulator. The modulator output is spectrally shaped by the modulator filter. Any linear signal distortions occurring in this part of the transmitter are modeled by a distortion filter. The signal then passes through a high-power amplifier which distorts the signal in a nonlinear fashion. On the uplink, white Gaussian noise is added to the signal.

At the input to the TDRS repeater the signal and noise are filtered. The power level is then adjusted to the specified value. The signal may be combined with other signals in a frequency division multiplex format. A nonlinear TWT amplifier provides the necessary power for the downlink and an output filter limits the transmitted spectrum. At the input to the receiver another white Gaussian noise is added. PN-spread channels are then despread before the carrier phase and bit timing are extracted. The soft-detected bits are
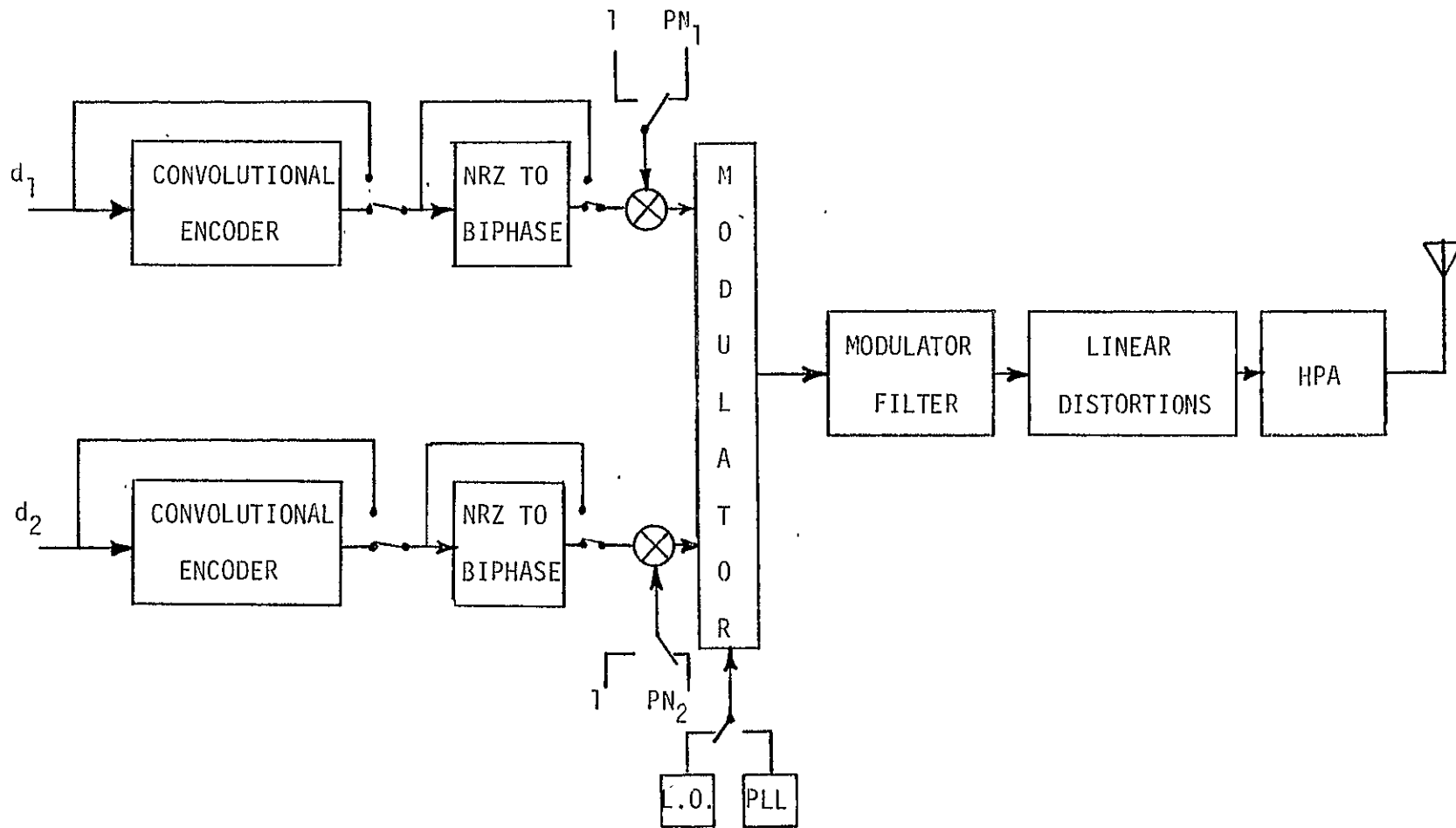
Figure 2.1.   Transmitter Model.

Signal

Thermal
Noise

Other
Signals

BPF

⊗

ALC

Σ

⊗

TWTA

BPF

L.O.

Figure 2.2.   TDRS Repeater Model.

SIGNAL +
UPLINK NOISE   DOWNLINK
NOISE

BPF

DESPREADER

PN CLOCK
RECOVERY

DEMOD

CARRIER
RECOVERY

MATCHED
FILTER

CLOCK
RECOVERY

H.L.

VITERBI
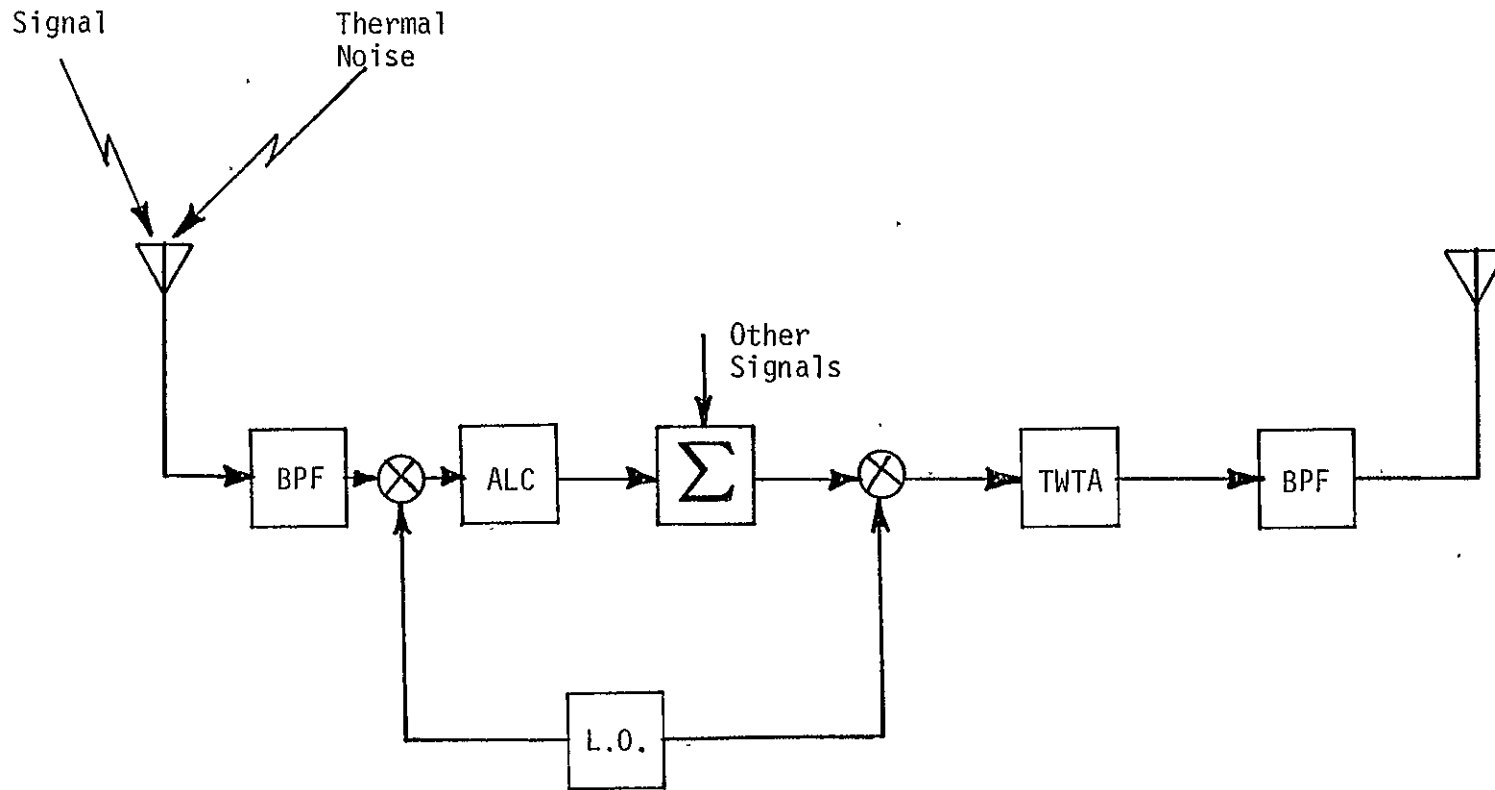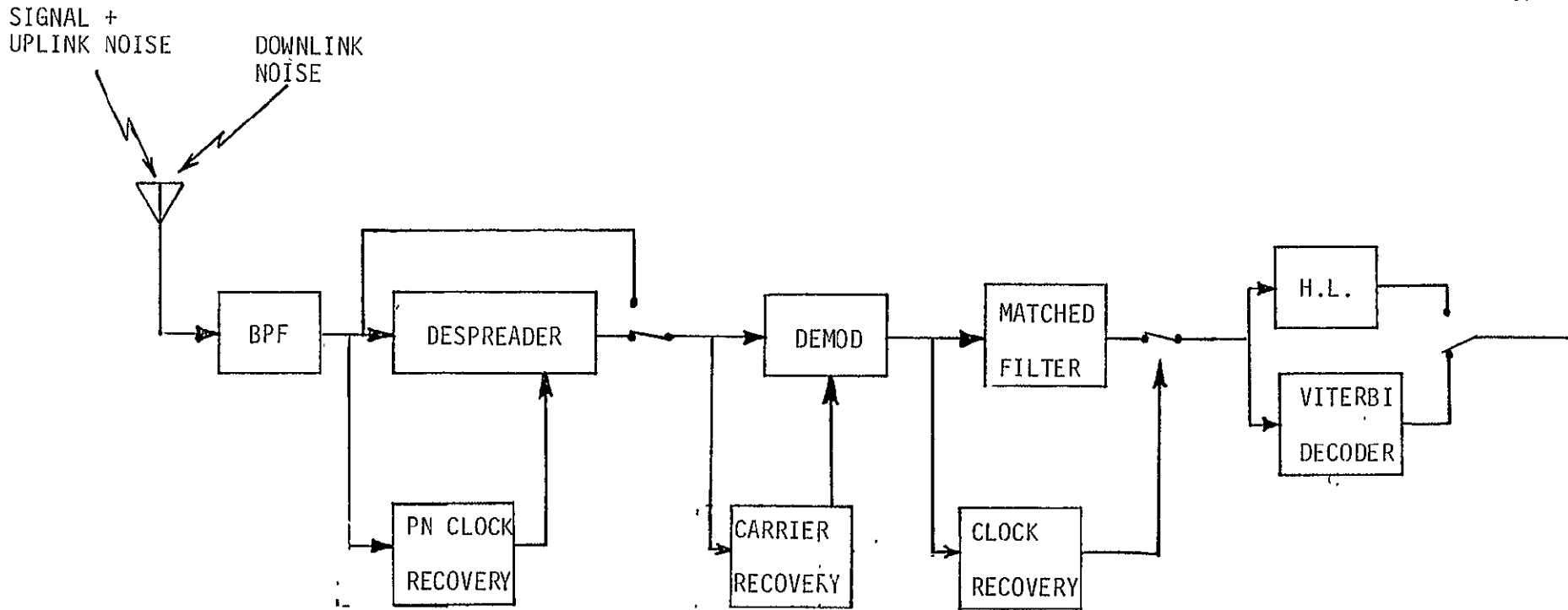DECODER

Figure 2.3. Receiver Model.

hardlimited for uncoded data or Viterbi-decoded for coded links.

2.2.3 Forward Link Models and Design Values

The models representing the forward service S-band and K-band
links are shown in Figs. 2.4 and 2.5, respectively, together with
some of the link characteristics. The design values for the
parameters defining each one of these models are summarized in
Tables 2.1 and 2.2. These values are stored in the program and are
used if the operator does not choose to override them.

2.2.4 Return Link Models and Design Values

The models for the return link services and their important
characteristics are shown in Figs. 2.6 through 2.8. Two different
models are defined, one based on a dedicated TWT amplifier (i.e.,
not shared with other signals), the other assuming a shared TWT
amplifier (composite link model). For the K-band link these models
correspond to the dedicated and composite links, respectively. For
the S-band link the dedicated link model is included to provide a
means of assessing the degradation due to the intermodulation effects
in the nonlinear amplifier. The two models are discussed in more detail
in Section 2.2.5.

The design values for all parameters of the return links are
summarized in Tables 2.3 and 2.4. Just as for the forward links,
these are the default parameter values stored in the program.

2.2.5 Dedicated vs Composite Channel Model for·the S-band Return
        Link

The S-band dedicated link model is provided as a tool to estimate
the effects of crosstalk generated in the shared nonlinear TDRS
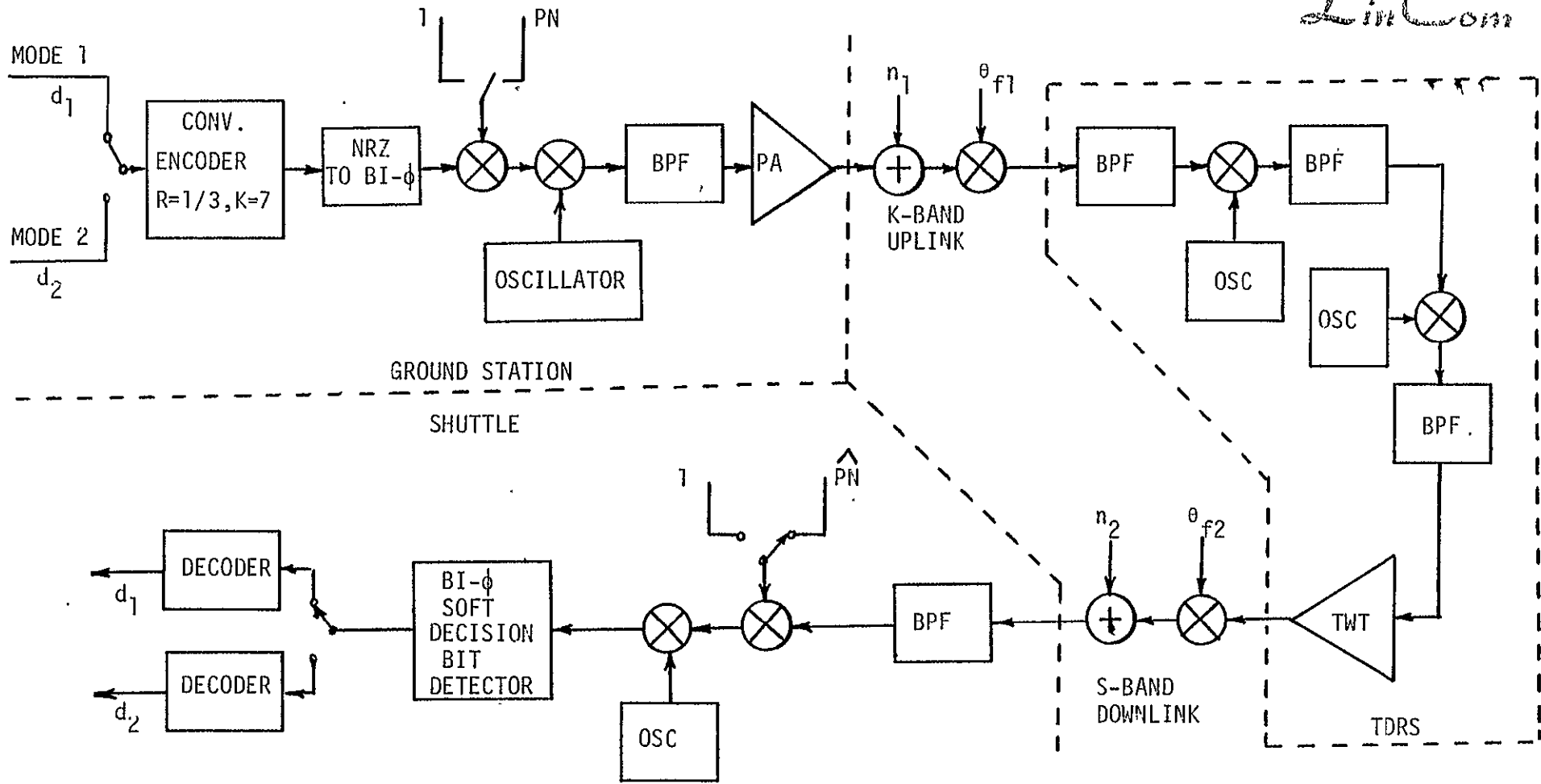amplifier on the bit error rate. To allow such a comparison the two

Fig. 2.4. S-Band Shuttle Forward Link

Data Rate: Mode 1: 32 Kbps
Mode 2: 72 Kbps

PN Chip Rate: 11.232 M chips/sec

PN Code Length: 1023 chips

Carrier Modulation: PSK$\pm\pi/2$ radians

78 0232

Table 2.1   <u>PARAMETER DESIGN VALUES FOR BER PROGRAM - SHUTTLE FORWARD LINK SSA</u>

PARAMETER	PRESENT VALUE	WHERE OBTAINED	DATE OBTAINED	OLD VALUE	SOURCE OLD VALUE
DATA RATE	72 Kb/sec	Harris PDR	3/30/78	72 Kb/sec	S-805-1
POWER SPLIT				1: 0	S-805-1
MODULATOR PHASE IMBALANCE (BPSK)	±3°	Harris PDR	3/30/78	± 3°	S-805-1
REL. PHASE BETWEEN I&Q CHANNELS	±3° peak	Harris PDR	3/30/78	±3° peak	S-805-1
DATA ASYMMETRY	±3%	Harris PDR	3/30/78	+3% peak	S-805-1
PN ASYMMETRY	< 1%	Harris PDR	3/30/78	±1% peak	S-805-1
DATA SKEW	--	--	--	N/A	--
PN SKEW	< 1%	Harris PDR	3/30/78	N/A	S-805-1
MODULATOR GAIN IMBALANCE	±0.25 dB	Harris PDR	3/30/78	±0.25 dB peak	S-805-1
XTR GAIN FLATNESS				±0.8 dB peak	S-805-1
XTR GAIN SLOPE	.3dB/ MHz	Harris PDR	3/30/78	±.1dB/MHz peak	S-805-1
XTR PHASE NON-LINEARITY	3°	Harris PDR	3/30/78	±8.6°peak/7MHz	S-805-1
XT FILTER BW				4.5 MHz	LinCom estimate
XT FILTER ORDER				4	LinCom estimate
XT FILTER RIPPLE				0.1 dB	LinCom estimate
XTR AM/AM				1 dB / dB	LinCom estimate
XTR AM/PM	< 4° dB	Harris PDR	3/30/78	3°	LinCom estimate
TDRS TWT MAX AM/PM	10°/dB	TPM	3/78	10°/dB	LinCom estimate
TDRS TWT AM/AM				0.2 dB/dB	LinCom estimate
TDRS TWT AM/PM	6°/dB	TPM	3/78	6°/dB	LinCom estimate
TDRS FRONT END FILTER BW	20 MHz	Harris PDR	3/30/78	20 MHz	Wu Proposal 7/76
ORDER				4	LinCom estimate
RIPPLE				0.1	LinCom estimate
TDRS TRANSMIT FILTER BW				4.5 MHz	LinCom estimate
ORDER				2	LinCom estimate
RIPPLE				0.2	LinCom estimate
PN TIMING OFFSET				1%	LinCom estimate
PN TIMING JITTER				1% peak	S-805-1
DATA TIMING OFFSET				1%	LinCom estimate
DATA TIMING JITTER				1% peak	S-805-1

Table 2.1. PARAMETER DESIGN VALUES FOR BER PROGRAM - SHUTTLE FORWARD LINK SSA

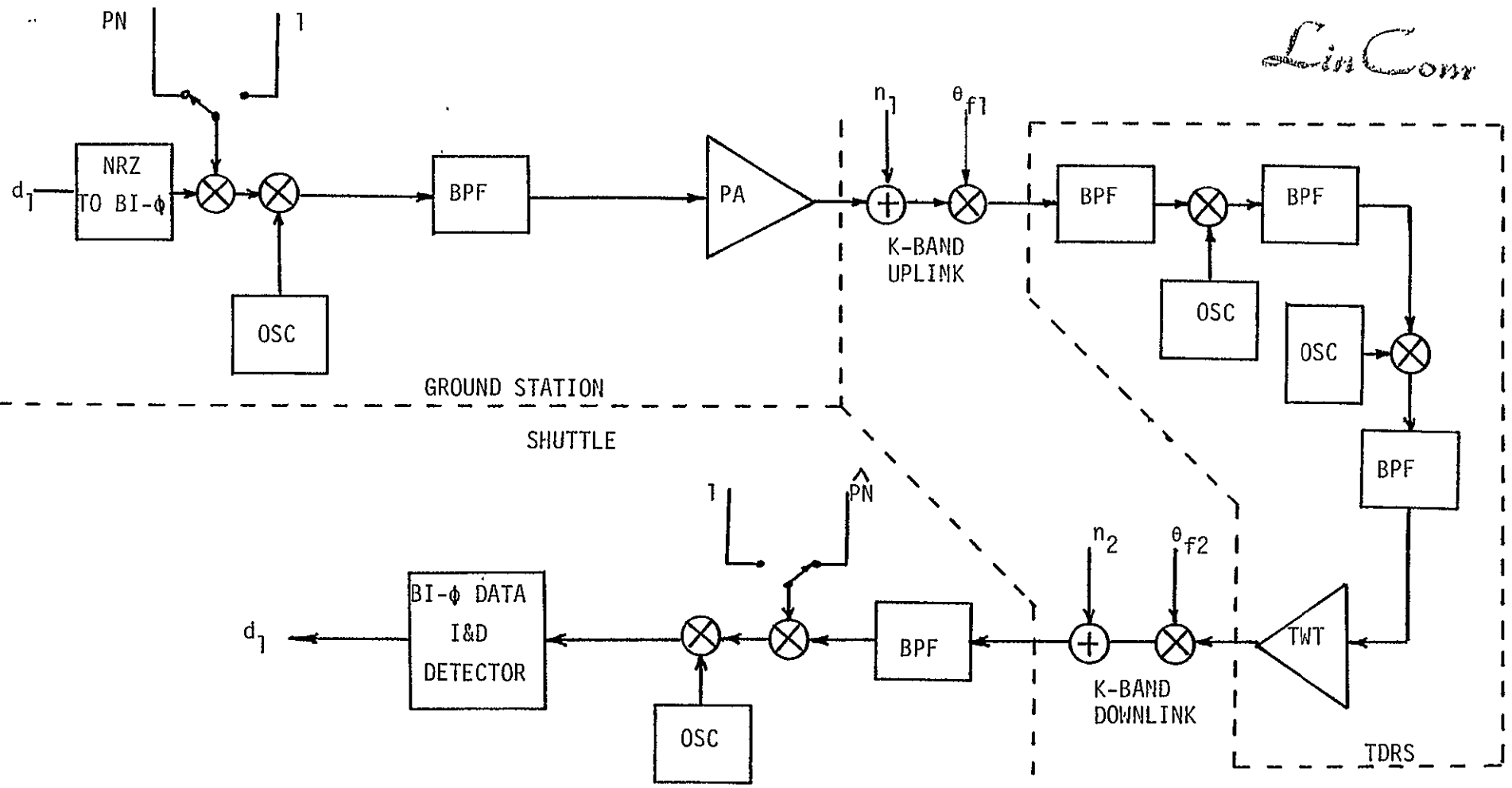| PARAMETER	PRESENT VALUE	WHERE OBTAINED	DATE OBTAINED	OLD VALUE	SOURCE OLD VALUE
LINK BUDGET					
XTR EIRP: UNCODED DATA	--	--	--	--	--
XTR EIRP.: CODED DATA	71.1 dBW	Harris PDR	3/30/78	71.1 dB	WU Proposal, 7
SPACE LOSS				208.1	WU Proposal, 7
POLARIZATION LOSS				0.1 dB	WU Proposal, 7
ATMOSPHERIC LOSS				0.8 dB	WU Proposal, 7
TDRS G/T				10. dB/°K	WU Proposal, 7
TDRS TWT MAX OUTPUT POWER	14.11 dBW	TPM	3/78	14.1 dBW	WU Proposal, 7
TDRS TWT OUTPUT BACKOFF				0	LinCom estimat
POWER ALLOCATION	0 dBW	TPM	3/78	0 dBW	LinCom estimat
CHANNEL POWER	14.11 dBW	TPM	3/78	14.1 dBW	LinCom estimat
TDRS HARDWARE LOSS				3.0 dB	LinCom estimat
TDRS ANTENNA GAIN				35.4 dB	WU Proposal,7/
POINTING LOSS				0.5	TDRSS Users Gu
SPACE LOSS	191.4	SS Circ Marg	1/77	191.6	TDRSS Users Gu
POLARIZATION LOSS				0.5	TDRSS Users Gu
ATMOSPHERIC LOSS				0	SS RF Circuit M
RX ANTENNA G/T				-30.1	SS RF Circuit M
PHASE NOISE BUDGET					
T OSCILLATORS 1-10 Hz				1.5° rms	S-805-1
10 to 32 Hz				1.5° rms	S-805-1
32 Hz to 1 KHz				4° rms	S-805-1
1 KHz to 6 MHz				2° rms	S-805-1
TDRS OSCILLATORS				3° rms	S-805-1
X Oscillators				1.4	S-805-1
X CARRIER TRACK-ING LOOP - STATIC HASE ERROR				3°	LinCom estimate
BANDWIDTH				32 Hz	LinCom estimate
DAMPING				2	LinCom estimate
SQUARING LOSS				2 dB	LinCom estimate

Fig. 2.5.   Shuttle Ku-Band Forward Link

Data Rate: 216 Kbps (Mode 1)/72 Kbps (Mode 2)   PN Code: PN_{f1}: $(2^{10}-1)$ Chip Gold Code

PN Chip Rate: 3 Mcps

'78 0233

Table 2.2. PARAMETER DESIGN VALUES FOR BER PROGRAM - SHUTTLE FORWARD LINK KSA

PARAMETER	PRESENT VALUE	WHERE OBTAINED	DATE OBTAINED	OLD VALUE	SOURCE OLD VALUE
TA RATE				216 Kb/sec	SSO ICD/IRN
WER SPLIT				1: 0	SSO ICD/IRM
DULATOR PHASE BALANCE (BPSK)	±3°	Harris PDR	3/30/78	±3° peak	S-805-1
L. PHASE BE-EEN I&Ω CHANNELS	±3°	Harris PDR	3/30/78		S-805-1
TA ASYMMETRY	±3%	Harris PDR	3/30/78	±3°	S-805-1
ASYMMETRY	1%	Harris PDR	3/30/78	1%	S-805-1
TA SKEW	--	--	--	N/A	--
SKEW				N/A	S-805-1
DULATOR GAIN BALANCE	±0.75 dB	Harris PDR	3/30/78	0.25 dB peak	S-805-1
R GAIN FLATNESS				0.8 dB peak	S-805-1
R GAIN SLOPE	±.3dB/MHz	Harris PDR	3/30/78	0.1dB/MHz	S-805-1
R PHASE NON-NEARITY	3°	Harris PDR	3/30/78	8.6°	S-805-1
FILTER BW	40 MHz	Harris PDR	3/30/78	50 MHz	LinCom estimate
FILTER ORDER				4	LinCom estimate
FILTER RIPPLE				0.1 dB	LinCom estimate
R AM/AM				1 dB/dB	LinCom estimate
R AM/PM	7°/dB	Harris PDR	3/30/78	3°/dB	LinCom estimate
RS TWT MAX AMPM	7.2°/dB	TPM	3/78	10°/dB	LinCom estimate
RS TWT AM/AM	0.9 dB	TPM	3/78	0.2dB/dB	LinCom estimate
RS TWT AM/PM				6°/dB	LinCom estimate
RS FRONT END .TER BW	50 MHz	TPM	3/78	50 MHz	WU Proposal, 7/76
ORDER				4	LinCom Estimate
RIPPLE				0.1 dB	LinCom estimate
RS TRANSMIT .TER BW				60 MHz	LinCom estimate
ORDER				2	LinCom estimate
RIPPLE				0.2 dB	LinCom estimate
TIMING OFFSET				1%	LinCom estimate
TIMING JITTER				1% peak	S-805-1
TA TIMING OFFSET				1%	LinCom estimate
TA TIMING JITTER				1% peak	S-805-1

Table 2.2.PARAMETER DESIGN VALUES FOR BER PROGRAM - SHUTTLE FORWARD LINK KSA

| PARAMETER	PRESENT VALUE	WHERE OBTAINED	DATE OBTAINED	OLD VALUE	SOURCE OLD VALUE
LINK BUDGET					
XTR EIRP: UNCODED DATA	75.9 dBW	Harris PDR	3/30/78	75.9 dBW	WU Proposal, 7/
XTR EIRP: CODED DATA	--	--	--	--	--
SPACE LOSS				208.4 dB	WU Proposal, 7/7
POLARIZATION LOSS				0.1 dB	WU Proposal, 7/7
ATMOSPHERIC LOSS				0.8 dB	WU Proposal, 7/7
TDRS G/T				10 dB/°K	WU Proposal, 7/7
TDRS TWT MAX OUTPUT POWER	2.16 dBW (spec)	TPM	3/78	1.8 dBW	WU Proposal, 7/7
TDRS TWT OUTPUT BACKOFF	0 dB	TPM	3/78	0 dBW	LinCom Estimate
POWER ALLOCATION	0 dB	TPM	3/78	0 dB	TDRSS Users Guide
CHANNEL POWER	2.16 dBW	TPM	3/78	0 dB	TDRS Users Guide
TDRS HARDWARE LOSS	1.68 dBW	TPM	3/78	1 dB	TDRS Users Guide
TDRS ANTENNA GAIN	51.85 dBW	TPM	3/78	52 dB	TDRS Users Guide
POINTING LOSS				0.7 dB	TDRSS Users Guide
SPACE LOSS				207.7 dB	TDRSS Users Guide
POLARIZATION LOSS				0.3 dB	TDRSS Users Guide
ATMOSPHERIC LOSS				0 dB	TDRSS Users Guide
RX ANTENNA G/T				5.3 dB/°K	TDRSS Users Guide
PHASE NOISE BUDGET					
XT OSCILLATORS 1 to 10 Hz				1.5° rms	S-805-1
10 to 32 Hz				1.5° rms	S-805-1
32 Hz to 1 KHz				4.0° rms	S-805-1
1 KHz to 25MHz				2.0° rms	S-805-1
TDRS OSCILLATORS				3°	S-805-1
RX OXCILLATORS				2.8°	S-805-1
RX CARRIER TRACKING LOOP					
STATIC PHASE ERROR				3°	LinCom estimate
BANDWIDTH				110 Hz	TRW, 8/77
DAMPING				2	LinCom estimate
SQUARING LOSS				2 dB	LinCom estimate

-23-
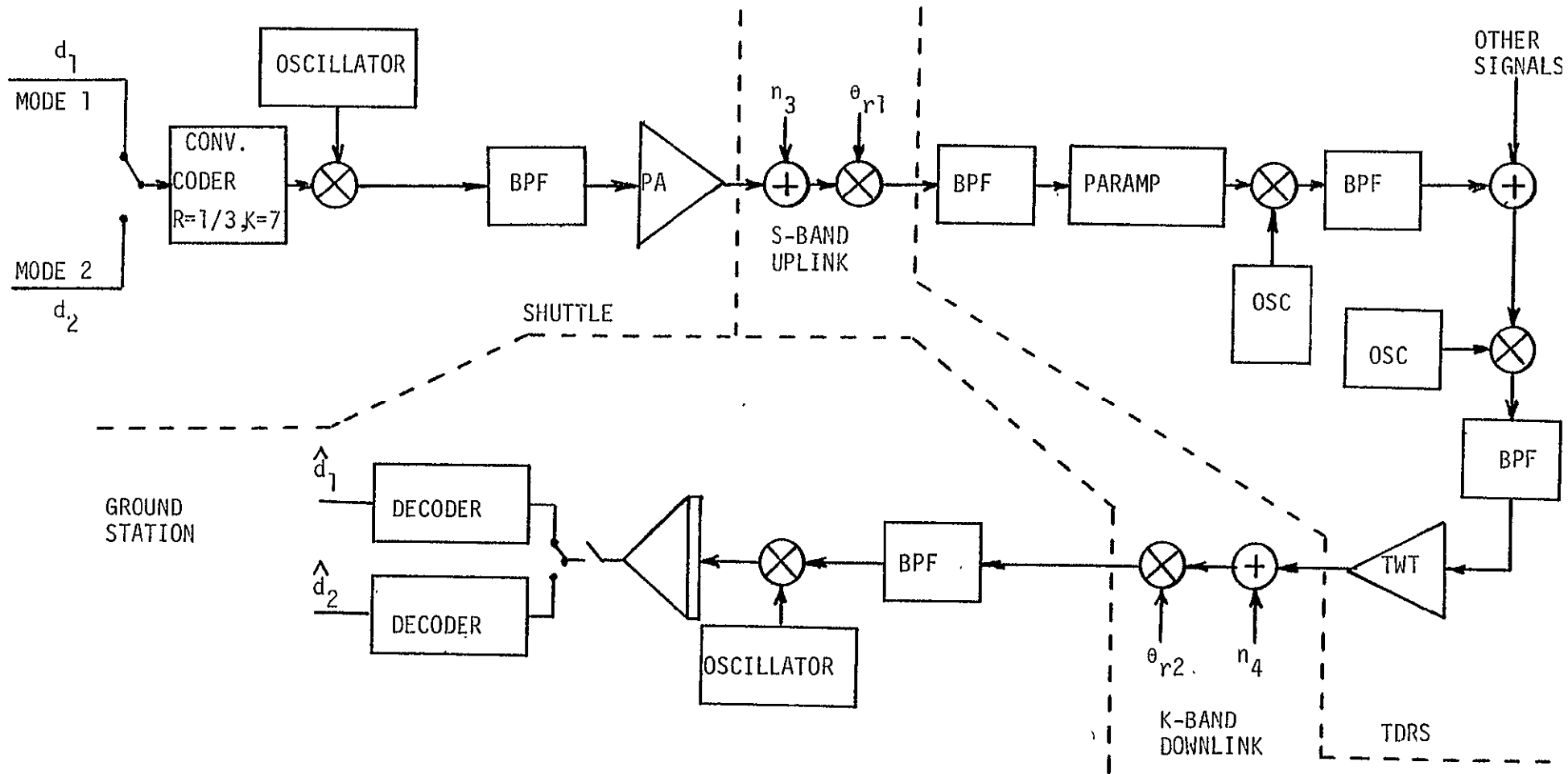
Fig. 2.6. S-Band Shuttle Return Link Model for Data Transmission.

Data Rates: Mode 1: 96 Kbps
             Mode 2: 192 Kbps

PN Code: Not Applicable

Convolution Coding: Data Coded in Both Mode 1 & Mode 2

Data Decoding: Rate 1/3, Constraint Length 7

Carrier Modulation: Bi-ϕ L Symbols PSK Modulate the
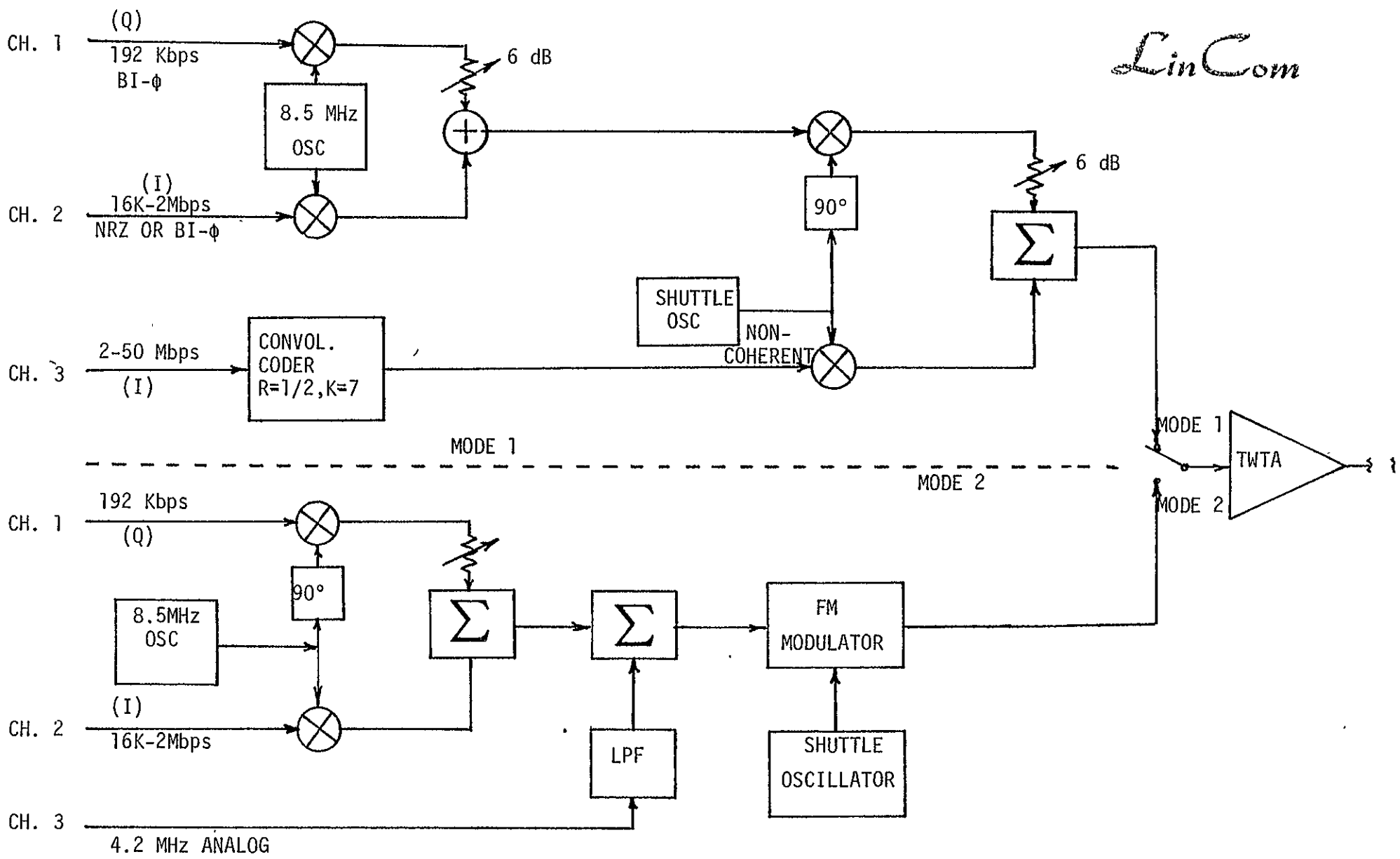   Carrier $\pm\pi/2$ Radians 78 0234

Table 2.3. PARAMETER DESIGN VALUES FOR BER PROGRAM — SHUTTLE RETURN LINK SSA.

PARAMETER	PRESENT VALUE	WHERE OBTAINED	DATE OBTAINED	OLD VALUE	SOURCE OLD VALUE
DATA RATE - I				192 Kbps	S-805-1
DATA RATE - Q				0	S-805-1
POWER SPLIT				1:0	S-805-1
MODULATOR PHASE IMBALANCE (BPSK)	11°	JSC	11/78	±3°	S-805-1
REL. PHASE BE-TWEEN I&Q CHANNELS				N/A	S-805-1
DATA ASYMMETRY	3.8%	JSC	11/78	±3%	S-805-1
PN ASYMMETRY				N/A	S-805-1
DATA SKEW				N/A	S-805-1
PN SKEW				N/A	S-805-1
MODULATOR GAIN IMBALANCE	.1 dB	JSC	11/78	+0.25 dB	S-805-1
XTR GAIN FLATNESS	.4 dB	JSC	11/78	+0.3 dB	S-805-1
XTR GAIN SLOPE				±0.1dB/MHz	S-805-1
XTR PHASE NON-LINEARITY				±3°	S-805-1
XT FILTER BW	100 MHz	JSC	11/78	1.2 MHz	S-805-1
XT FILTER ORDER				4	LinCom estimate
XT FILTER RIPPLE				0.1 dB	LinCom estimate
XTR AM/AM				1 dB/dB	LinCom estimate
XTR AM/PM	14°/dB	JSC	11/78	12°/dB	S-805-1
TDRS TWT MAX AM/PM				10°/dB	LinCom estimate
TDRS TWT AM/AM				0 dB/dB	LinCom estimate
TDRS TWT AM/PM				6°/dB	LinCom estimate
TDRS FRONT END FILTER BW				10 MHz	LinCom estimate
ORDER				4	LinCom estimate
RIPPLE				0.1 dB	LinCom estimate
TDRS TRANSMIT FILTER BW				621 MHz	LinCom estimate
ORDER				2	LinCom estimate
RIPPLE				0.2 dB	LinCom estimate
PN TIMING OFFSET				1%	LinCom estimate
PN TIMING JITTER				1% peak	S-805-1
DATA TIMING OFFSET				1%	LinCom estimate
DATA TIMING JITTER	6%	JSC	11/78	1% peak	S-805-1

PARAMETER	PRESENT VALUE	WHERE OBTAINED	DATE OBTAINED	OLD VALUE	SOURCE OLD VALUE
			LINK BUDGET		
XTR EIRP: UNCODED DATA					
XTR EIRP: CODED DATA	16.7 dBW	JSC	3/78	15.2 dBW	SS Circuit Margin
SPACE LOSS				192.1 dB	SS Circuit Margin, 1/77
POLARIZATION LOSS				0.5 dB	SS Circuit Margin, 1/77
ATMOSPHERIC LOSS				0 dB	SS Circuit Margin, 1/77
TDRS G/T	9.55(nominal)	TPM	3/78	8.3 dB/°K	SS Circuit Margin, 1/77
TDRS TWT MAX OUTPUT POWER	13..4 dB	TPM	3/78	12.5 dBW	WU Proposal, 7/76
TDRS TWT OUTPUT BACKOFF	2.0 dB	TPM	3/78	2.0 dB	WU Proposal, 7/76
POWER ALLOCATION	-10.0 dB	TPM	3/78	-9.9 dB	WU Proposal, 7/76
CHANNEL POWER	1.4 dBW	TPM	3/78	0.6 dBW	WU Proposal, 7/76
TDRS HARDWARE LOSS	2.46 dB	TPM	3/78	1.7 dB	WU Proposal, 7/76
TDRS ANTENNA GAIN	45.90 dB	TPM	3/78	41.3 dB	WU Proposal, 7/76
POINTING LOSS	0.65 dB	TPM	3/78	0.7 dB	WU Proposal, 7/76
SPACE LOSS				207.7 dB	WU Proposal, 7/76
POLARIZATION LOSS				0.1 dB	WU Proposal, 7/76
ATMOSPHERIC LOSS				0.8 dB	WU Proposal, 7/76
RX ANTENNA G/T				40.3 dB/°K	WU Proposal, 7/76
			PHASE NOISE BUDGET		
OSC, COHERENT RNAROUND					
to 10 Hz				1° rms	S-805-1
0 Hz to 1 kHz				1° rms	S-805-1
kHz to 6 MHz				1° rms	S-805-1
OSC NONCOHERENT RNAROUND					
to 10 Hz				2° rms	S-805-1
0 to 100 Hz				1° rms	S-805-1
00 Hz to 1 kHz	10° rms	JSC	11/78	1° rms	S-805-1
kHz to 6 MHz				1° rms	S-805-1
RS OSCILLATORS	3.2° rms	TPM	3/78	3°	S-805-1
OSCILLATORS				1°	S-805-1
CARRIER TRACKING OP					
TATIC PHASE ERROR				3°	LinCom Estimate
ANDWIDTH				40 Hz	TRW, 8/77
AMPING				2	LinCom Estimate
QUARING LOSS				DG1: 2 dB DG2: 8 dB	LinCom Estimate

Fig. 2.7. K-Band Shuttle Return Transmitter.

Data Rates: Mode 1   FM: Mode 2

I Channel (Carrier QDSB) 4-50 Mbps   Bandwidth (Predetection) 50 MHz

78 0235

PARAMETER	PRESENT VALUE	WHERE OBTAINED	DATE OBTAINED	OLD VALUE	SOURCE OLD VALUE
ATA RATE - I Ch.1				192 Kb/s	
Ch.2				2 Mb/s	S-805-1
Ch.3				50 Mb/s	
WER SPLIT				20:-4: 1	S-805-1
DULATOR PHASE BALANCE (BPSK)				+3°	S-805-1
L. PHASE BE- EEN I&Q CHANNELS				+3°	S-805-1
TA ASYMMETRY				+3%	S-805-1
ASYMMETRY				N/A	S-805-1
TA SKEW				N/A	S-805-1
SKEW				N/A	S-805-1
DULATOR GAIN BALANCE				+0.25 dB	S-805-1
R GAIN FLATNESS				+0.3 dB	S-805-1
R GAIN SLOPE				+0.1dB/MHz	S-805-1
R PHASE NON- NEARITY				±3°	S-805-1
FILTER BW				225 MHz	LinCom Estimate
FILTER ORDER				4	LinCom estimate
FILTER RIPPLE				0.1	LinCom estimate
AM/AM				1 dB/dB	LinCom estimate
AM/PM				12°/dB	S-805-1
S TWT MAX AMPM				10°/dB	LinCom estimate
S TWT AM/AM				0 dB/dB	LinCom estimate
S TWT AM/PM				6°/dB	LinCom estimate
S FRONT END TER BW				225 MHz	WU Proposal, 7/76
ORDER				4	LinCom estimate
RIPPLE				0.1	LinCom estimate
S TRANSMIT TER BW				225 MHz	LinCom estimate
ORDER				4	LinCom estimate
RIPPLE				0.2	LinCom estimate
TIMING OFFSET				+1%	LinCom estimate
TIMING JITTER				1%peak	S-805-1
A TIMING OFFSET				1%	LinCom estimate
A TIMING JITTER				1% peak	S-805-1

PARAMETER	PRESENT VALUE	WHERE OBTAINED	DATE OBTAINED	OLD VALUE	SOURCE OLD VALUE
LINK BUDGET					
XTR EIRP				48.1 dBW	SSRF Circuit Ma 1/77
SPACE LOSS				208.5 dB	SSRF Circuit Ma 1/77
POLARIZATION LOSS				-0.3 dB	SSRF Circuit Ma 1/77
ATMOSPHERIC LOSS				0 dB	SSRF CircuitMarg
TDRS G/T				22.6 dB/°K	SSRF Circuit Mar
TDRS TWT MAX OUTPUT POWER				12.5 dB	WU Proposal, 7/
TDRS TWT OUTPUT BACKOFF				Composite,2.dB Dedicated,.5dB	WU Proposal, 7/
POWER ALLOCATION	-2.5 dB	TPM#8	3/78	-2.4 dB	WU Proposal, 7/
CHANNEL POWER				Composite,8.0dBW Dedicated,12dBW	WU Proposal,
TDRS HARDWARE LOSS				1.2 dB	LinCom estimate
TDRS ANTENNA GAIN				41.3 dB	WU Proposal, 7/
POINTING LOSS				0.7 dB	WU Proposal, 7/
SPACE LOSS				207.7 dB	TDRSS Users Gui
POLARIZATION LOSS				0.1 dB	TDRSS Users Gui
ATMOSPHERIC LOSS				0.8 dB	TDRSS Users Gui
RX ANTENNA G/T				40.3 dB	TDRSS Users Gui
PHASE NOISE BUDGET					
TX OSC, COHERENT TURNAROUND					
1 to 10 Hz				3° rms	S-805-1
10 Hz to 1 kHz				3° rms	S-805-1
1 kHz to 150 MHz				1° rms	S-805-1
TX OSC, NONCOHERENT TURNAROUND					
1 to 10 Hz				15° rms	S-805-1
10 to 100 Hz				7.5° rms	S-805-1
100 Hz to 1 kHz				2° rms	S-805-1
1 kHz to 150 MHz				2° rms	S-805-1
TDRS OSCILLATORS	3.4°	TPM#8	3/78	3°	S-805-1
RX OSCILLATORS				1°	S-805-1
RX CARRIER TRACKING LOOP					
STATIC PHASE ERROR				3°	LinCom Estimat
BANDWIDTH				1000 Hz	TRW, 8/77
DAMPING				2	LinCom Estimat
SQUARING LOSS				DG1: 2 dB DG2: 8 dB	LinCom Estimate
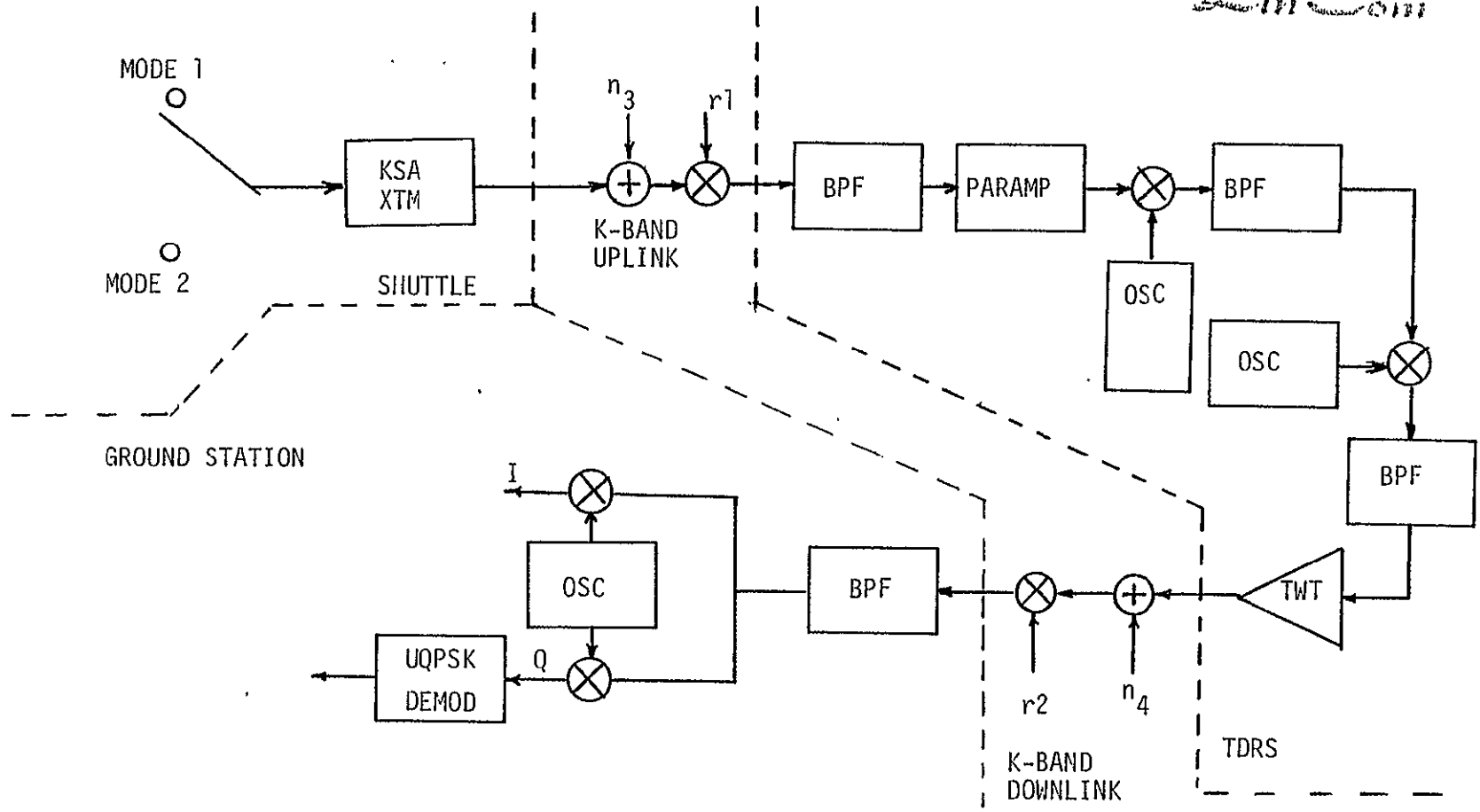
Fig. 2.8.   Dedicated KSA Return Link Model.

models are made to agree in every respect except for the sharing of the amplifier. In particular, the S-band channel power into the TWTA and the amplifier characteristic and maximum TWT output power are identical.

2.2.6 Ideal Channel Model

Along with the error rate for the specified channel the program prints the error probability for an "ideal channel." This is assumed to be an infinite bandwidth, linear channel with additive white Gaussian uplink and downlink noise as the only distortions. Uplink and downlink carrier-to-noise ratios as well as the repeater input noise bandwidth (affecting the power robbing in the satellite) are matched to the actual channel. The printed error rate is therefore the optimum performance achievable with the given link power budget and a nonprocessing satellite.

2.3 Subsystem Models

2.3.1 Introduction

This chapter extends the channel model description to the subsystem level. The implementations chosen are based on the actual Shuttle, TDRS or ground station hardware implementation whenever such information was available. Otherwise, a reasonable state-of-the-art guess was used. The Shuttle transmitter implementation has enough flexibility to model the user constraint distortions.

2.3.2 Modulator

The modulator accepts two binary switching waveforms and phase-modulates them onto a carrier. The phase transitions are instantaneous. The resulting waveform may exhibit the following types of distortions:

●Gain Imbalance

●Phase Imbalance (for BPSK)

●Nonorthogonal Channels (for QPSK and UQPSK)

●Data Asymmetry

●PN Asymmetry

●I/Q Data Skew (for equal rates and no PN spreading)

●I/Q PN Skew

●Data Bit Jitter

●PN Chip Jitter

●Carrier Phase Jitter

which are defined in Section 2.5.3.

2.3.3 Filters ·

All filters are modeled as Chebyshev filters. They are defined by the three parameters bandwidth, ripple and number of poles. The number of poles refers to the transfer function of the equivalent baseband filter. The ripple is defined as $20 \log(v_1/v_2)$ where v_1, v_2 are shown in Fig. 2.9. The bandwidth is the two-sided ripple-bandwidth as shown in the figure, i.e. it does usually not agree with either the noise bandwidth or the 3 dB bandwidth. However, if the ripple is specified as 0 dB a Butterworth filter characteristic results and the 3 dB bandwidth is used.

In the transmitter some linear distortion may be specified in terms of the following parameters:

●Gain Flatness

●Gain Slope

●Phase Nonlinearity
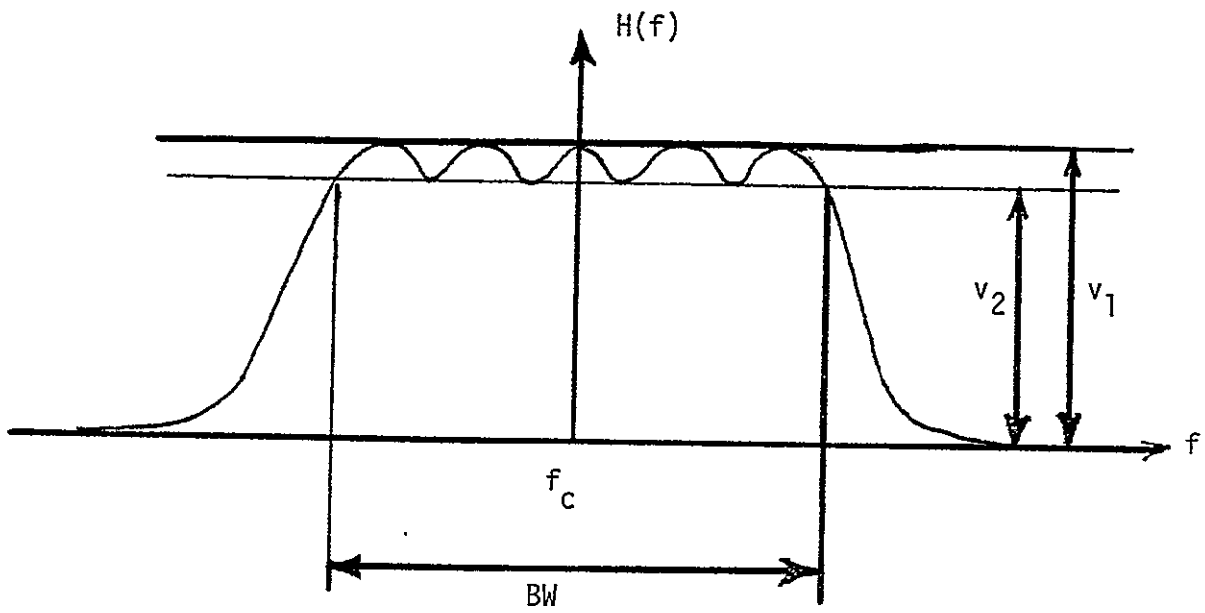
Figure 2.9. Chebyshev Filter Characteristic.

The transfer characteristic used is described in Section 2.5.3. In order to obtain the phase nonlinearity specified and no more, the transmit Chebyshev filter has a linear phase characteristic. All other filters exhibit the unequalized Chebyshev phase characteristic.

Note that the filter in the transmitter inherently sets the following parameters which are specified as user constraints in Ref. [1]:

- Data Transition Time
- Minimum 3 dB Bandwidth Prior to Power Amplifier

2.3.4 Power Amplifiers

2.3.4.1 Introduction

The power amplifiers are modeled as memoryless devices with a gain characteristic which may depend on the instantaneous value of the signal envelope and with an envelope-dependent phase shift between the input and output. The transmitter HPA characteristic therefore sets the following distortion parameters:

- AM-PM
- Data Transition Induced PM

There are three different characteristics built into the program: a linear amplifier, a measured TWT characteristic and a characteristic with constant AM-AM and AM-PM distortion. These models are discussed below. An important parameter for a nonlinear power amplifier is the operating point. Its definition is discussed at the end of this section.

2.3.4.2 Linear Amplifier

The linear amplifier has a constant arbitrary gain and no phase

shift. The input power is automatically adjusted so that the output power agrees with the specified amplifier output power, viz., the output saturation power (dBW) minus the output backoff (dB). It is understood that the terms "output saturation power" and "output backoff" are meaningless for a linear amplifier; however, they are used in the above definition of output power in order to reach a closer agreement with the TWT amplifier operating point definition which is given below.

2.3.4.3 TWT Characteristic

The measured TWT characteristic corresponds to the Hughes 261H tube and is shown in Fig. 2.10. In order to provide more flexibility the model includes two parameters which allow one to adjust the scale on the gain and phase nonlinearity separately to meet the output saturation power and maximum AM-PM specifications.

The AM-PM distortion is defined as

$$AM\text{-}PM = \frac{dg(R)}{d[20 \log_{10} R]} = \frac{\ln(10)}{20} \frac{R dg(R)}{dR} \left[\frac{deg}{dB}\right]$$

The normalized AM-PM function is plotted in Fig. 2.11. Note that it peaks at approximately 8 dB input backoff. This means that the worst degradation due to AM-PM can be expected if the TWT input signal power is 8 dB below the saturation power.
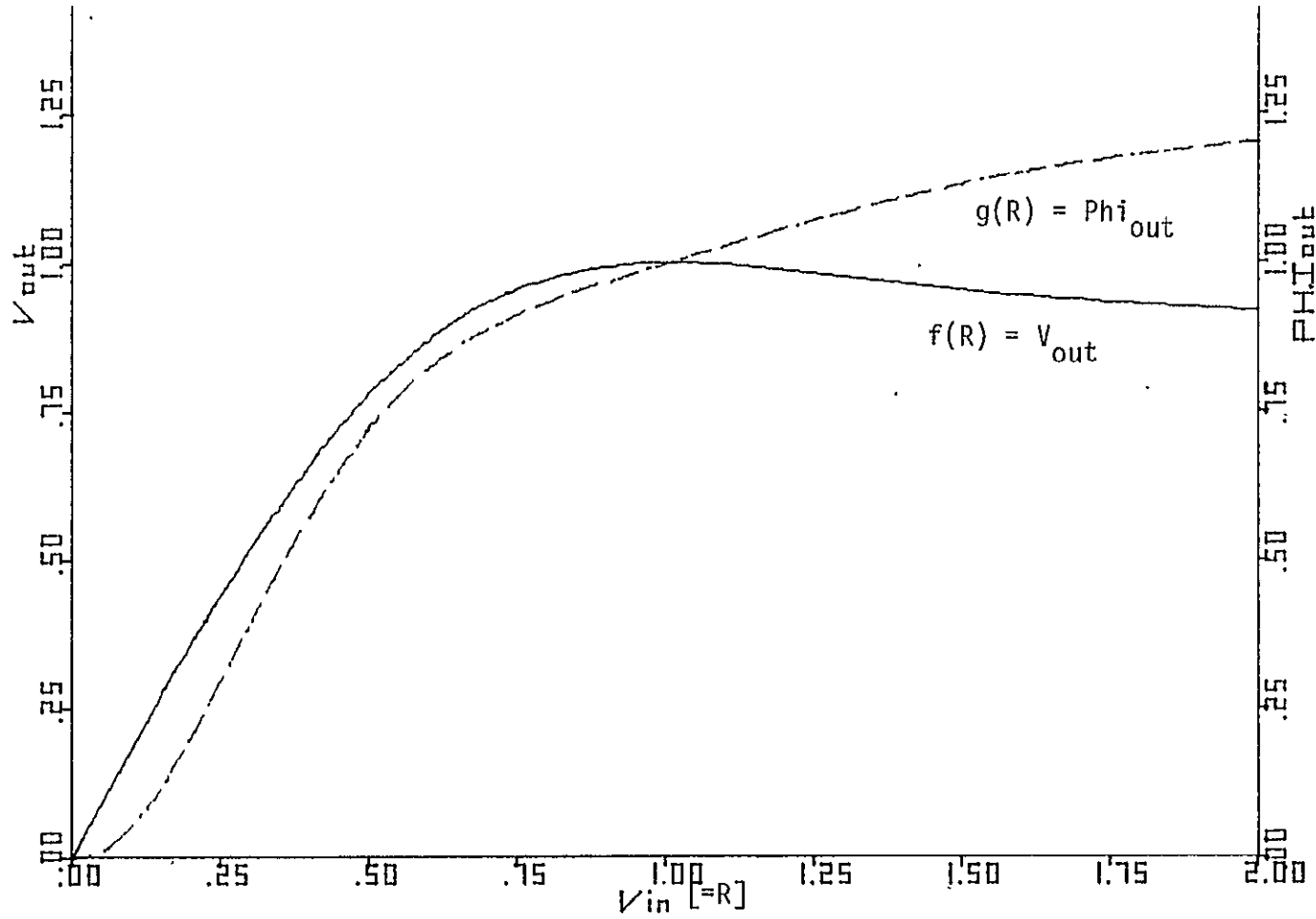
Figure 2.10. Normalized TWT AM-AM and AM-PM Characteristics.

2.3.4.4 Constant AM-AM, AM-PM Model

The AM-AM distortion is defined as

$$\text{AM-AM} = \frac{d[20 \log_{10} f(R)]}{d[20 \log_{10} R]} = \frac{R}{f(R)} \frac{df(R)}{dR} \quad [\frac{dB}{dB}]$$

and the AM-PM distortion is

$$\text{AM-PM} = \frac{dg(R)}{d[20 \log_{10} R]} = \frac{\ln(10)}{20} \frac{Rdg(R)}{dR} \quad [\frac{deg}{dB}]$$

Using

$$f(R) = R^{\text{AM-AM}}$$

$$g(R) = \begin{cases} \text{AM-PM } 20 \log_{10} R & R \geq \varepsilon \\ \text{AM-PM } 20 \log_{10} \varepsilon & R < \varepsilon \end{cases}$$

where ε is some small (with respect to the r.m.s. signal) number we obtain a characteristic with a constant AM-AM and AM-PM value over all operating points. This model is implemented with AM-AM and AM-PM as parameters. A typical characteristic is plotted in Fig. 2.12. This model can also simulate a hard-limiter by setting AM-AM = AM-PM = 0.

As in the case of the linear amplifier the terms "output saturation power" and "output backoff" are not applicable to this characteristic. They are however used to define the output power in the same way as for the linear amplifier.
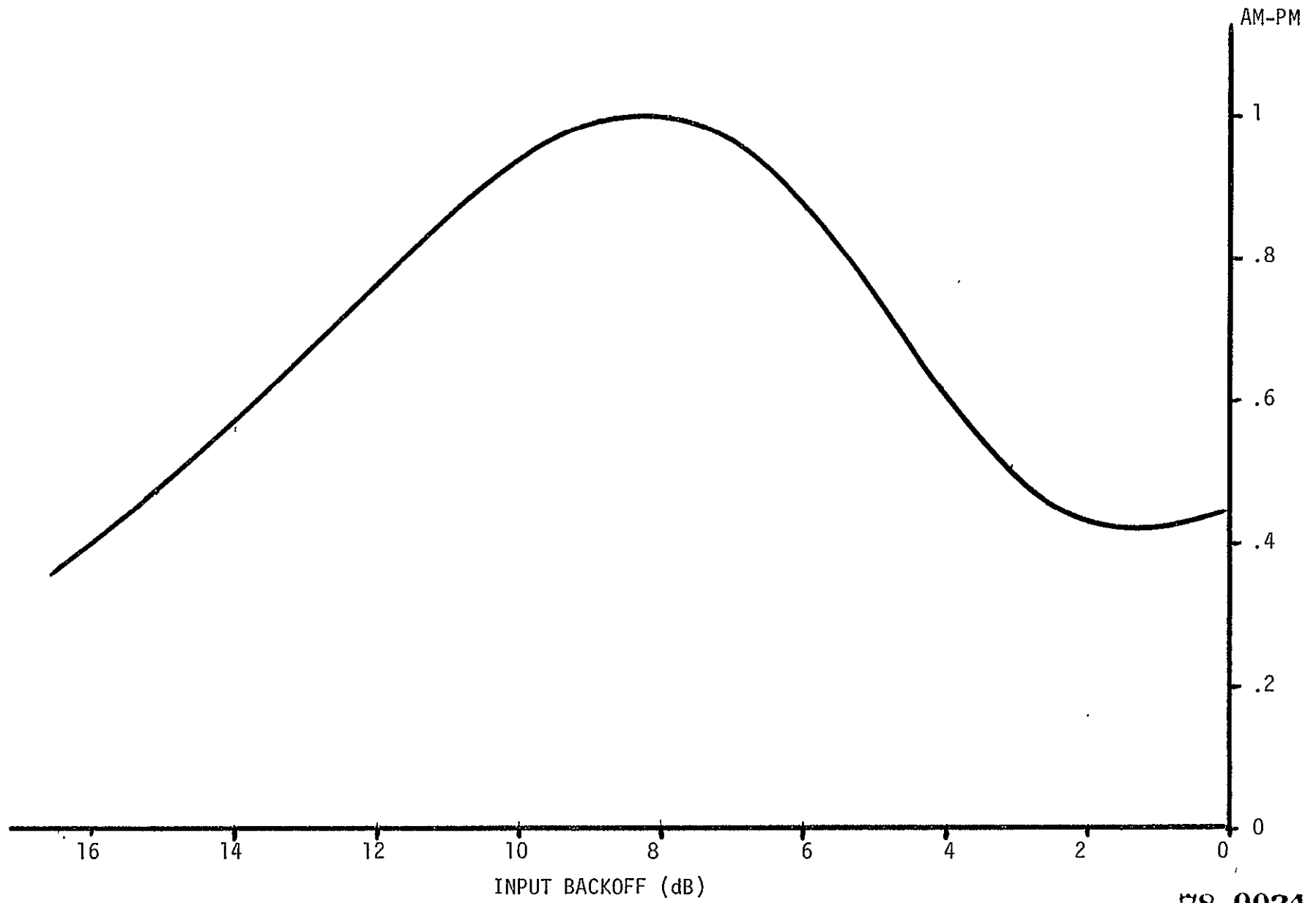
Figure 2.11. Normalized AM-PM Characteristic.

'78 0024

$f(R) = V_{out}(.9\ dB/dB)$

$g(R) = Phi_{out}$

$f(R) = V_{out}\ (.1\ dB/dB)$
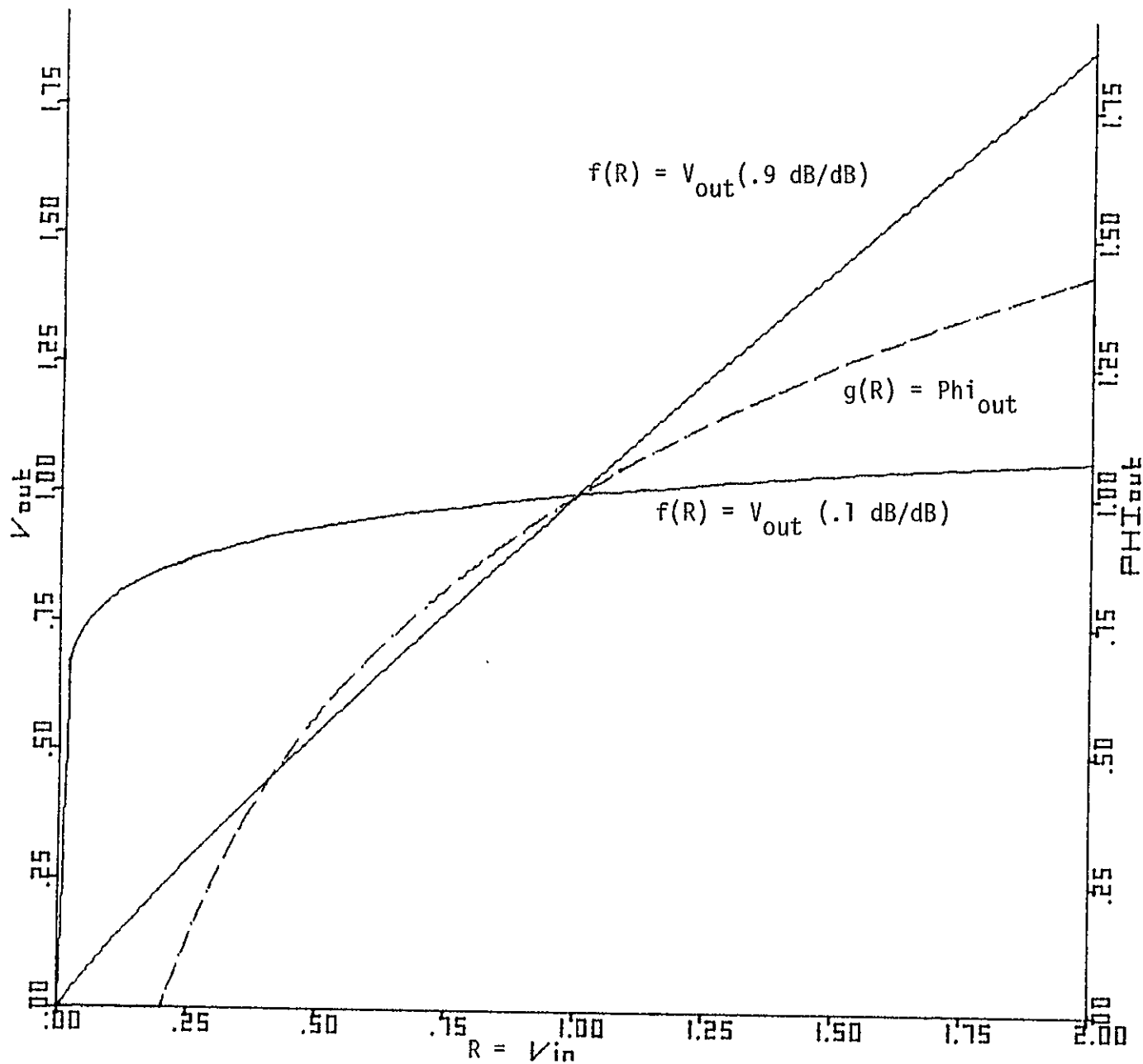
Figure 2.12. Normalized Characteristic for Constant AM-AM, AM-PM.

'78 0025

2.3.4.5 Definition of Operating Point

For the linear amplifier and the constant AM-AM, AM-PM model performance is insensitive to the amplifier operating point, viz., the power level of the signal into the amplifier. For the TWT model, however, it is an important parameter. Here the operating point is characterized by the input backoff, which is defined as the ratio of the input power (signal plus noise) to the input saturation power, where the input saturation power is the power of a CW input signal which produces the maximum output power. The input backoff is computed from the specified output backoff on the basis of a noise-free CW signal.

2.3.5 PN Despreader

The despreader implementation is shown in Fig. 2.13. For a four-phase signal, only one quadrature component (the higher-power channel for unbalanced QPSK signals) is used to find the PN epoch. Both PN sequences are then derived from the same PN generator.

2.3.6 Carrier Recovery

The carrier tracking loop is modeled as a Costas loop for BPSK signals and for PN-spread signals and as a two-channel Costas loop with hard-limiters (Fig. 2.14) for balanced and unbalanced QPSK signals. For PN-spread QPSK or UQPSK signals a single loop tracks the carrier in one of the quadrature channels and its phase estimate is used for the demodulation of both channels.

2.3.7 Data Clock Recovery

The data tracking loop implementation is shown in Fig. 2.15. The baseband input signal is hard-limited and multiplied with a delayed copy of itself. This produces a line in the spectrum which
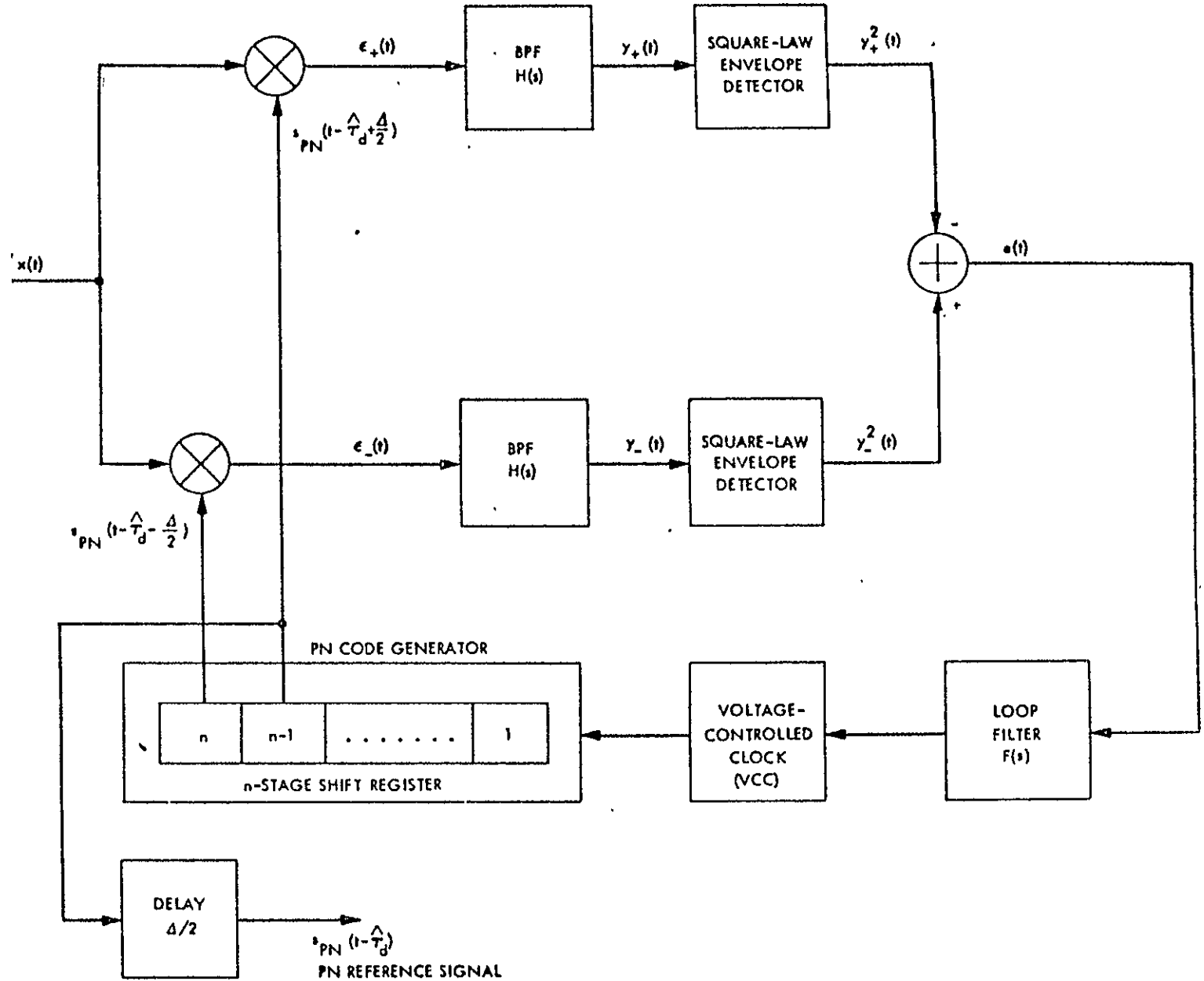
Figure 2.13. A Noncoherent "One Δ" Delay-Locked Loop

'78 0026
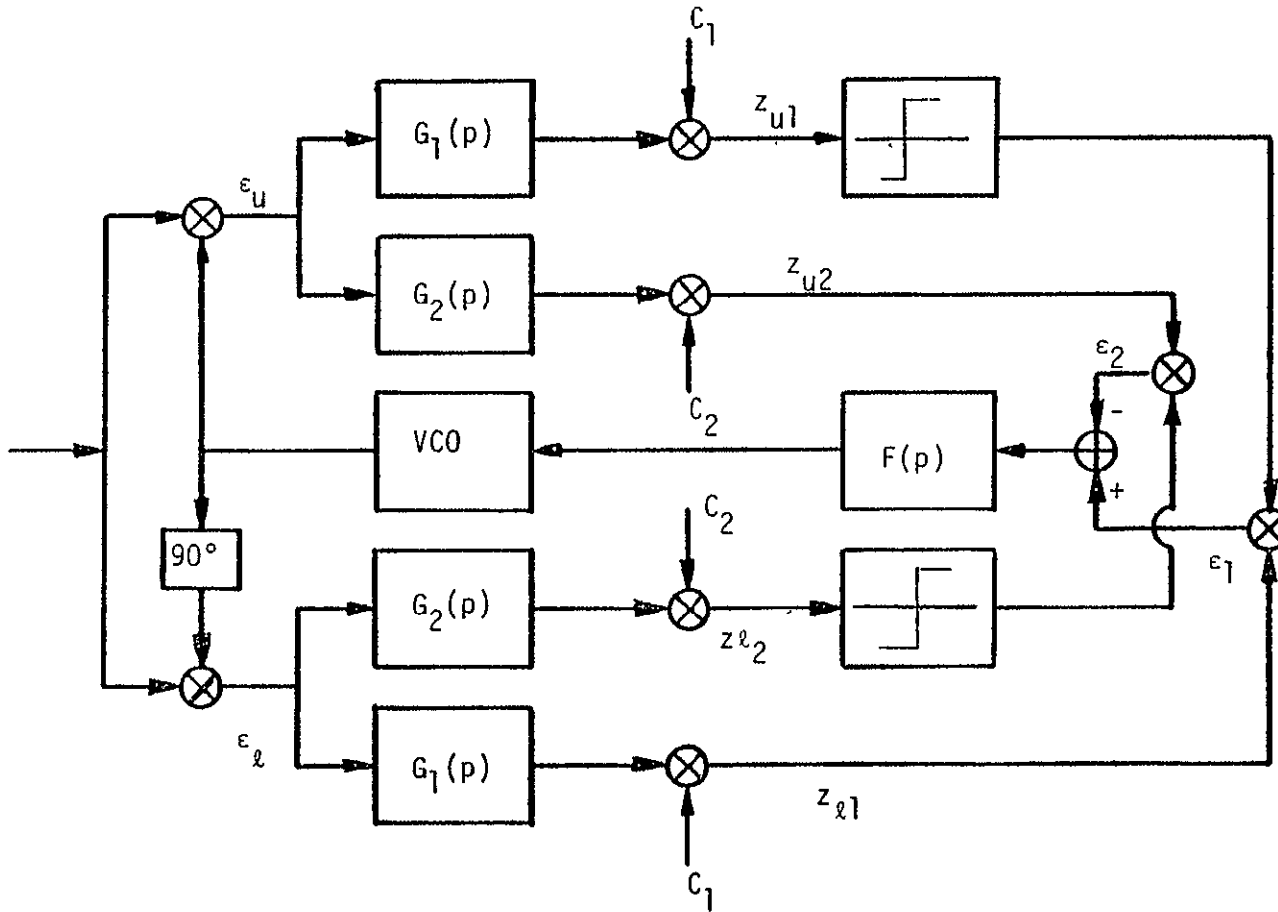
Figure 2.14. Two Channel Costas with Hard-Limiters.
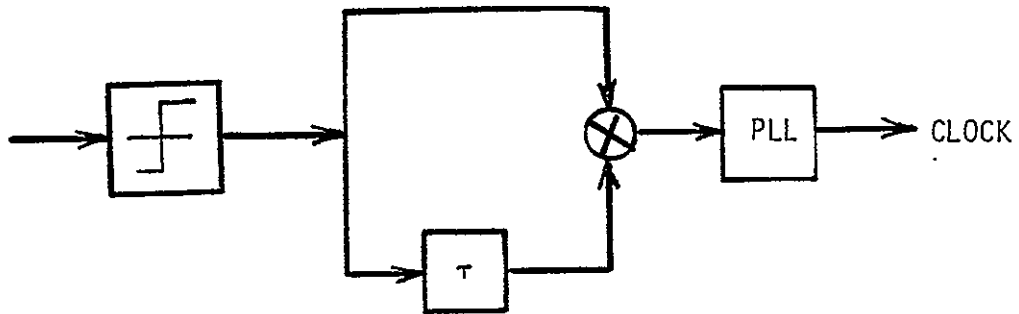
Figure 2.15. Data Clock Recovery Implementation.

is being tracked by a phase-locked loop. The delay τ can be selected; a typical value is half a bit time for NRZ symbols and one quarter of a bit time for biphase symbols. The resulting spectral line is at the data rate or twice the data rate, respectively. The loop bandwidth is set at 1/1000 of the data rate or 10 Hz, whichever is more.

2.3.8 Data Detector

The data detector is modeled as a hard-limiter for uncoded data and as a three-bit quantizer for convolutionally encoded data.

2.4 Definition and Modelling of User Constraints

2.4.1 Introduction

This section lists all the user constraint parameters specified in [1], Table 3-14, along with their official definition ([1], Appendix I) and the model used in LinCsim. An effort was made to find for every parameter the worst-case model meeting the specifications.

2.4.2 User Constraints

Modulator Phase Imbalance (BPSK Only)

Definition: The steady state phase difference between the phase
separation of the BPSK modulated +1 and -1 data bits
and 180 degrees.

Model:
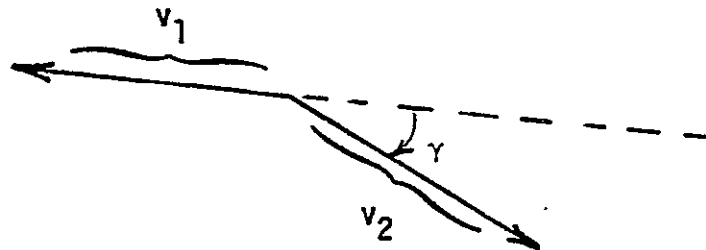
γ = Phase Imbalance

Modulator Gain Imbalance (dB)

1. BPSK

Definition: $10 \log P_1/P_0 = 20 \log[\frac{X+\Delta X}{X}]$ where P_1 is the power in an
all 1's data pattern as measured at the modulator output,
P_0 is the power in an all 0's data pattern as measured
at the modulator output, X is the steady state amplitude
gain of the modulator phase state one, $X+\Delta X$ is the steady
state amplitude gain of modulator phase state two, and
$\Delta X \geq 0$.

Model:
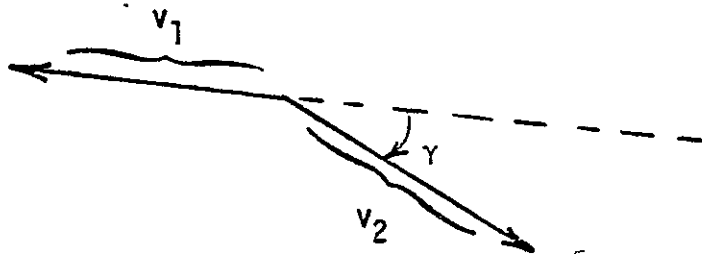
$$|20 \log(v_1/v_2)| = \text{modulator gain imbalance}$$

$$\frac{1}{2}[\max(v_1,v_2)]^2 = \text{design modulator output power}$$

2. QPSK and UQPSK

Definition: 20 log $\left[\dfrac{X+(\Delta X_i)_{max}}{X}\right]$ where the four modulator phase

states have steady state amplitude gains X, $X+\Delta X_1$,

$X+\Delta X_2$ and $X+\Delta X_3$, and where $\Delta X_i \geq 0$.

Model:
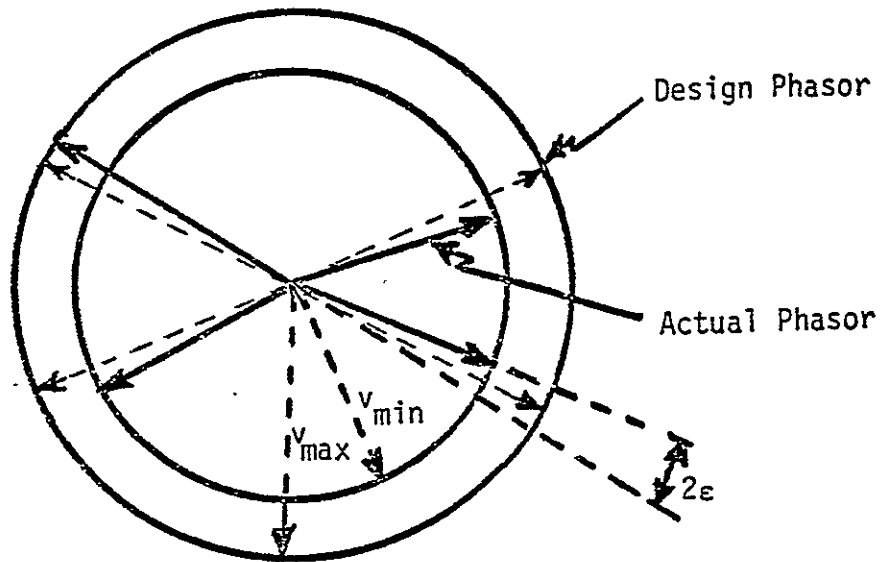
$20 \log(v_{max}/v_{min})$ = modulator gain imbalance

$v_{max}^2/2$ = design modulator output power

Relative Phase Between I and Q Channels

Definition: The difference in phase, as shown below, between the best fit orthogonal reference phase vectors and the actual phase vectors.

PHASE DIFFERENCE

BEST FIT REFERENCE

ACTUAL PHASE

Model:

Design Phasor

Actual Phasor

V_{min}

V_{max}

2ε
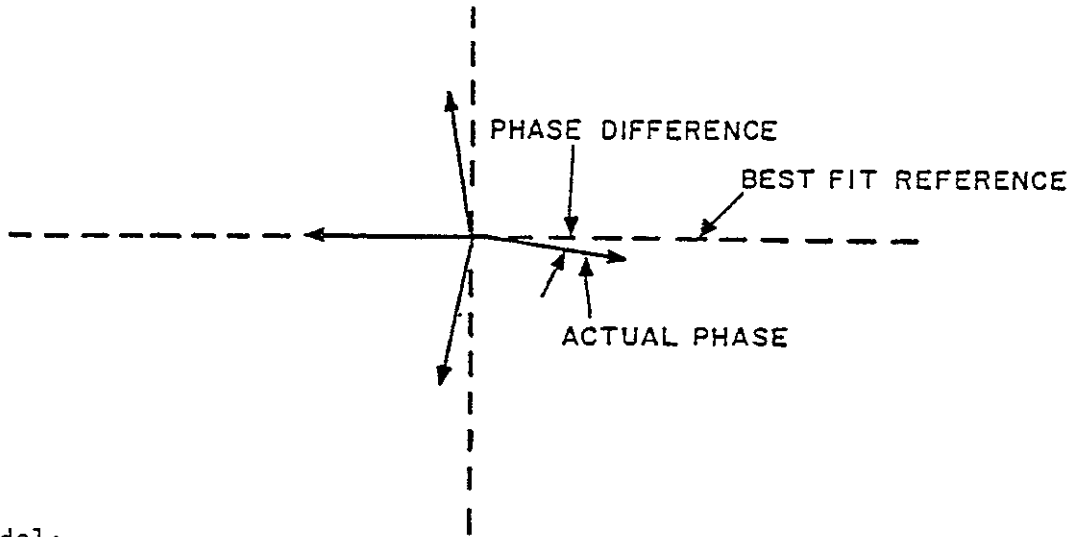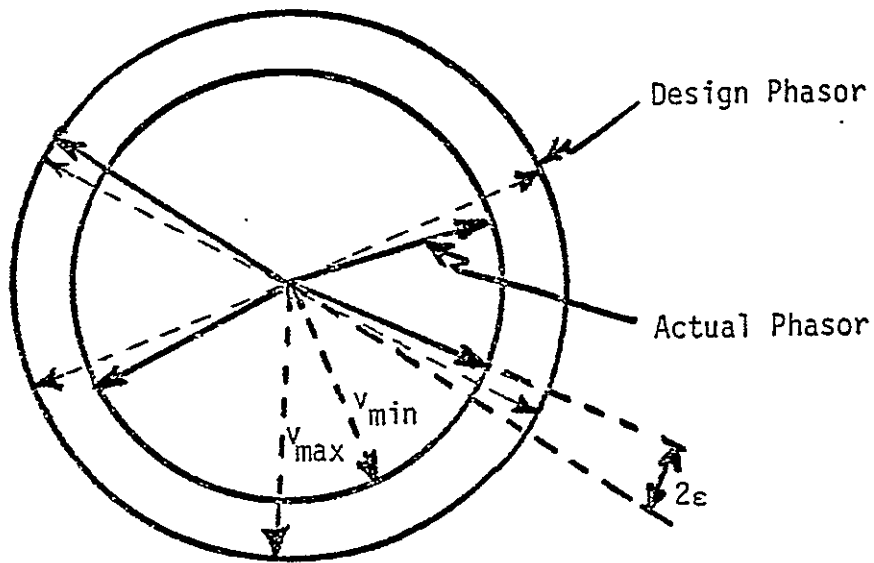
ε = relative phase between I and Q channel

Data Asymmetry

Definition:

1. For an NRZ format signal:

$$\left[\frac{\text{length of long bit} - \text{length of short bit}}{\text{length of long bit} + \text{length of short bit}}\right] \times 100\%$$

2. For a bi-ϕ format signal, data asymmetry applies to both the entire bit as well as to each half symbol pulse. For data bits, data asymmetry is:

$$\left[\frac{\text{length of long bit} - \text{length of short bit}}{\text{length of long bit} + \text{length of short bit}}\right] \times 100\%$$

For half symbol pulse, data asymmetry is:

[length of long half symbol pulse - length of short half symbol pulse]/[length of long half symbol pulse + length of short half symbol pulse] x 100%

Model:

Each positive-going pulse transition is advanced by $\alpha T_s/2$, each negative going transition is retarded by $\alpha T_s/2$ with respect to a perfect clock, where T_s = symbol time for NRZ, T_s = 1/2 symbol time for Bi-ϕ data. Then

Length of long pulse: $T_s(1+\alpha)$

Length of short pulse: $T_s(1-\alpha)$

$$\text{Data Asymmetry} = \frac{T_s(1+\alpha)-T_s(1-\alpha)}{T_s(1+\alpha)+T_s(1-\alpha)} \cdot 100 = \alpha \cdot 100$$

Data Transition Time

Definition: The time required to switch from 90% of the initial

data state to 90% of the final data state, illustrated

as follows:
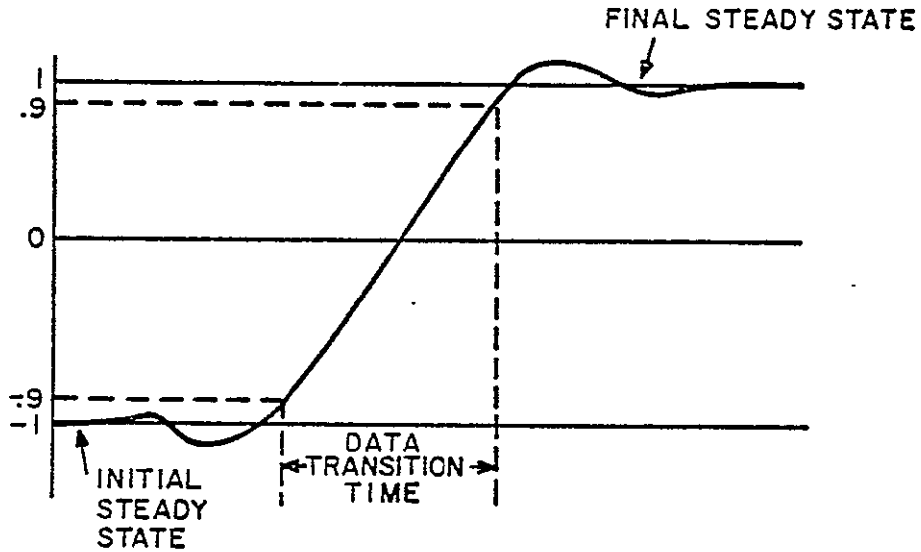
DATA TRANSITION TIME DEFINITION

Model: The data transition time is set by the pulse-shaping filter

characteristic.

Phase Nonlinearity

Definition: The peak deviation of the phase from the best linear fit
to the actual phase versus frequency relationship over
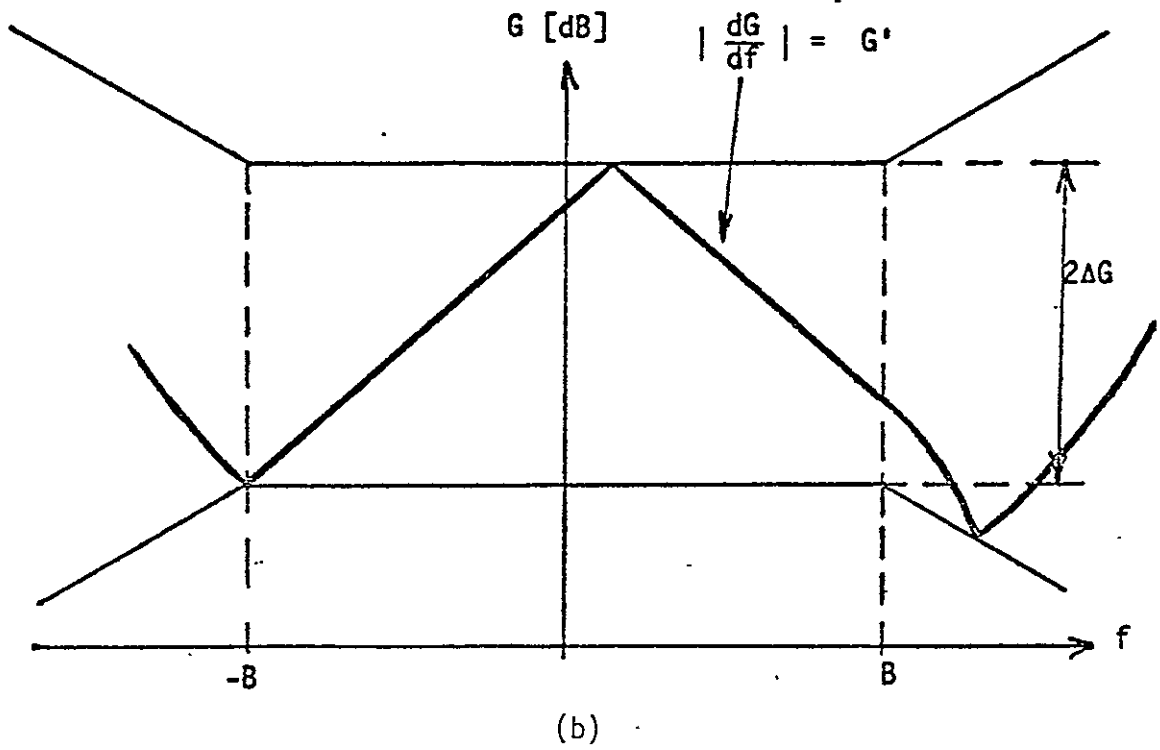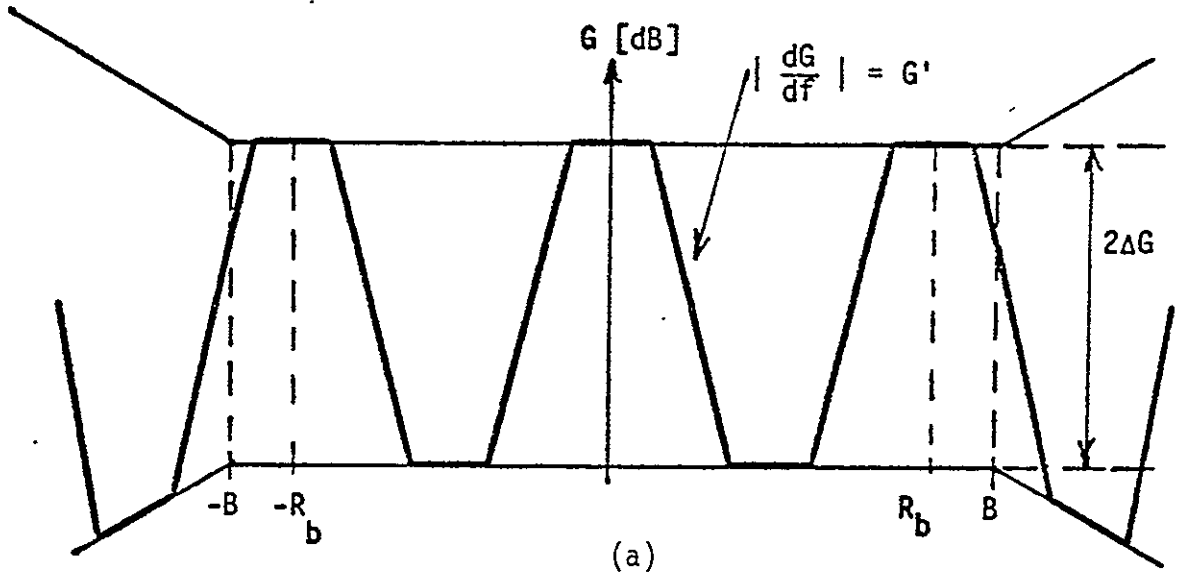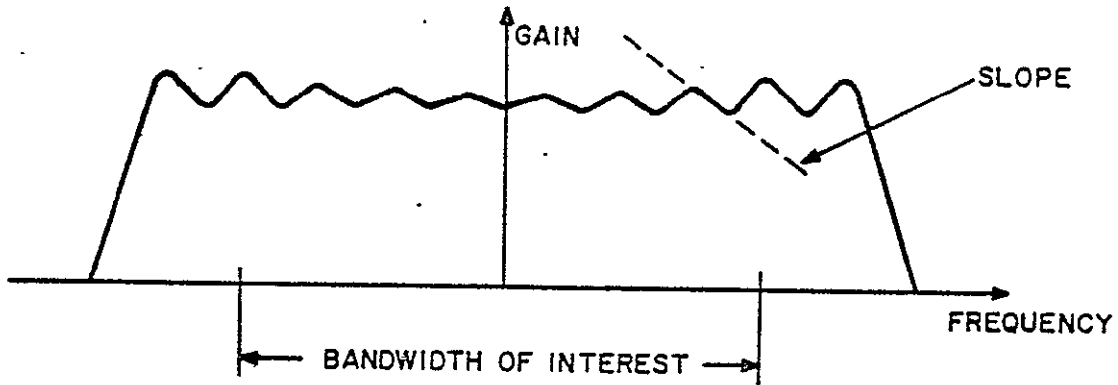the bandwidth of interest, illustrated as follows:
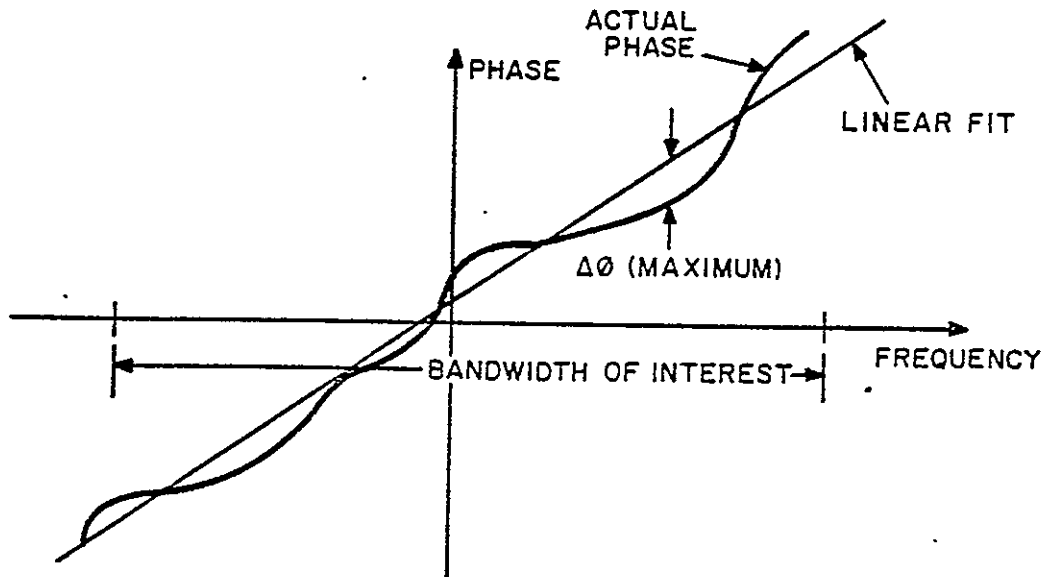
PHASE NONLINEARITY ($\Delta\emptyset$) DEFINITION

Model: The phase nonlinearity is modeled as a sinusoidal ripple
within the specification bandwidth B. Outside, it flares out
linearly as shown below. The ripple period is equal to the
data rate, the amplitude ϕ_{max} is equal to the specified phase
nonlinearity.
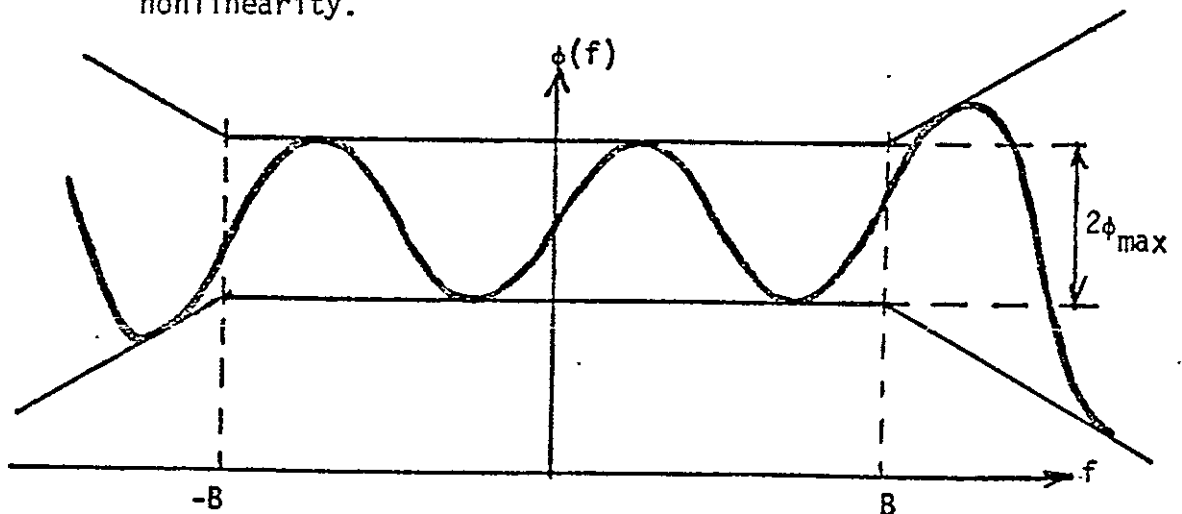
Gain Flatness

Definition: The peak deviation of the gain from the best horizontal

fit to the actual gain versus frequency relationship over

the bandwidth of interest, illustrated as follows:

Model: If the specified gain slope is sufficiently large the

logarithmic gain characteristic is modeled as a trapezoidal

waveform with a peak-to-peak amplitude of twice the

specified gain flatness ΔG with a slope equal to the gain

slope G' specified. Outside of B it flares out. The

ripple period is equal to the data rate. The resulting

characteristic is illustrated in (a). If the gain slope is

too small to obtain the above characteristic a triangular

waveform is used with the same peak-to-peak amplitude and

with the given gain slope. The period of this waveform

is determined by these parameters. The phase is adjusted

to assure that the positive and negative peaks are reached

within ±B. Outside of B the characteristic flares out

again, see (b)

(a)

(b)

Gain Slope

Definition: The rate of change in gain versus frequency at any
point within the bandwidth of interest, illustrated
as follows:

GAIN

SLOPE

FREQUENCY

BANDWIDTH OF INTEREST

Model: If the specified gain slope is sufficiently large the
logarithmic gain characteristic is modeled as a trapezoidal
waveform with a peak-to-peak amplitude of twice the specified
gain flatness ΔG with a slope equal to the gain slope G'
specified. Outside of B it flares out. The ripple period
is equal to the data rate. The resulting characteristic
is illustrated in (a). If the gain slope is too small
to obtain the above characteristic a triangular waveform
is used with the same peak-to-peak amplitude and with the
given gain slope. The period of this waveform is determined
by these parameters. The phase is adjusted to assure that
the positive and negative peaks are reached within $\pm B$. If
the gain slope specified is too small, i.e., G'B < ΔG the
slope is readjusted to G' = $\Delta G/B$. Outside of B the
characteristic flares out again, see (b).

(a)

(b)
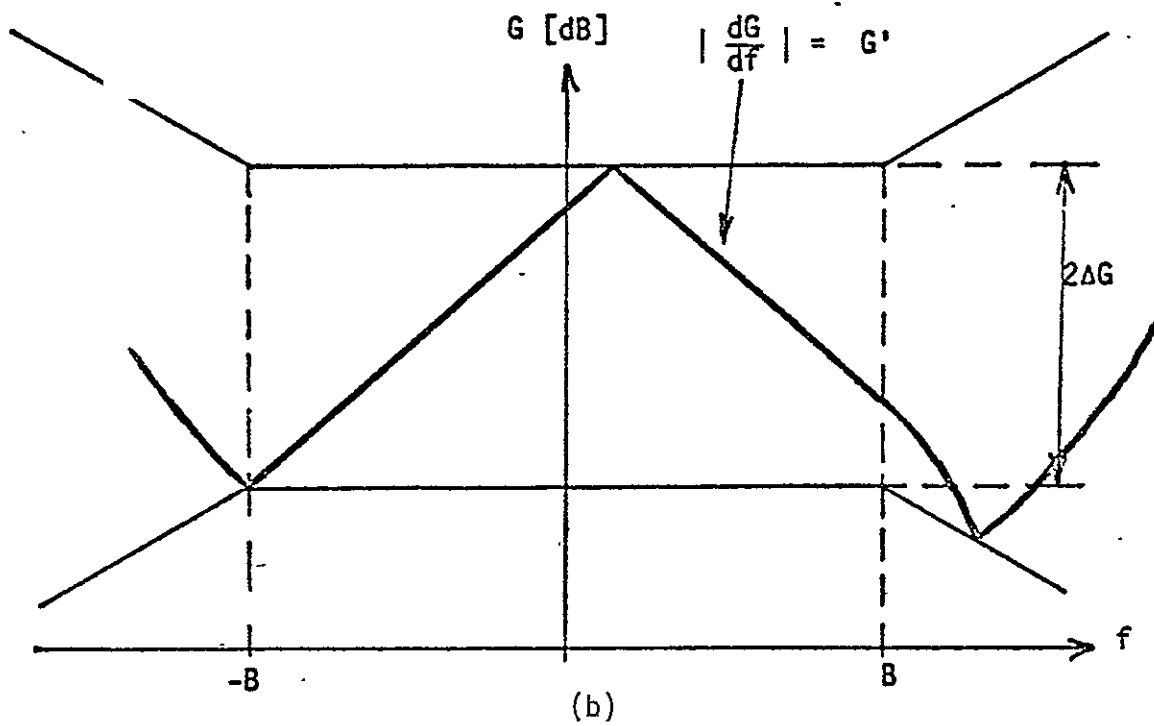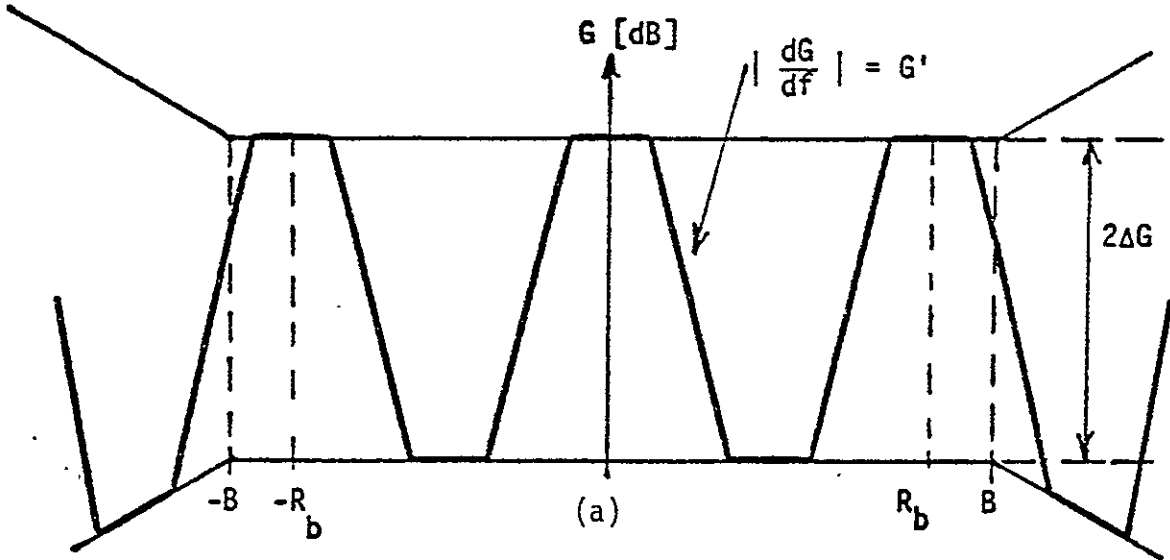
AM/PM

Definition: AM/PM = worst case $\dfrac{d\phi_{out}}{dP_{in}}$ over the range of operating

points where P_{in} = RF power input to power amplitier,

in dB and ϕ_{out} = RF phase output from power amplifier,

in degrees.
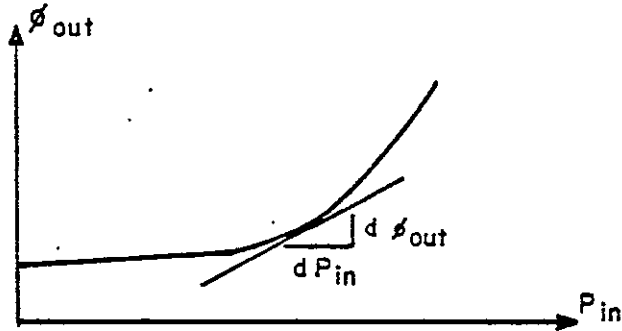
Model: The envelope-dependent phase shift is given by

$$g(R) = \begin{cases} AM/PM\ 20\ \log_{10}(R) & R \geq \varepsilon \\ AM/PM\ 20\ \log_{10}(\varepsilon) & R < \varepsilon \end{cases}$$

where

R = RF input envelope (V)

ε = some small voltage (with respect to r.m.s.

signal)

This results in a constant value for the AM/PM.

Data Transition Induced PM

Definition: Phase variation at the power amplifier output which
is correlated with the modulation on the carrier. This
phase variation results from the combined effects of
bandlimiting followed by AM/PM conversion.

Model: The data transition induced PM is determined by the choice
of type and bandwidth of the pulse shaping filter together
with the selected value of transmitter AM/PM.

PN Chip Jitter

Definition: Let εT be the error in seconds between the actual chip transition time and the correct transition, when T is the chip period and ε is a random variable. Then PN chip jitter is the square root of the variance of ε multiplied by 100 percent.

PN chip jitter is measured as the rms phase error in a baseband bandwidth of 1 MHz using a high gain second-order PN Code Tracking Loop with a damping factor of 0.707 and a two-sided noise bandwidth $(2B_L)$ of 0.2 Hz. This user constraint is based upon zero TDRSS forward link PN jitter.

INPUT SIGNAL → PN CODE TRACKING LOOP $2B_L = 0.2$ HZ → PHASE DETECTOR OUTPUT → FILTER BW = 1 MHZ → MEASURE PHASE ERROR
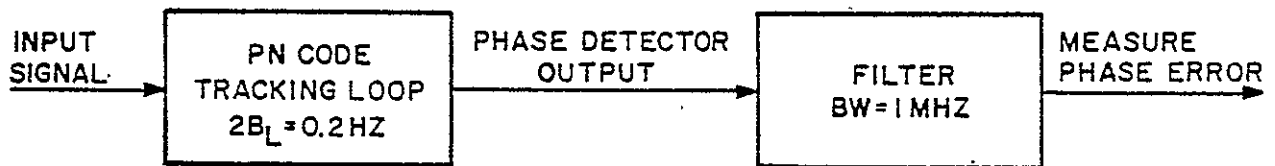
Model: This parameter describes the random variation of the PN clock phase. A Gaussian distribution is assumed and the rms value is set to one third of the peak value specified.

Minimum 3 dB Bandwidth Prior to Power Amplifier

Definition: (No official definition available.)

Model: This is the 3 dB bandwidth of the pulse-shaping filter.

Data Bit Jitter

Definition: User spacecraft peak clock frequency jitter and peak jitter rate (sinusoidal or 3σ random) as percent of the symbol clock rate.

Model: This parameter describes the random variation of the data clock phase. A Gaussian distribution is assumed. Note that this definition deviates from the definition above.

Spurious PM

Definition: Consider a carrier

$$\sin[\omega_c t + \phi(t)]$$

$\phi(t)$ = PM spurs + phase noise.

-PM spurs are discrete phase modulated components on the carrier.

-Phase noise is random phase modulation.

Then each PM spur can be written as

$$B_i \sin(\omega_i t)$$

and the resulting rms spurious PM will be

$$\text{Spurious PM} = \sqrt{\sum_i \frac{B_i^2}{2}} \ .$$

where the sum is taken over all i for which ω_i is within the specified frequency range.

Spurious PM can be determined by measuring the power in each spur and calculating the rms value for these powers.

Model: This parameter is not modelled presently.

Short Term EIRP Stability for KSA Acquisition Sequence No. 1.

Definition: The short-term EIRP stability is determined by measuring the peak-to-peak variations in signal EIRP in dB and dividing by the specified averaging periods in seconds.

Model: This parameter has no effect on the bit error performance and is therefore not modelled.

Spurious Outputs

Definition: The sum of the power in all spurs within the
                specified bandwidth measured relative to the total
                signal power. (dBc indicates dB below total signal
                power). Data bandwidth is the bandwidth between the
                first nulls of the signal. That is, two times the
                symbol rate for NRZ data and four times the symbol
                rate for Bi-∅ formatted data. The channel bandwidth
                is 6 MHz for MA; 10 MHz for SSA, S-band Shuttle, and
                S-band IF service; and 225 MHz for KSA, Ku-band
                Shuttle, and Ku-band IF service.

Model: This parameter is not modelled presently.

Frequency Stability (Peak)

Definition: The peak instantaneous carrier frequency deviation from the nominal carrier frequency (Δf) normalized to the nominal carrier frequency as observed over the specified time interval of interest. This includes frequency deviation due to all sources including deviations induced by environmental changes. (This parameter only applies to the non-coherent modes of operation.)

Model: This parameter has no effect on the bit error performance and is therefore not modelled.

Incidental AM

Definition: Consider an ideal RF signal of the form:

$$A \cos[\omega_c t + \phi(t)]$$

Then a signal with amplitude modulation m_i at frequencies ω_i with phase ϕ_i will be of the form:

$$A[1 + \sum_i m_i \cos(\omega_i t + \phi_i)]\cos[\omega_c t + \phi(t)]$$

The peak of the amplitude modulation will then occur when all of the incidental AM components line up. Therefore, the peak incidental AM will be:

$$\sum_i m_i \times 100\%$$

Model: This parameter has little effect on the bit error performance and is therefore not modelled.

Axial Ratio

Definition: For circularly polarized antennas, the electrical field

vector usually produced describes an ellipse instead of

a circle. The axial ratio is a measure of ellipticity and

is the ratio of the minor axis of the ellipse to the major

axis.

Model: This parameter has little effect on the bit error performance

and is therefore not modelled.

Phase Noise

Definition: Phase noise is the random component of the phase modulation on the carrier. If the spectrum of the phase noise is taken as $S_\phi(f)$, then the rms phase from f_1 to f_2 is:

$$\text{Phase Noise} = \sqrt{\int_{f_1}^{f_2} S_\phi(f)df}$$

Phase nosie can be determined by measuring the power in each frequency band and then subtracting the power in the spurs within that band.

Phase noise values for the coherent turnaround mode assume no phase noise on the signal received by the user and therefore represent the phase noise added by the user. Values indicated for the noncoherent mode represent total output phase noise of the user.

Model: The phase noise is modelled as a Gaussian random process with a flat spectrum in each of the frequency bands specified.

I/Q Data Skew

Definition: Relative time delay of the data transitions between I and Q channels measured as a percent of a bit time. This parameter is determined by data, clock, and modulator characteristics.

Model: This parameter applies to balanced staggered QPSK only. It defines the relative time delay between the pulse center in the one channel and the pulse transition in the other channel. Due to the ground station hardware implementation this parameter has a negligible effect on the performance of an unspread link and no effect on a PN spread link.

Permissible EIRP Variation

Definition: Range over which the user EIRP measured along the

user/TDRS line-of-sight may vary without requiring

user reconfiguration. Performance is determined from

user transmitter power variation, transmit antenna

pattern, worst case user orientation, and maximum

variation in range between the user and TDRS over the

duration of a pass.

Model: This parameter has no effect on the bit error performance

and is therefore not modelled.

Permissible Rate of EIRP Variation

Definition: The time derivative of EIRP.

Model: This parameter has no effect on the bit error performance and is therefore not modelled.

LinCom

Maximum User EIRP

Definition: (No official definition available.)

Model: This parameter has no effect on the bit error performance

and is therefore not modelled.

Frequency Error of 8.5 MHz Subcarrier

Definition: Difference between subcarrier frequency and 8.5 MHz.

Model: The frequency error itself has no effect on the bit error
performance and is therefore not modelled. The effect of
the loop stress in the receiver is modelled through the
resulting static phase offset.

Subcarrier Phase Noise

Definition: Phase noise on the 8.5 MHz subcarrier (see phase
noise definition).

Model: The subcarrier phase noise is modelled as a Gaussian random
process whose power is concentrated outside the subcarrier
tracking loop bandwidth but considerably below the data
rate (worst-case assumption).

I/Q PN Skew

Definition: Relative time delay of the chip transitions between

I and Q channels measured as a percent of a chip time.

Model: Relative time delay between the chip center in one channel

and the chip transition in the other channel of a SQPN

signal.

PN Asymmetry

Definition: PN chip asymmetry is defined as:

$$\left[\frac{\text{length of long chip - length of short chip}}{\text{length of long chip + length of short chip}}\right] \times 100\%$$

Model: Each positive going chip transition is advanced by $\alpha T_c/2$,

each negative going transition is retarded by $\alpha T_c/2$ with

respect to a perfect clock, where T_c = chip time. Then

$$\text{PN Asymmetry} = \frac{T_c(1+\alpha) - T_c(1-\alpha)}{T_c(1+\alpha) + T_c(1-\alpha)} \times 100 = \alpha \cdot 100.$$

REFERENCE

[1] Tracking and Data Relay Satellite System (TDRSS) Users'
    Guide, Revision 3, STDN No. 101.2, Goddard Space Flight
    Center, Greenbelt, MD, January, 1978.

3.0 LinCsim PERFORMANCE PREDICTION

3.1 Introduction

The Shuttle/TDRSS link simulation software package (LinCsim) has been used to predict the Shuttle/TDRSS S-band return link bit error rate performance based on current link budgets user constraint values and TDRS/ground station hardware data. The results of this effort are presented in this section.

3.2 Performance Prediction for Shuttle S-band Return Link

This section presents the sensitivity of the Shuttle S-band return link BER performance to variations of the user constraint values based on current link budgets, nominal user constraint value estimates and TDRS/ground station hardware data. This simulation is based on the link models presented in Chapter 2 and on the system parameters listed in Table 2.3.

The link characteristics assumed are summarized in Table 3.1. The nominal values of the user constraints are listed in Table 3.2. They agree with the expected Shuttle values obtained from JSC. The link budget is reproduced in Table 3.3. It is based on the budgets contained in Ref. 1 with some updates obtained from Dr. Kwei Tu. Table 3.4 lists the user constraints whose effect on performance was studied.

The results are shown in two different forms. The BER curves show the bit error probability as a function of Shuttle-to-TDRS link carrier-to-noise ratio (CNR) variation around the nominal link budget of Table 3.3. The horizontal distance between the bit error rate curve and the design point shown represents

Table 3.1. Shuttle S-band Return Link Characteristics
Used for LinCsim

Data Rate	192 Kbps
Data Format	BPSK, Biphase, Unspread
Coding	Rate 1/3 Convolutional Code
Carrier	Noncoherent with Forward Link
Design Error Rate	10^{-4}

Table 3.2. Nominal User Constraint Values Used for LinCsim

Data Bit Jitter (3σ)	.6%
Modulator Phase Imbalance	11°
Modulator Gain Imbalance	.1 dB
Data Asymmetry	3.8%
Phase Nonlinearity	3°
Gain Flatness	.4 dB peak
Gain Slope	.1 dB/MHz
AM/PM	14°/dB
3 dB Bandwidth	100 MHz
Phase Noise	
1 Hz - 10 Hz	0°
10 Hz - 100 Hz	1°
100 Hz - 1 kHz	10°
1 kHz - 6 MHz	1°

Table 3.3. Shuttle S-Band Return Link Power Budget.

Shuttle-to-TDRS Link

Shuttle EIRP	16.7 dBW
Space Loss	192.1 dB
Polarization Loss	.5 dB
TDRS G/T.	9.55 dB/°K

TDRS-to-Ground Link

TDRS TWT max Output Power	13.4 dBW
TWT Output Backoff	2 dB
SSA Power Allocation	-10 dB
TDRS Hardware Losses	2.46 dB
TDRS Antenna Gain	45.9 dB
Pointing Loss	.65 dB
Space Loss	207.7 dB
Polarization Loss	.1 dB
Atmospheric Loss	.8 dB
Ground Station G/T	40.3 dB/°K

Table 3.4. Parameters Studied.

Modulator Gain Imbalance

Modulator Phase Imbalance

Data Asymmetry

Data Bit Jitter

Data Static Timing Offset

XTR AM/AM

XTR AM/PM

Static Phase Error

XTR Gain Slope

XTR Gain Flatness

XTR Phase Nonlinearity

Phase Noise R.M.S.

the margin in carrier-to-noise ratio which can be allocated to the various subsystems for hardware degradations. The sensitivity curves show the increase in Shuttle-to-TDRSS CNR needed to offset the performance degradation (relative to the nominal performance) due to the variation of a single parameter at the design error rate of 10^{-4}.

The error rate curve in Fig. 3.1 represents the BER performance of a Shuttle transponder transmitting a perfect signal (i.e. all user constraints are set to zero). The CNR loss shown (.9 dB) can be attributed to the TDRS and the ground station. This BER curve is reproduced on all other BER plots and labeled "Perfect User." The horizontal distance between this curve and one of the other BER curves represents the CNR loss due to the combined effect of all the user constraints. For the nominal conditions this loss amounts to .75 dB.

Fig. 3.20 shows that by far the biggest contribution of degradation comes from the phase noise which is specified as 10° rms in the 0 to 270 Hz frequency range. As a worst-case assumption this noise power was concentrated in the 100-270 Hz range (i.e. outside the tracking loop bandwidth). A more accurate performance prediction could be made if the noise power inside and outside the tracking loop bandwidth were known separately.
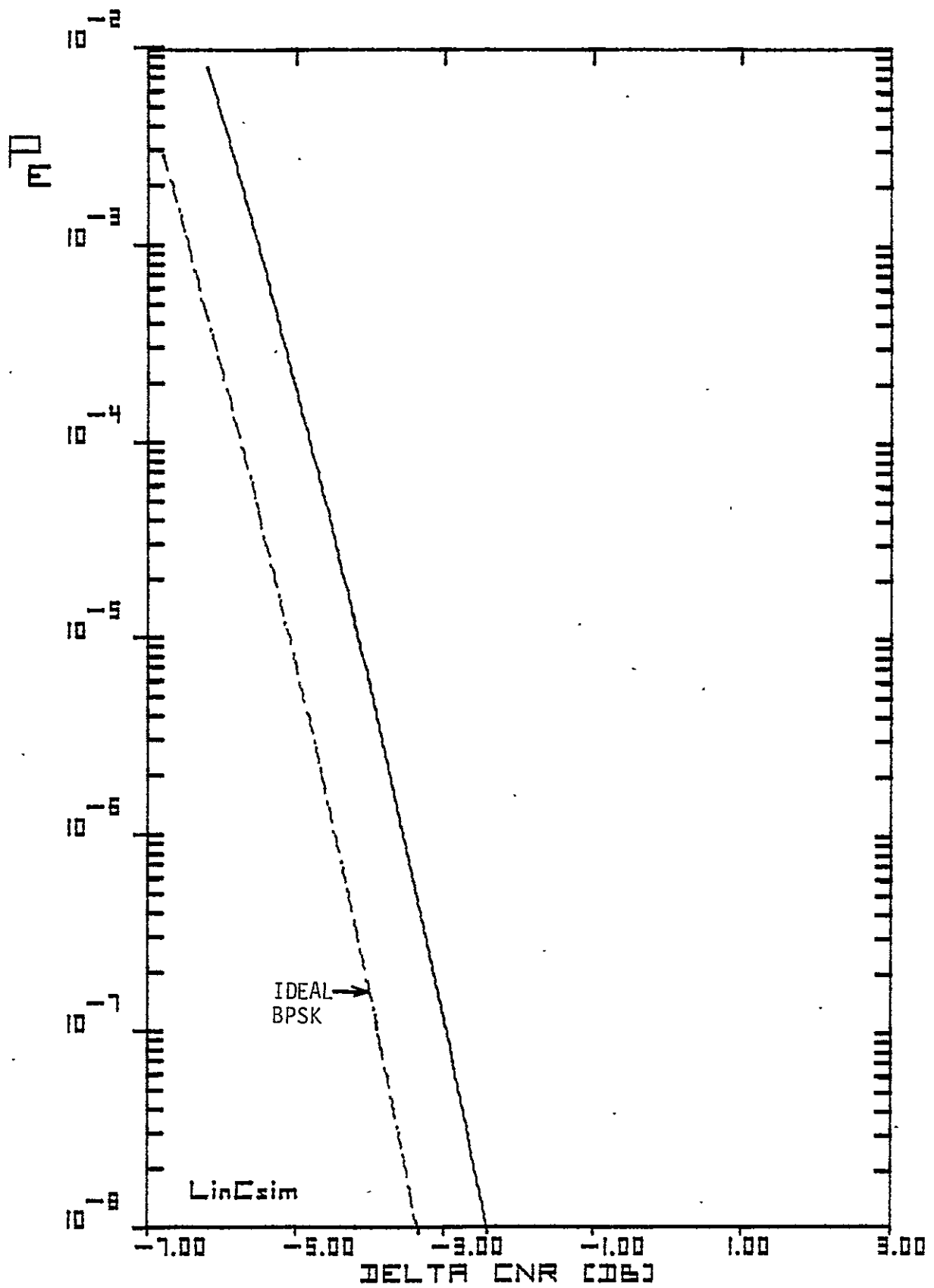
Figure 3.1.BER Plot for Perfect Shuttle Transmitter.

MODULATOR GAIN IMBALANCE

◊
DESIGN POINT

0 dB

.2

.4

.6

.8

1 dB

PERFECT USER

IDEAL
BPSK

LinCsim

10^{-2}

10^{-3}

10^{-4}

10^{-5}

10^{-6}

10^{-7}

10^{-8}

-6.00   -4.00   -2.00   .00   2.00

DELTA CNR [DB]
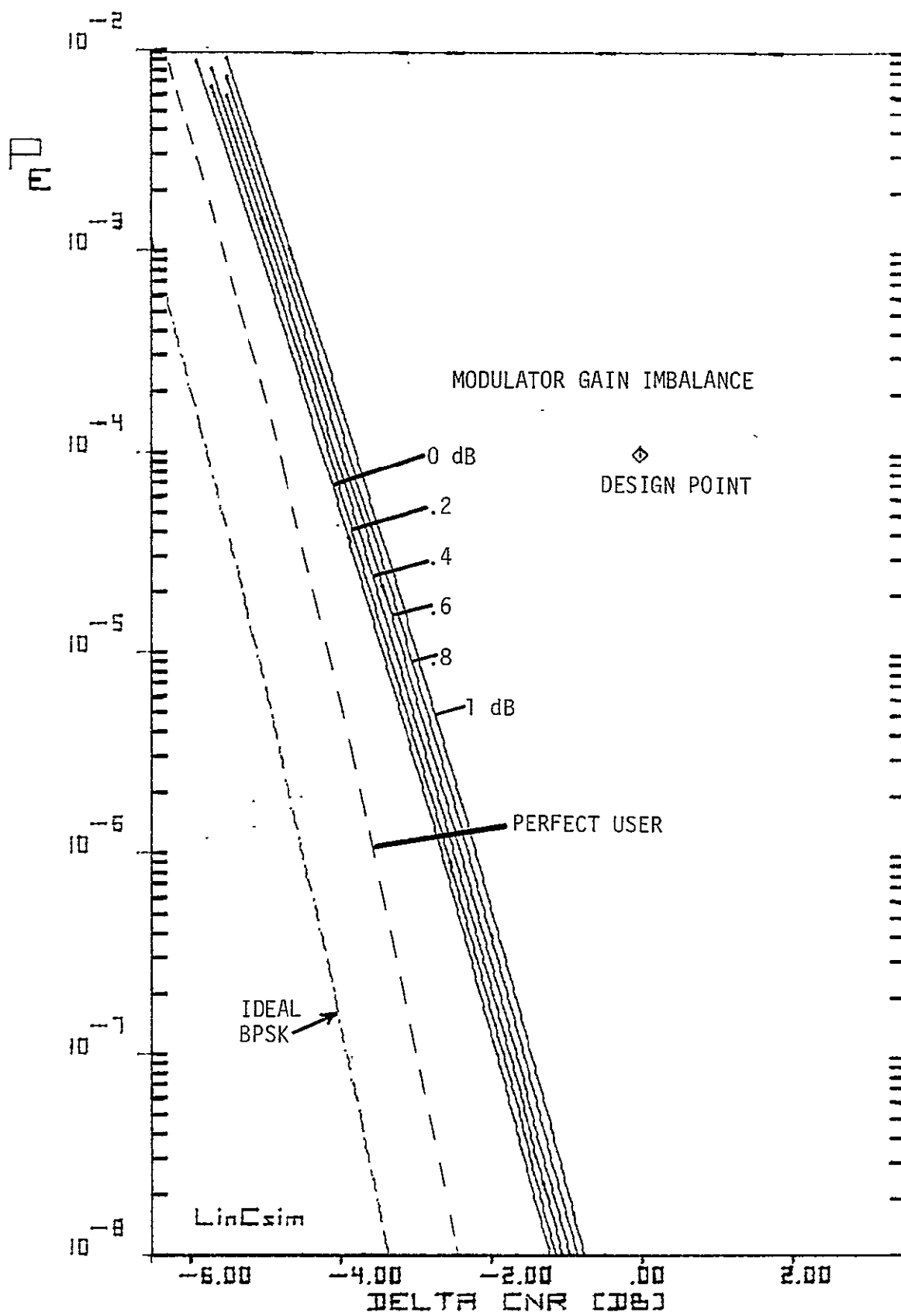
Figure 3.2. BER Plot for Gain Imbalance.
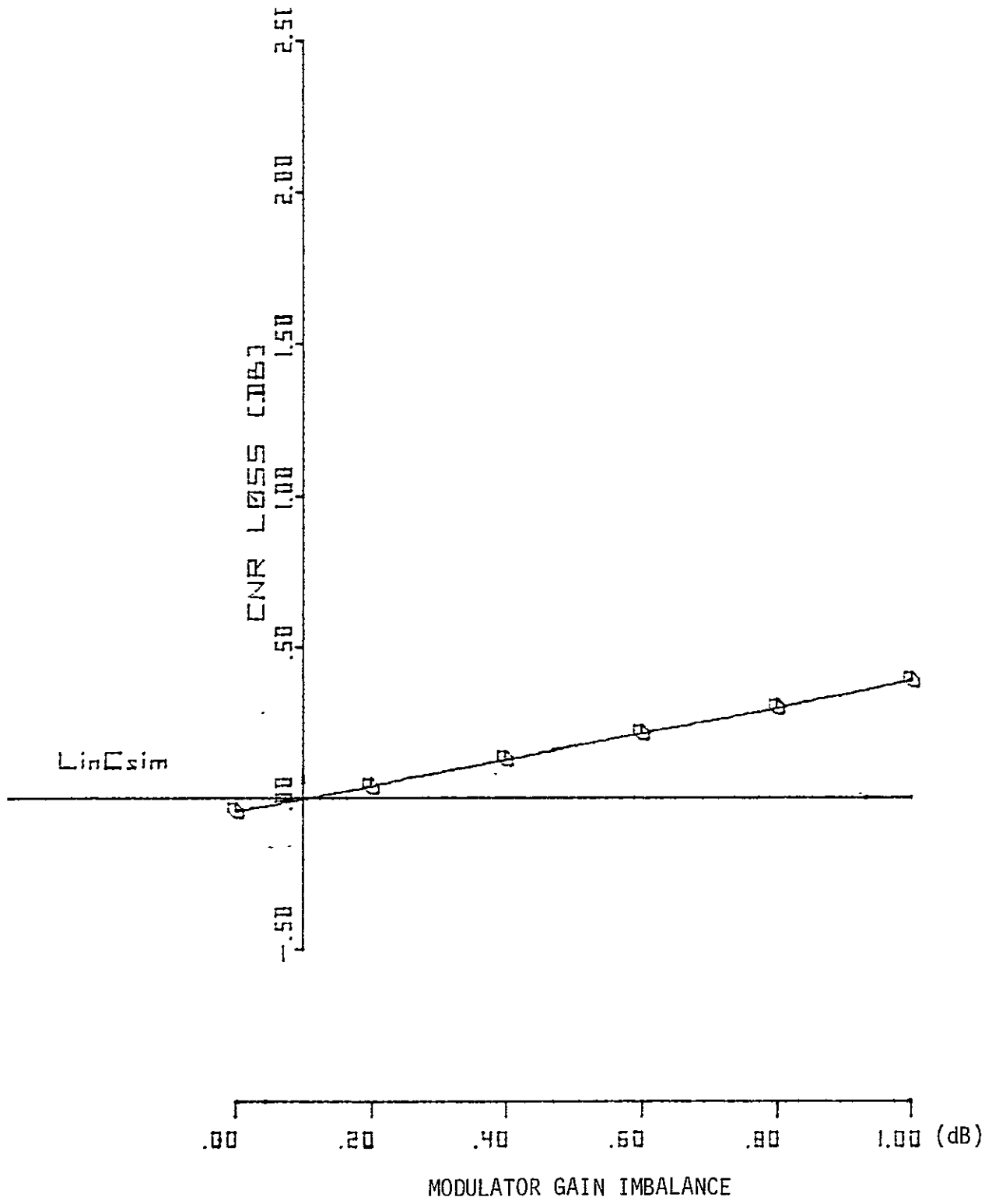
Figure 3.3. Sensitivity Curve.

-85-
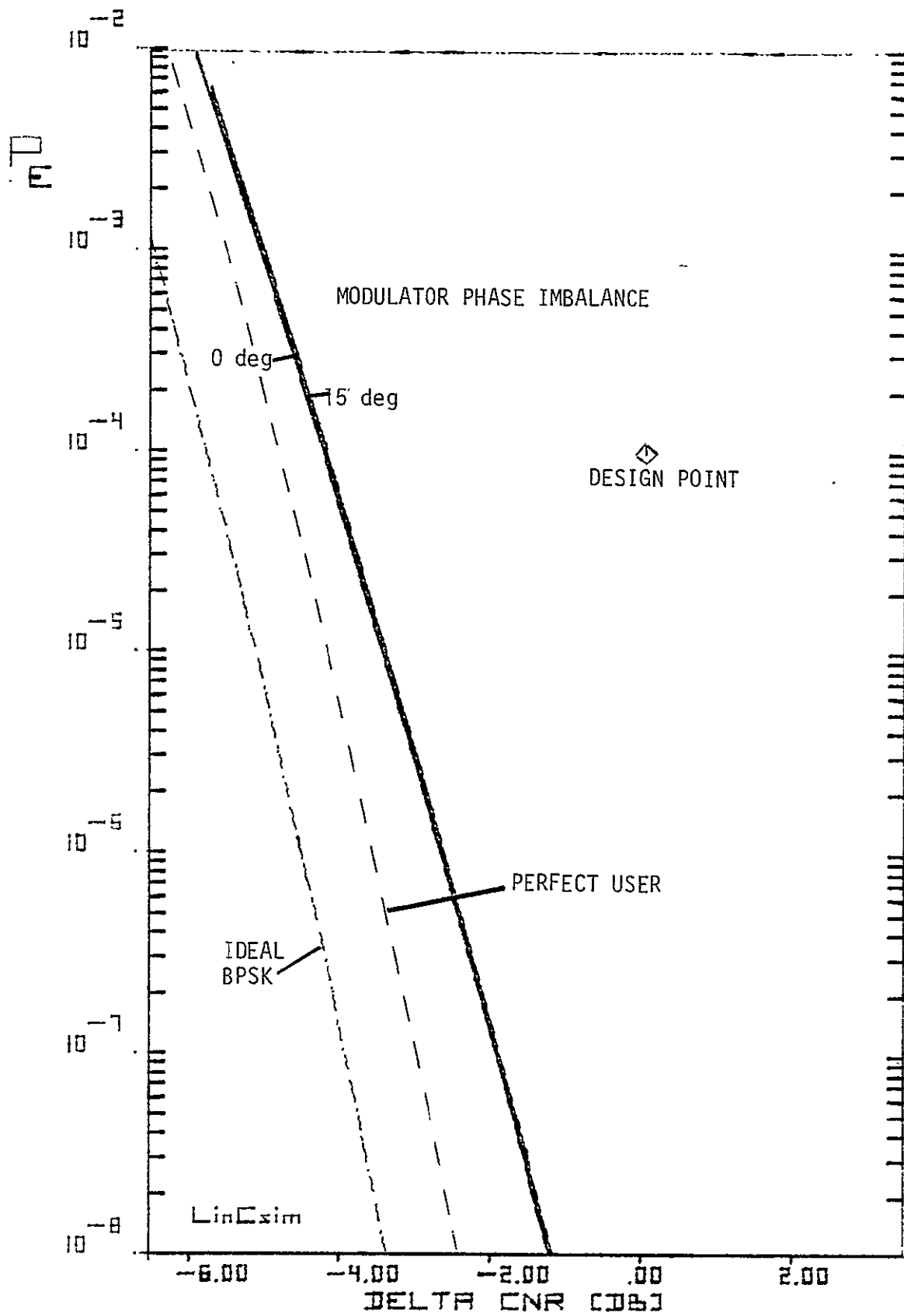
Figure 3.4. BER Plot for Phase Imbalance.
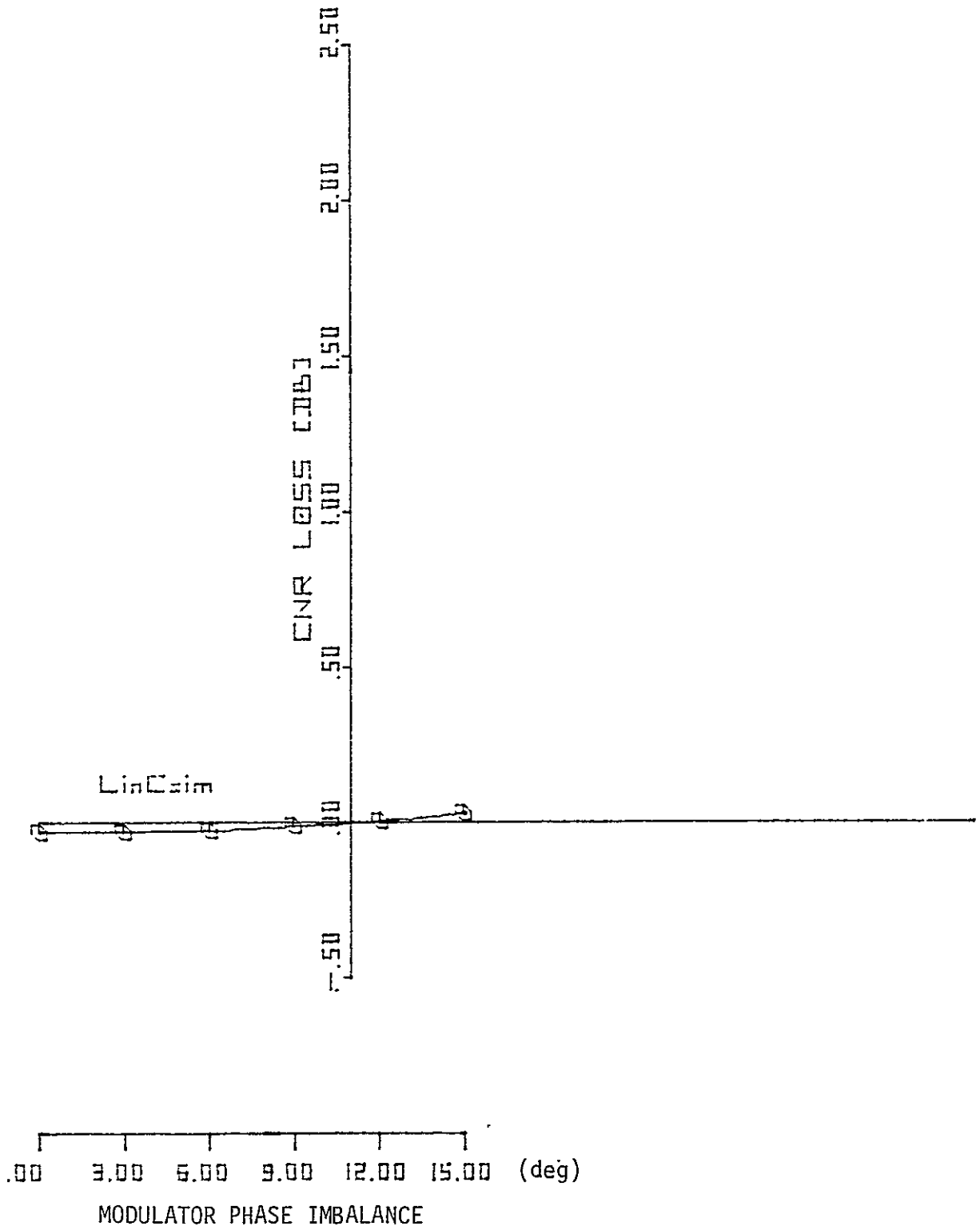
Figure 3.5 Sensitivity Curve.
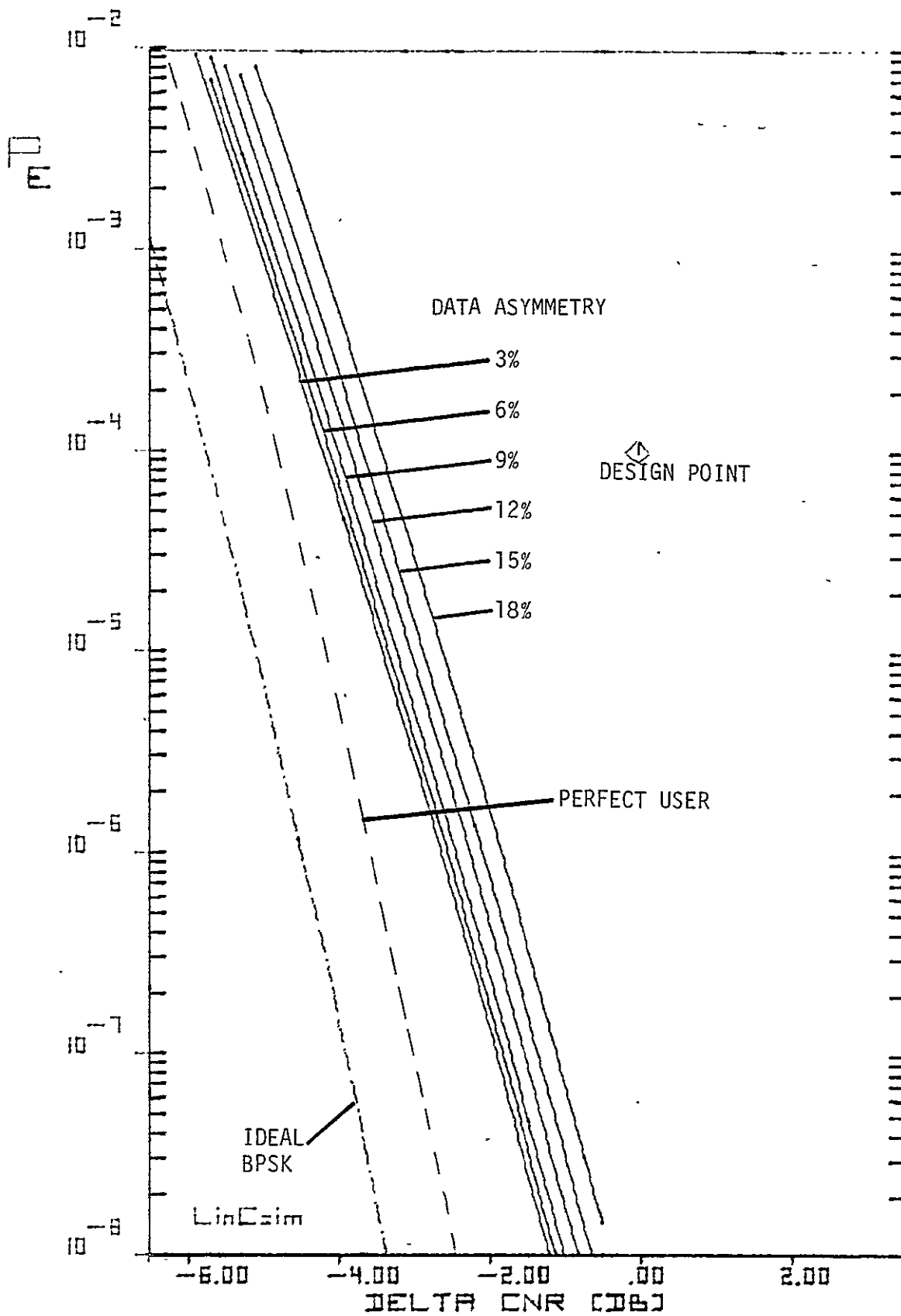
Figure 3.6. BER Plot for Data Asymmetry.
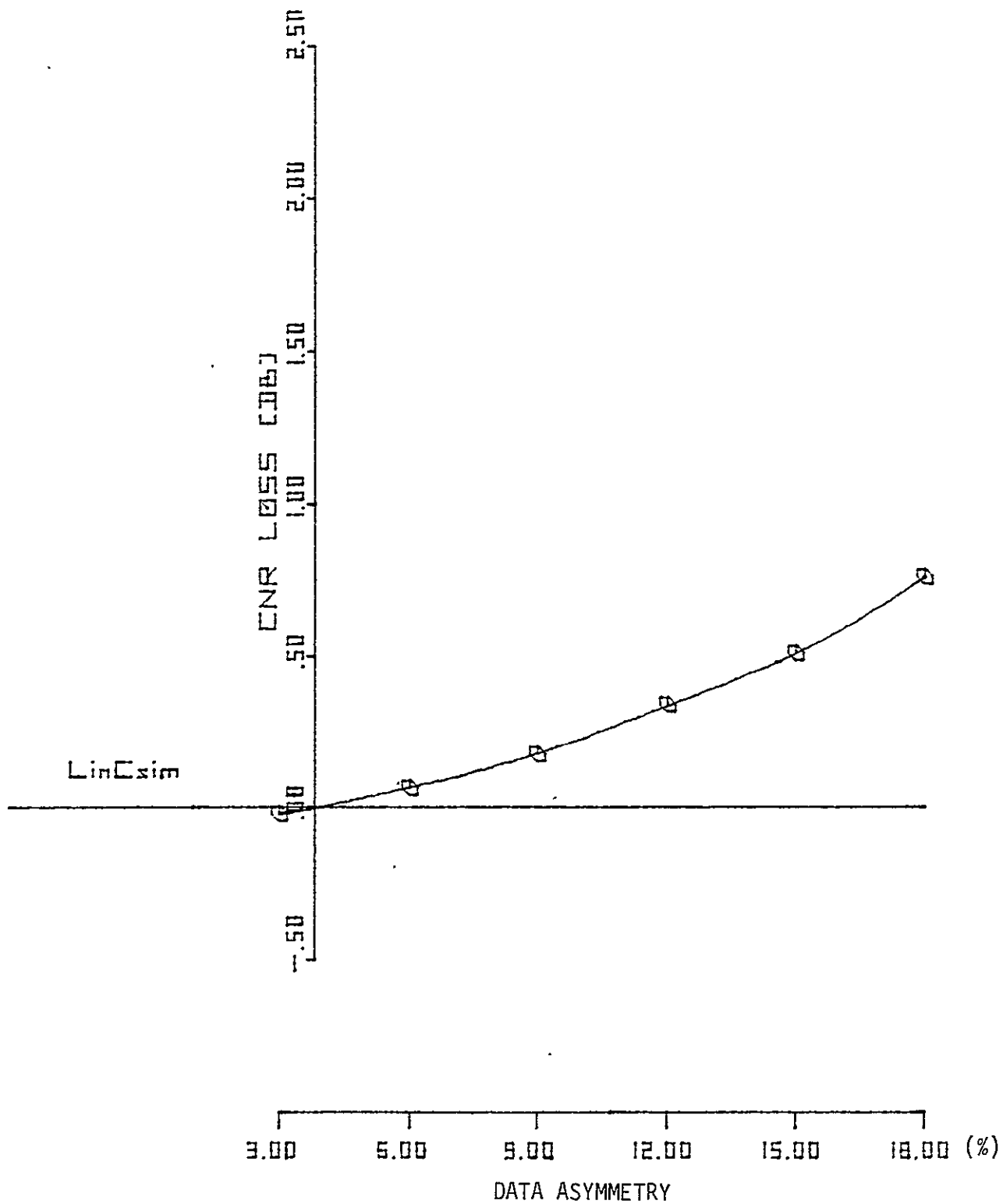
Figure 3.7. Sensitivity Curve.
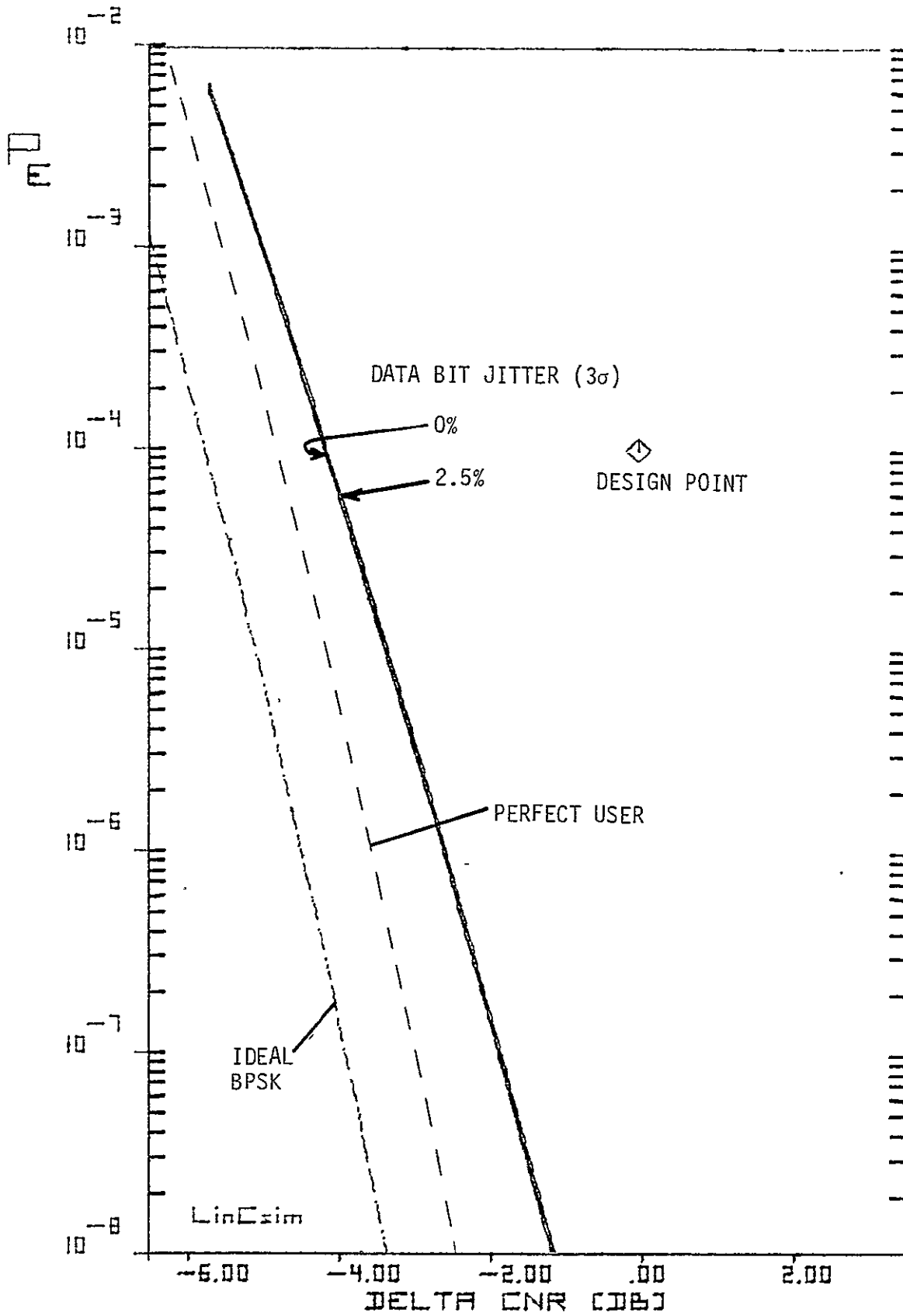
Figure 3..8. BER Plot for Bit Jitter.

79 0056
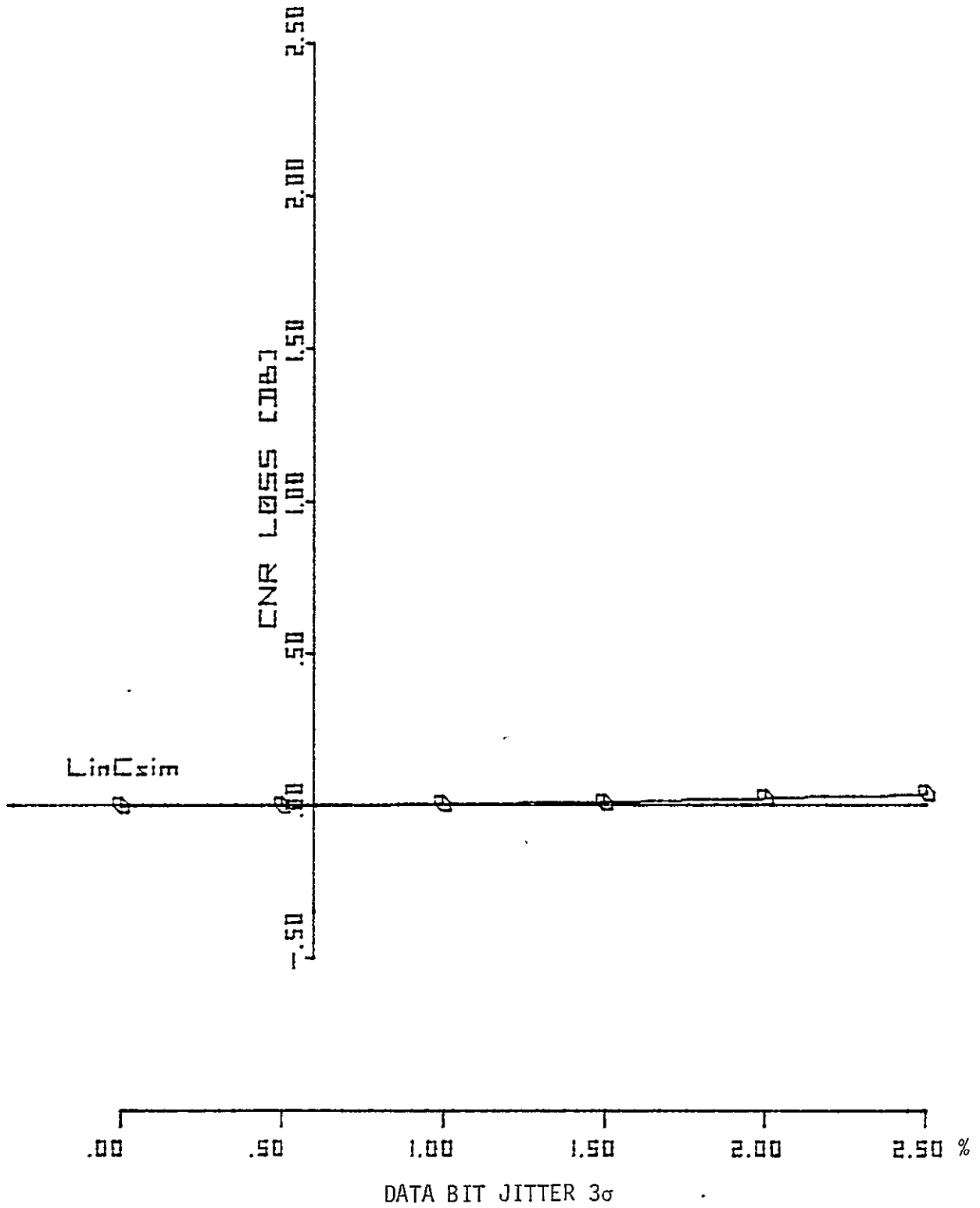
Figure 3.9 .Sensitivity Curve.

79 0057
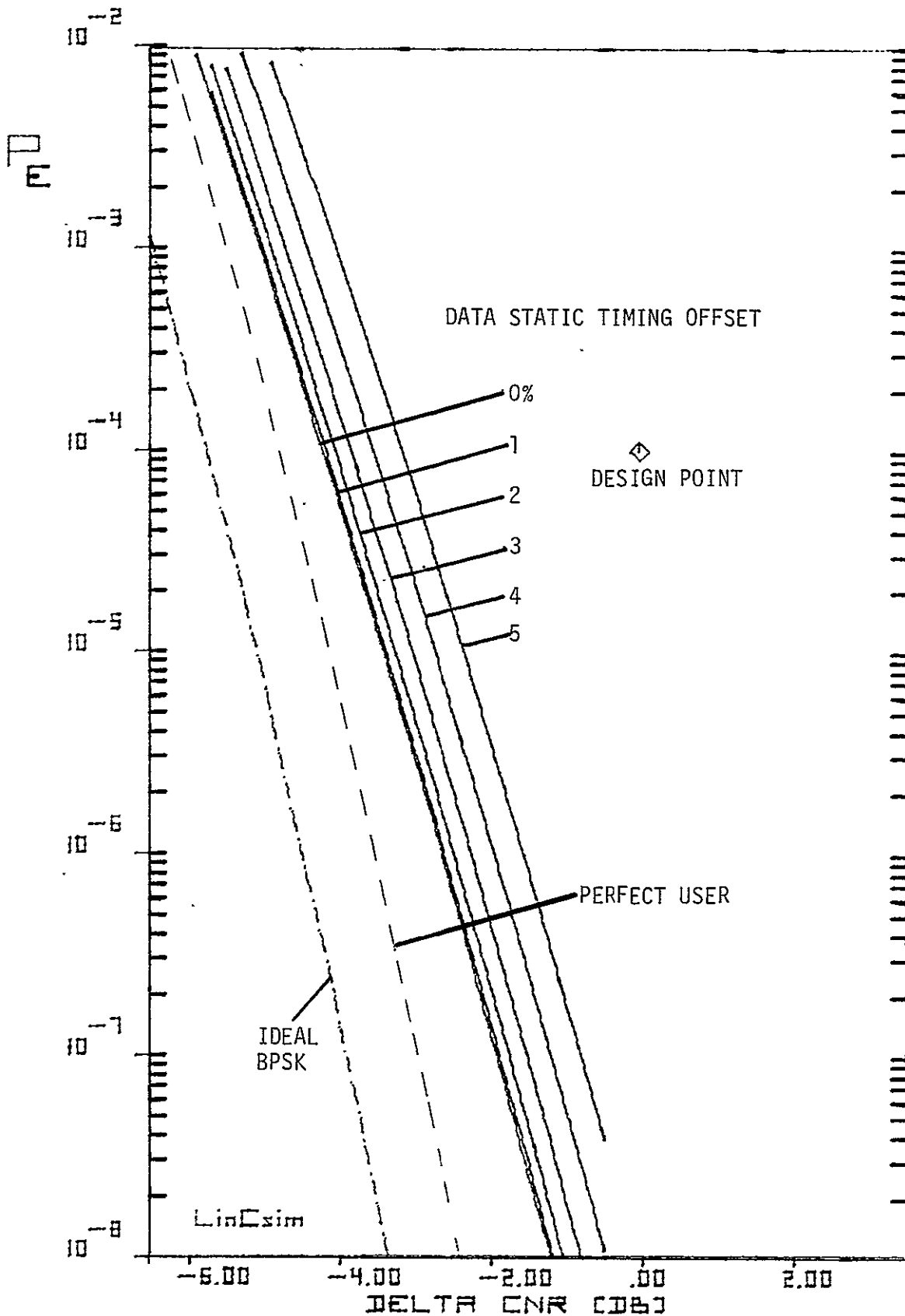
Figure 3.10 BER Plot for Timing Offset.

79 0058
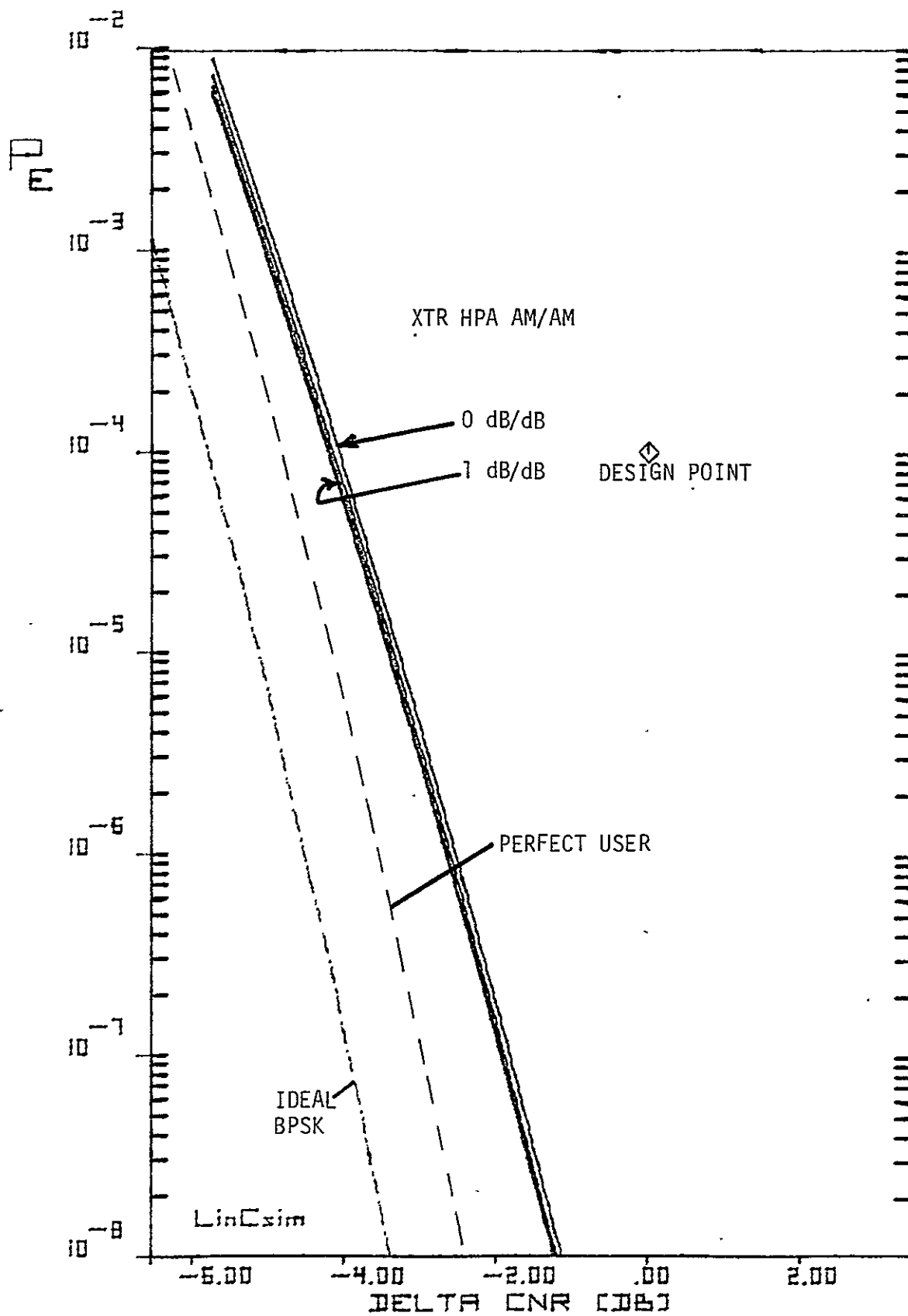
Figure 3.11. BER Plot for AM/AM.

C-2

79 0053
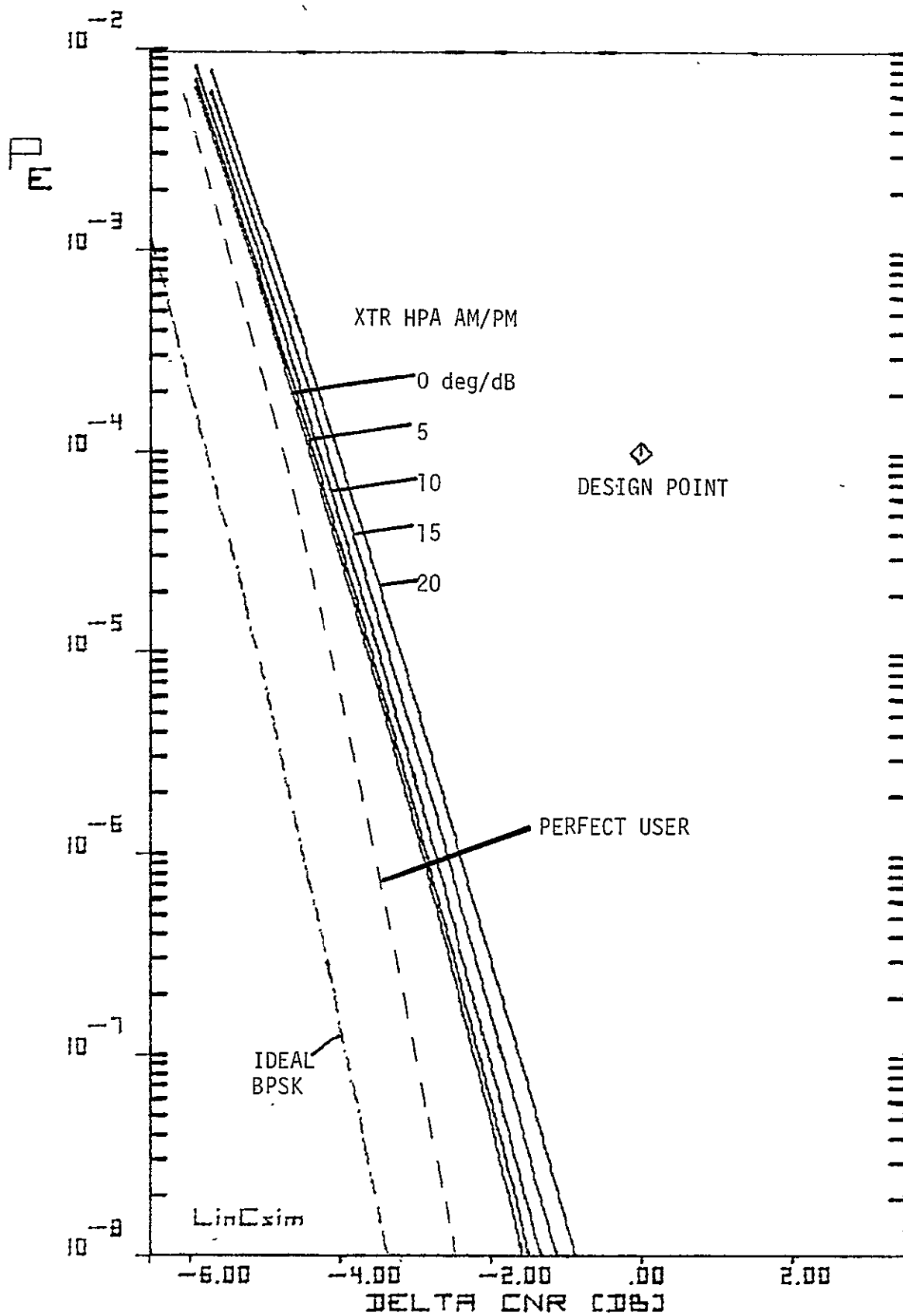
Figure 3.1.2. BER Plot for AM/PM

The plot shows BER ("E" vertical axis, logarithmic from 10^{-2} to 10^{-8}) versus DELTA CNR [DB] (horizontal axis from -6.00 to 2.00).

Labels on the figure:

XTR HPA AM/PM

0 deg/dB
5
10
15
20

DESIGN POINT

PERFECT USER

IDEAL BPSK

LinCsim

79 0060
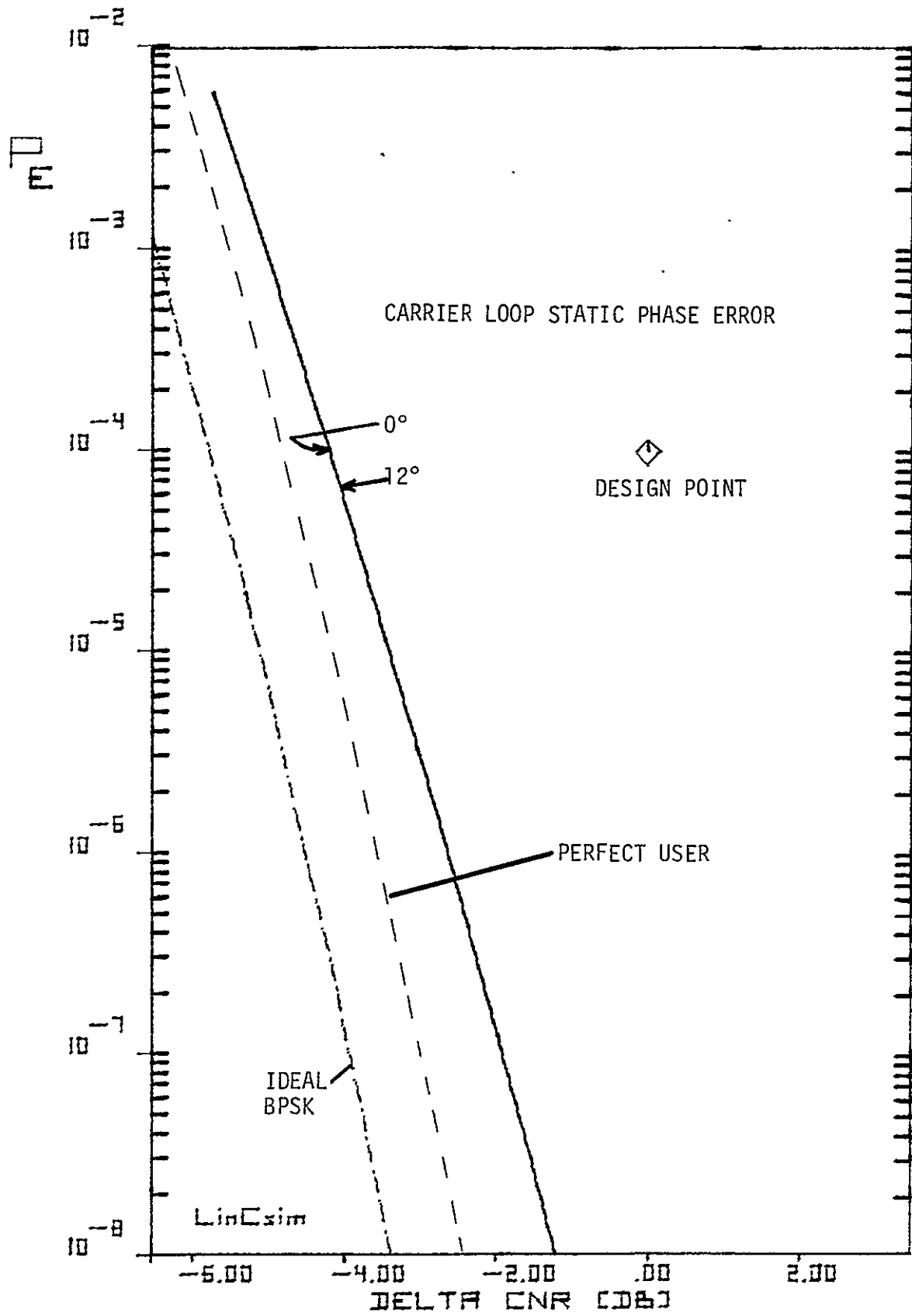
Figure 3.13.BER Plot for Static Phase Error.
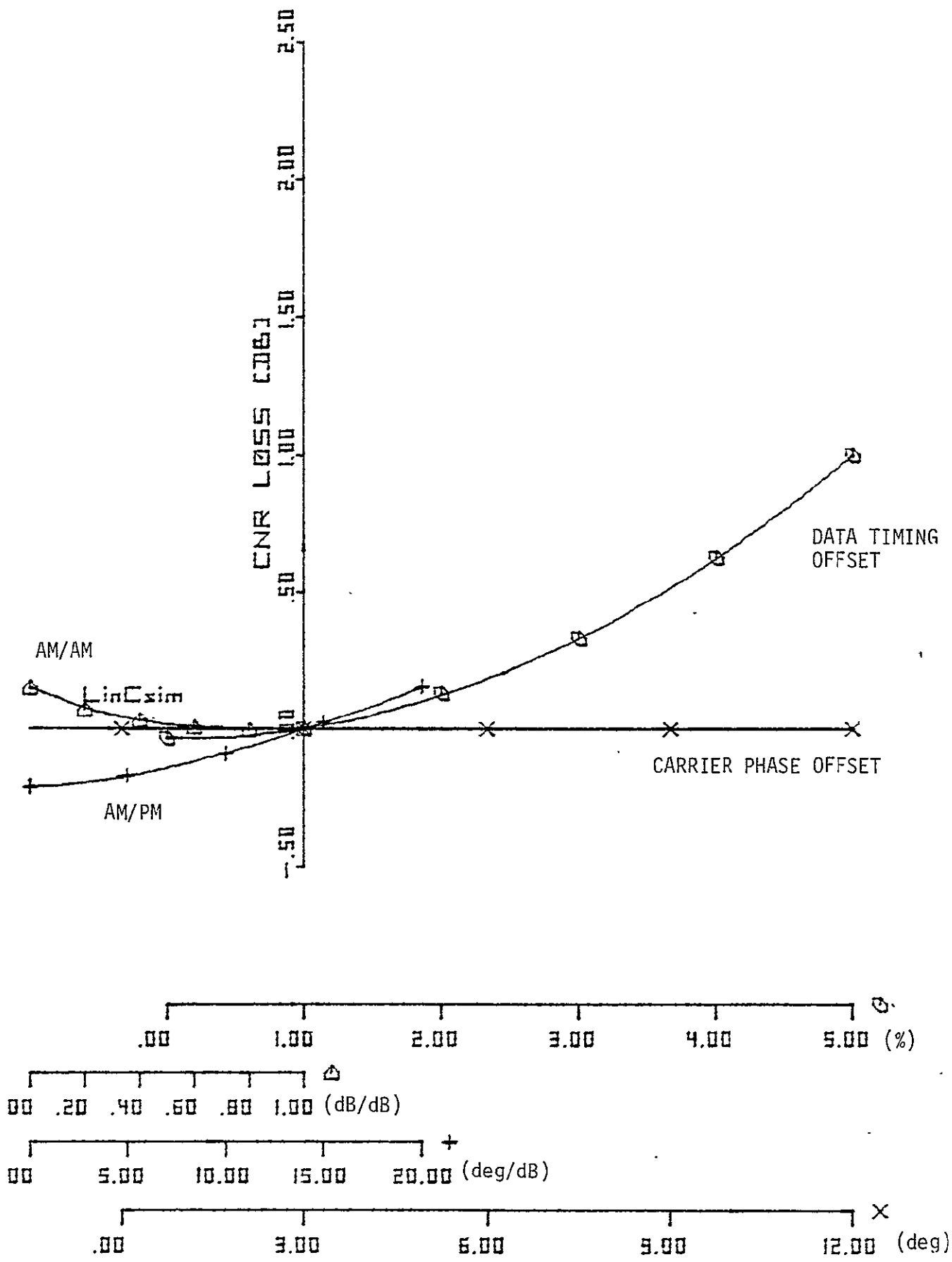
Figure 3.14. Sensitivity Curves.

-96-
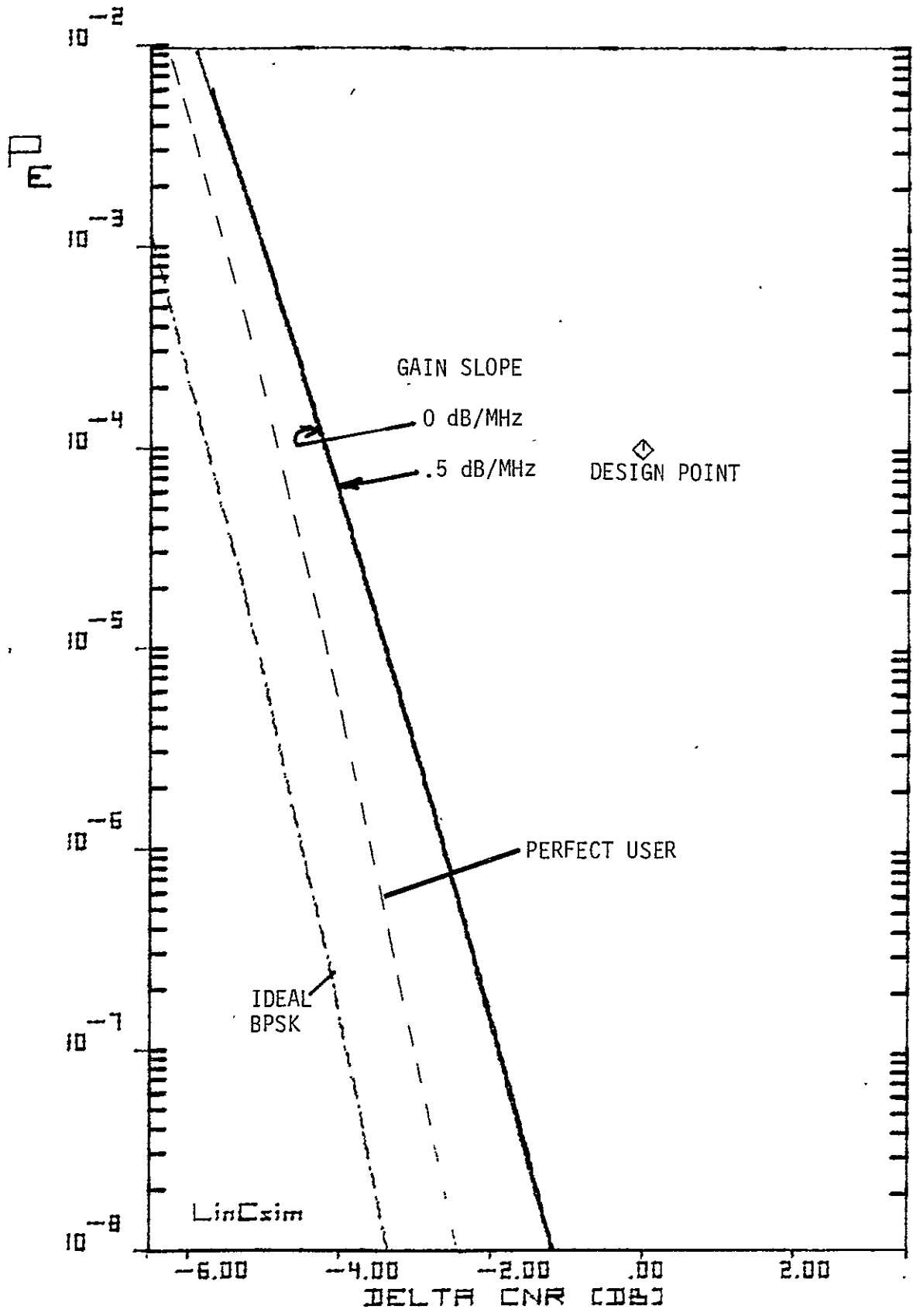
Figure 3.15.BER Plot for Gain Slope.
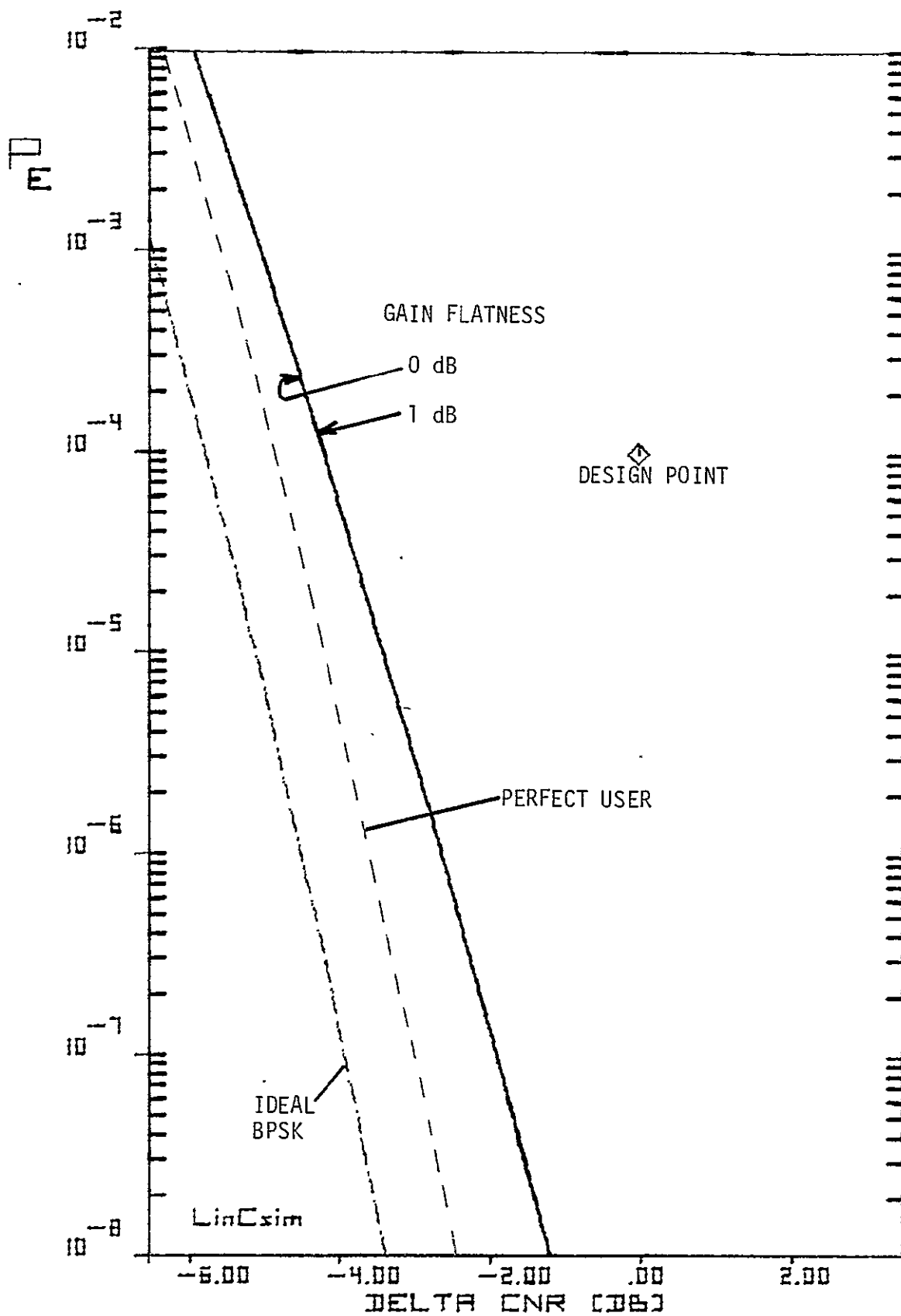
Figure 3..16.BER Plot for Gain Flatness.
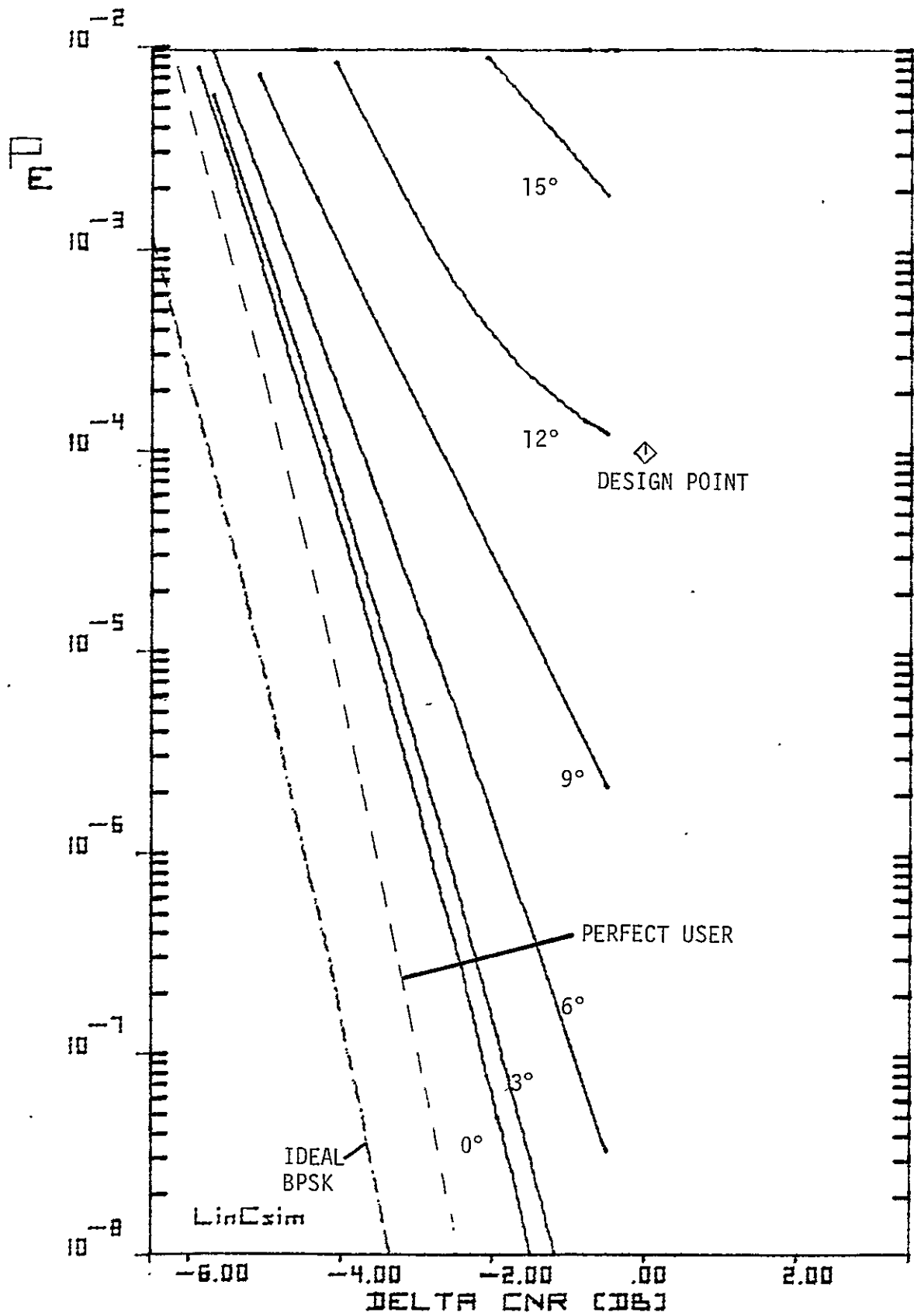
Figure 3.17.BER Plot for Phase Nonlinearity.
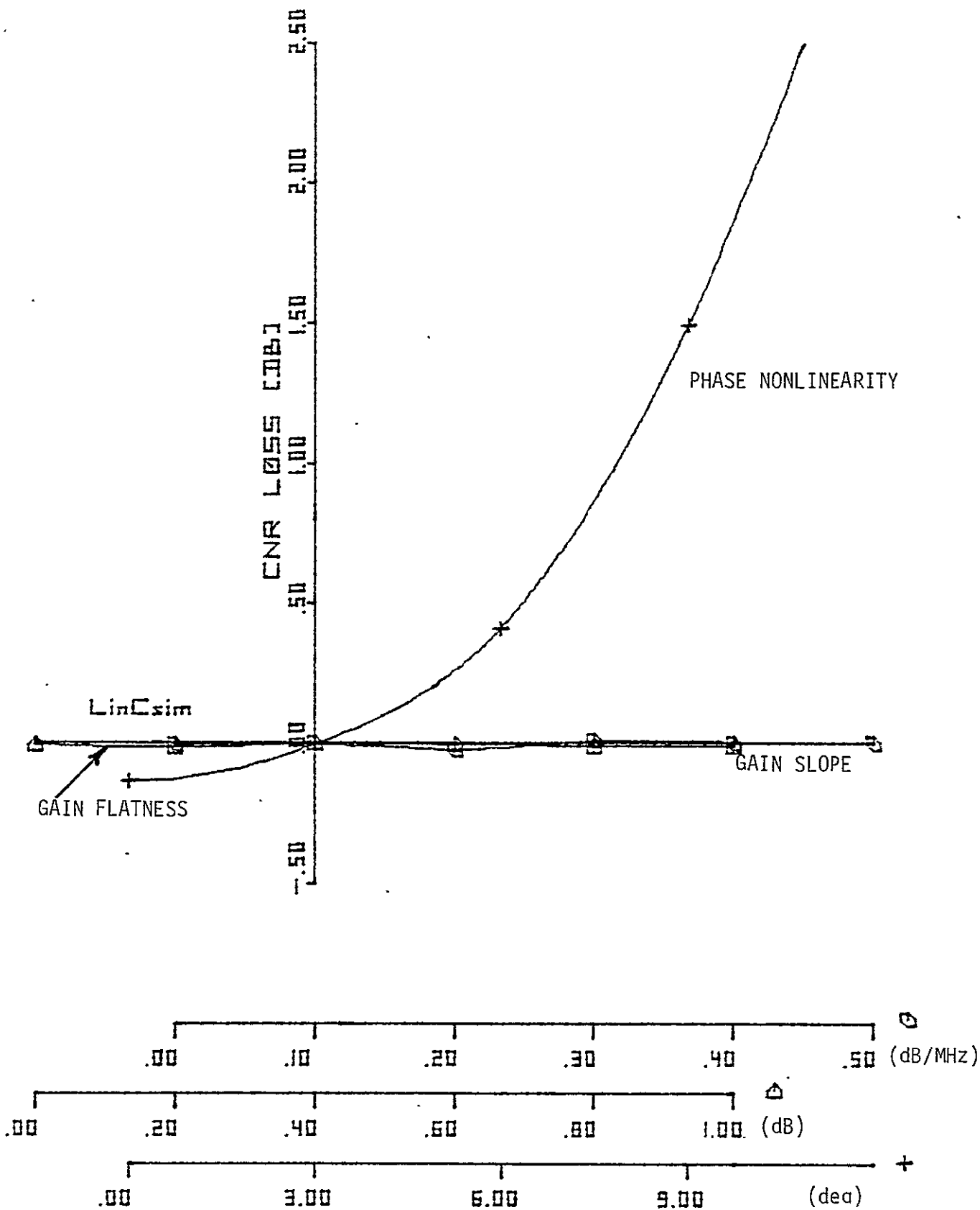
Figure 3.18. Sensitivity Curves.

79 0066
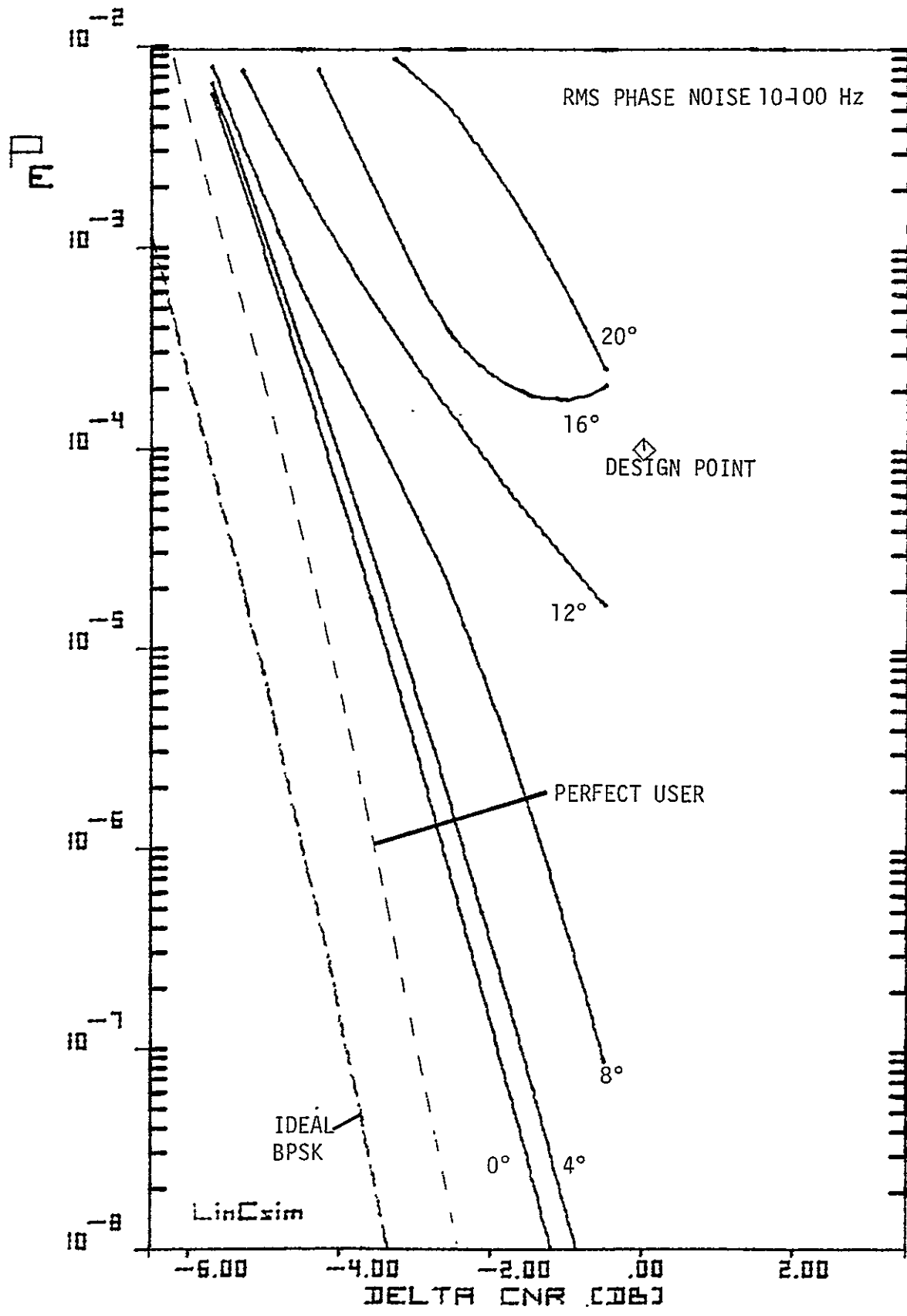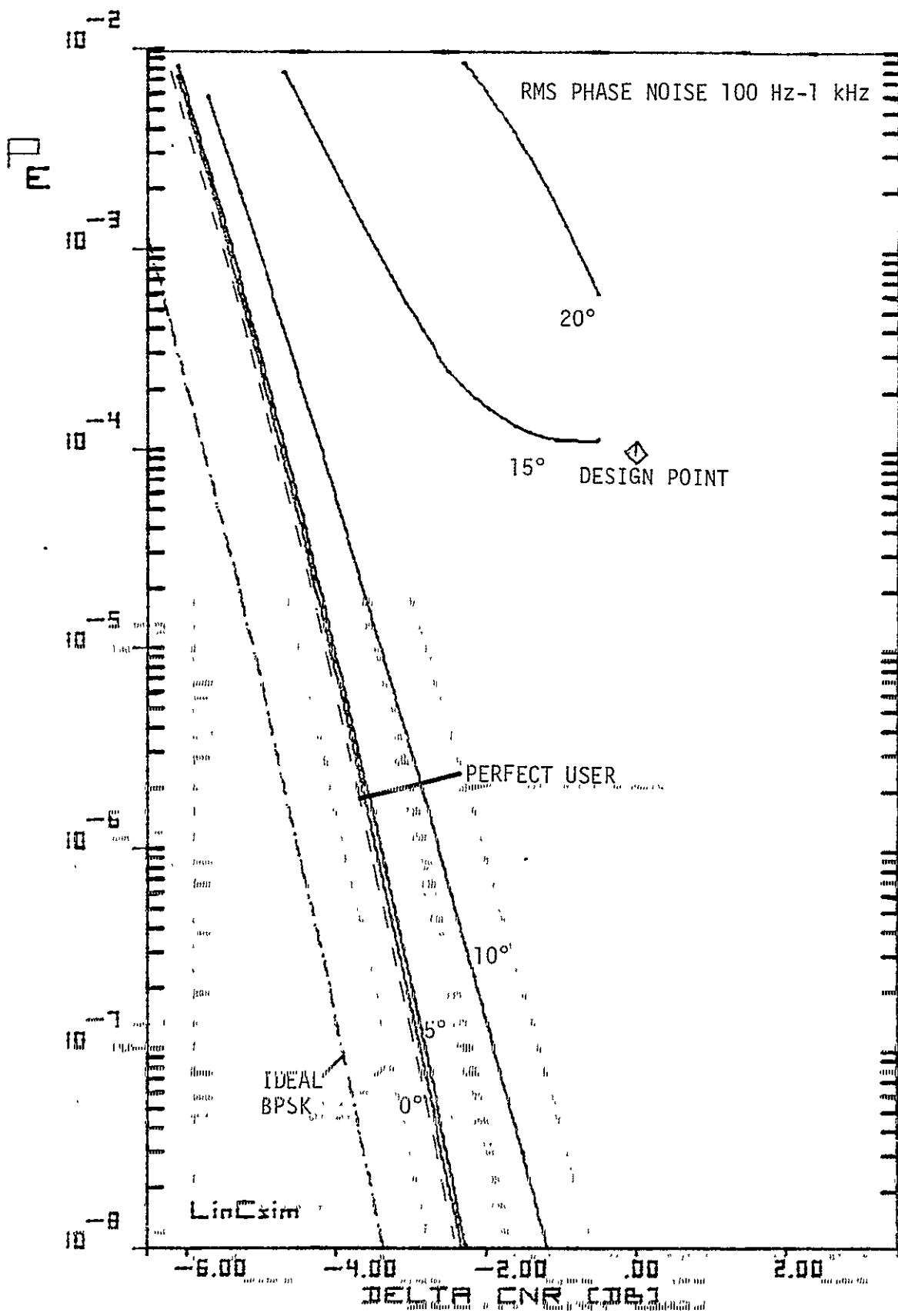
Figure 3.19.BER Plot for Low Frequency Phase Noise.
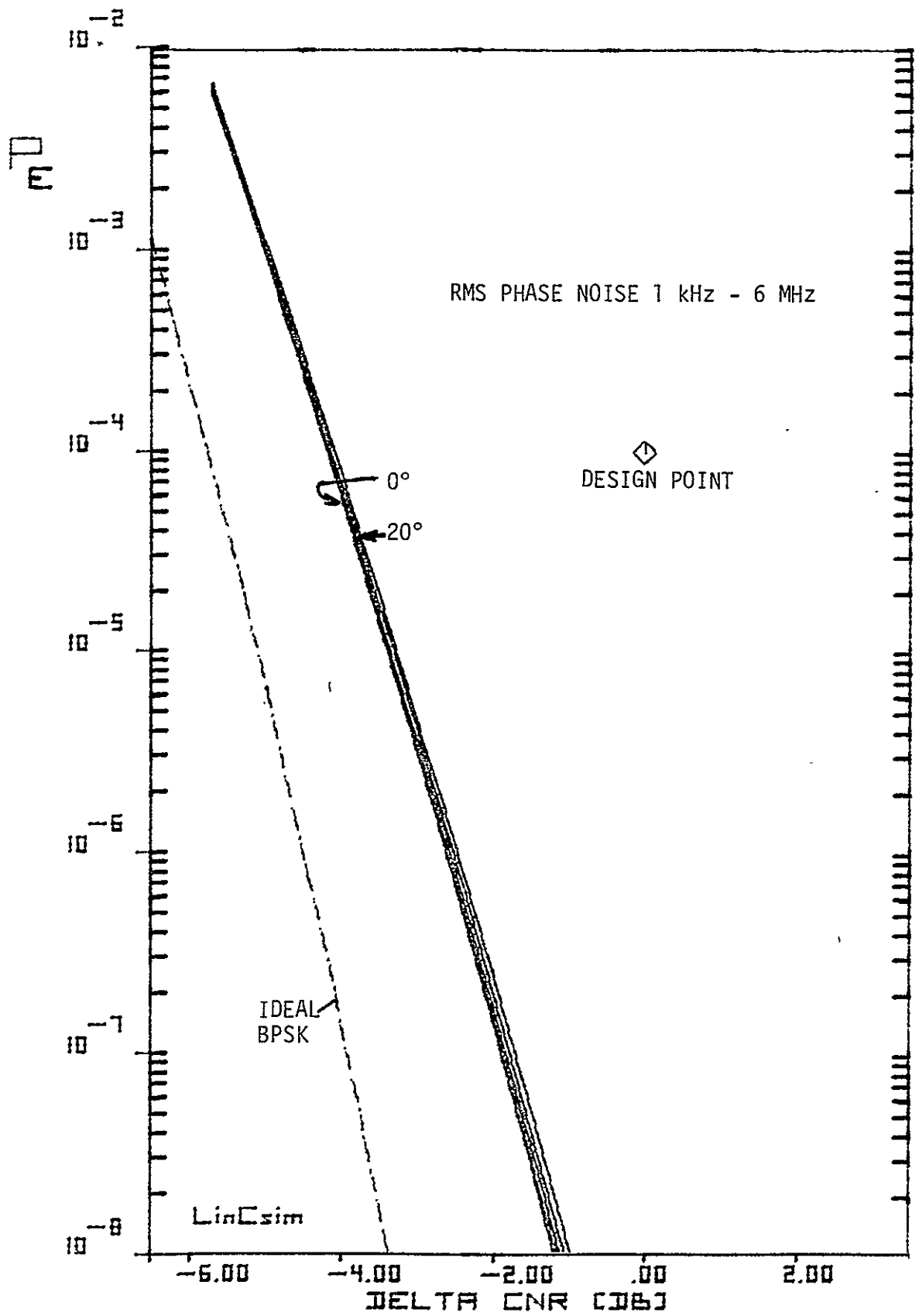
Figure 3-20. BER Plot for Medium Frequency Phase Noise.
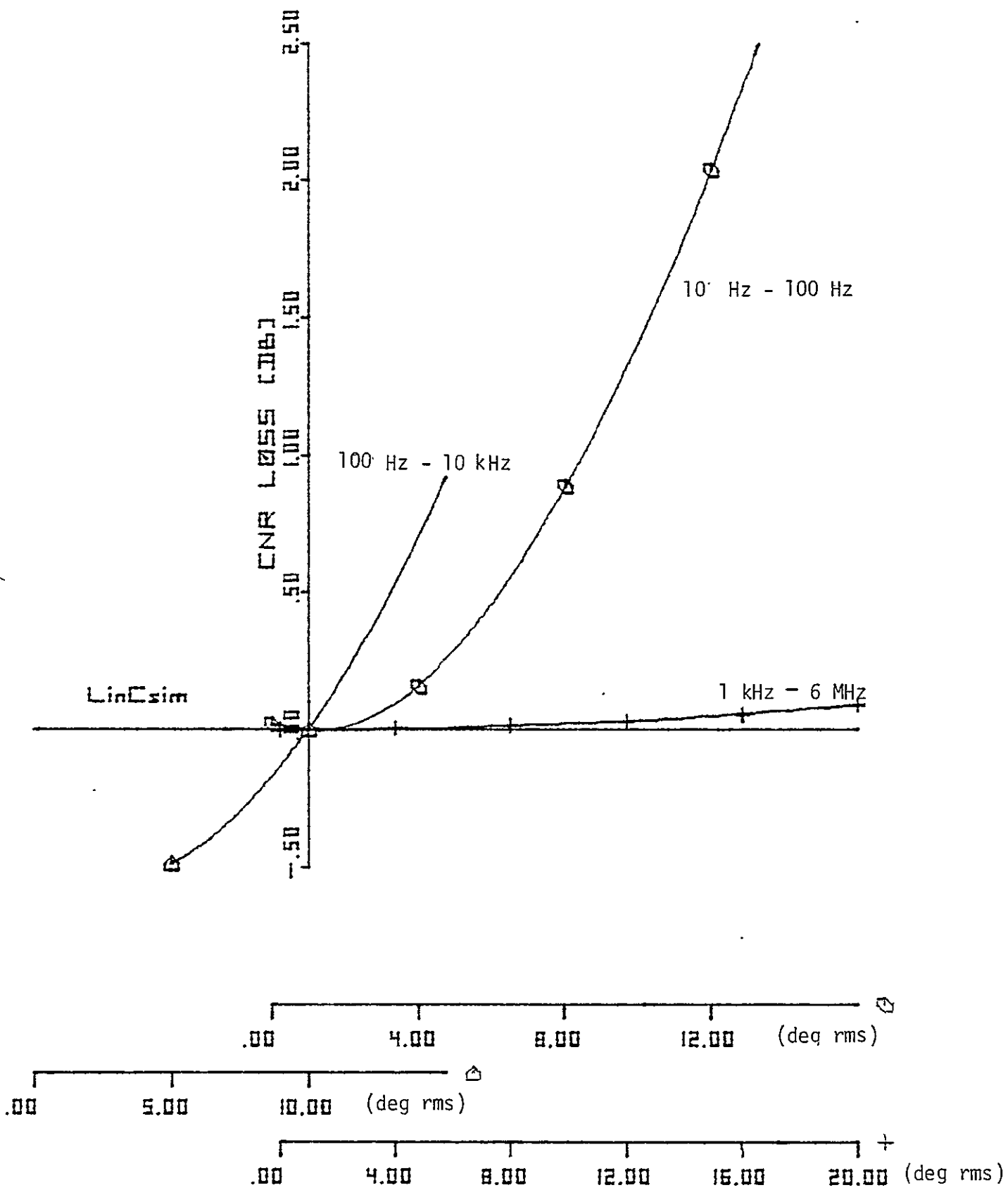
Figure 3.21.BER Plot for High Frequency Noise.

Figure 3.22. Sensitivity Curves for Phase Noise.

REFERENCE

[1] Tracking and Data Relay Satellite System (TDRSS) Users'
     Guide, Revision 3, STDN No. 101.2, Goddard Space Flight
     Center, Greenbelt, MD, January, 1978.

4.0 ATTACHED SPACELAB PAYLOAD BIT JITTER PERFORMANCE

4.1 Introduction

In this section the problem of bit jitter on the attached spacelab payload link is studied and the effect on the bit error rate performance is predicted. The analysis also includes the effect of data asymmetry. The results show that the limiting level of acceptable clock jitter at the output of the attached spacelab payload is determined by the sensitivity of the Viterbi decoder to imperfect pulses at the ground station receiver. In Section 4.2 we introduce the mathematical model we have adopted for our analysis. We also present in this section the model we have selected for clock jitter, bit jitter and data asymmetry. Based on laboratory measurements, we have determined the shape of the possible data sequences out of the attached spacelab into the Ku-band Space Shuttle equipment. These various pulse shapes are also presented in Section 4.2. In Section 4.3 we derive an expression for the bit error rate at the spacelab Ku-band transmitter interface due to imperfect timing. We then show that for the available SNR the effect of an acceptable level of clock jitter at the ground receiver has a negligible impact on the overall link performance even for a biased sampling time of $\pm 12.5\%$ in the Shuttle repeater. (This figure for the maximum bias was given to LinCom by JSC personnel. Note, however, that this does not agree with the description in [3]. According to this source the worst-case sampling point is 5 nsec from the transition. At the highest data rate of 50 Mbits/sec this is equivalent to 25% of the bit-

time. Hence the maximum bias would also be 25%.) The coded link

bit jitter performance is analyzed in Section 4.4. We show in

this section how a completely soft Viterbi decoder significantly

ameliorates the effect of imperfect pulses at the output of the

Ku-band transmitter. Finally, in Section 4.5 we summarize the

results and present some conclusions on the effect of clock and

bit jitter on the overall system performance.

4.2 System Model, Clock Jitter and Data Asymmetry

The mathematical system model we have adopted for our analysis

is as shown in Figure 4.1. Notice that although this is a simplified

model of the overall system it allows us to accurately represent

the various sources of link performance degradation. It is assumed

first that the data flow from the attached spacelab payload to the

Ku-band Shuttle transmitter is at baseband. The shape of the pulses

carrying the data has been determined from laboratory measurement (4.2)

and for the purpose of our analysis they will be assumed to be as

shown for a typical case in Figure 4.3a Other typical pulse sequences

are shown in Figure 4.3b. The clock information entering into the

Ku-band transmitter is assumed to be emanating from an imperfect oscillator.

The phase detector output $\varepsilon(t)$ of the clock regenerator circuit will

then be a random process whose statistics depend on the oscillator

phase noise characteristic. If we now sample this process $\varepsilon(t)$ at

times t* and t*+$\overline{T}$ where $\overline{T}$ is the inverse of the symbol rate, then we

obtain two random variables $\varepsilon(t*)$ and $\varepsilon(t*+\overline{T})$. Pictorially we have
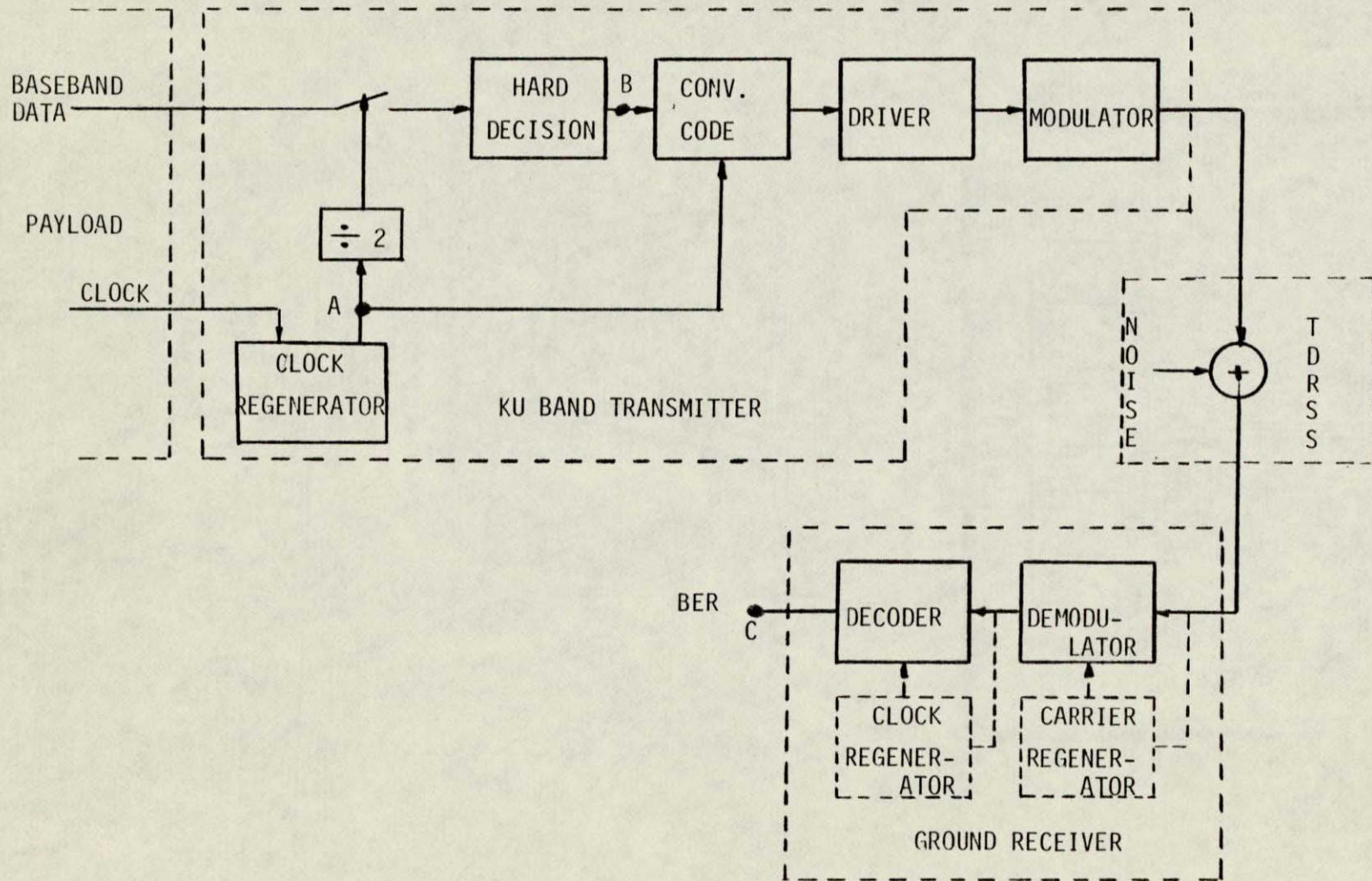
the following situation:
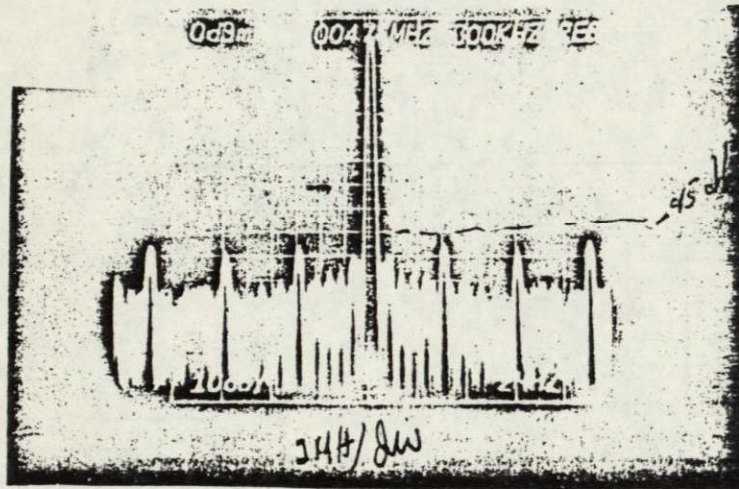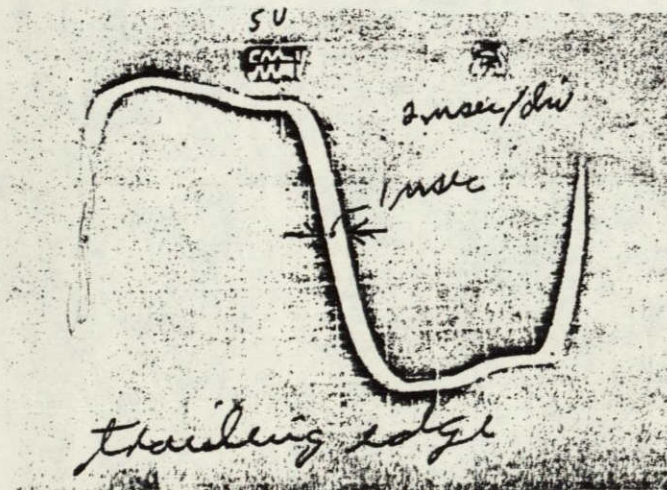
LinCom

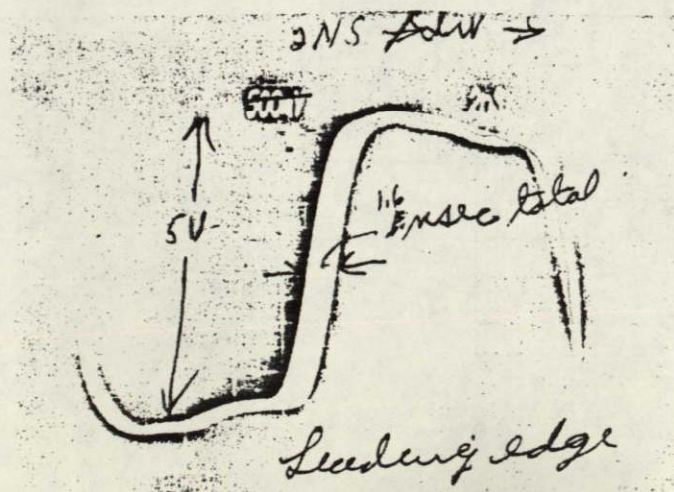Figure 4.1.   MATHEMATICAL SYSTEM BLOCK DIAGRAM

78 0193

Figure 4.2. HRM Clock Analysis.

(a)   Spectrum characteristic

(b)   Pulse shape characteristic.   Trailing edge.

(c)   Pulse Characteristic.   Leading edge

78 0539

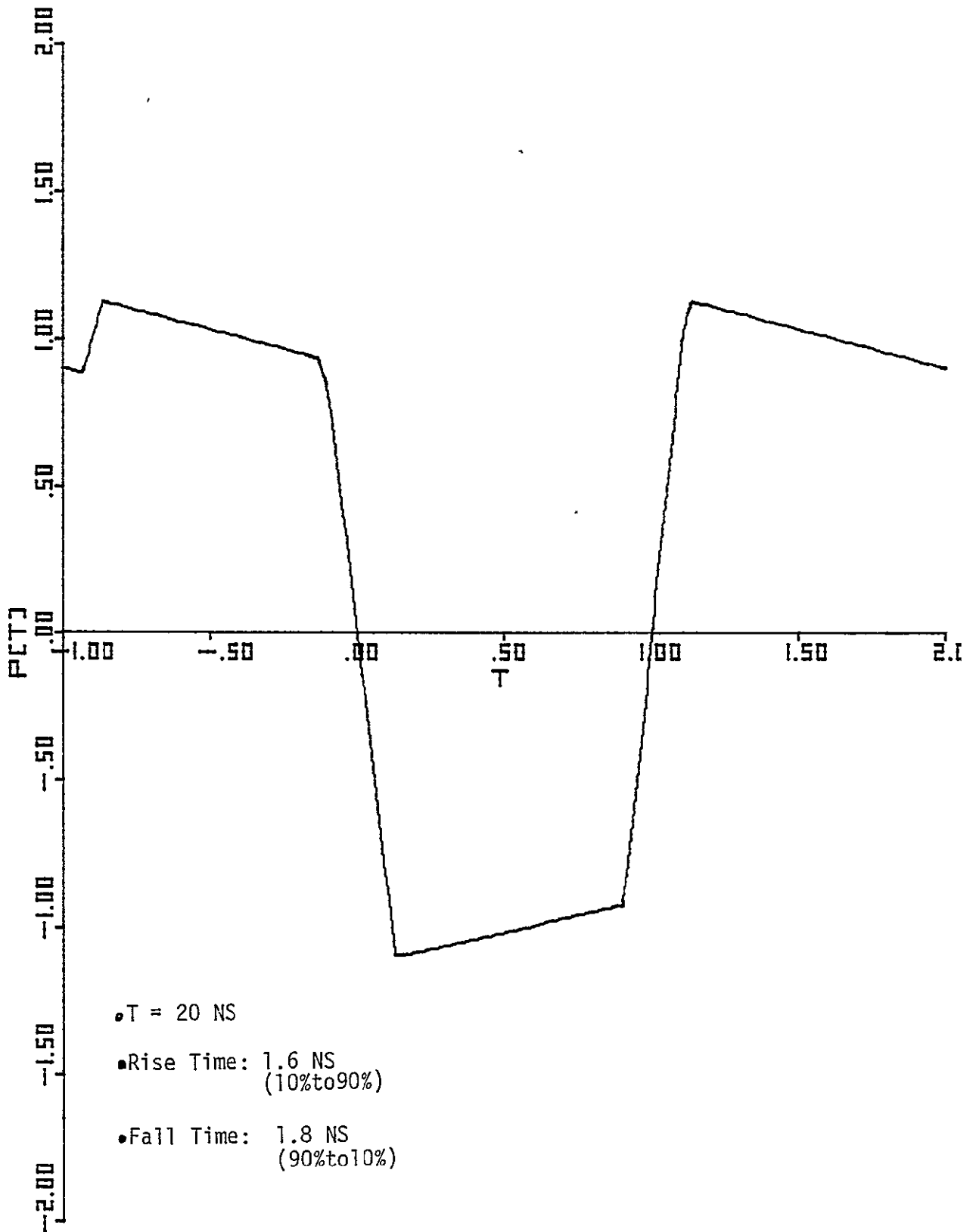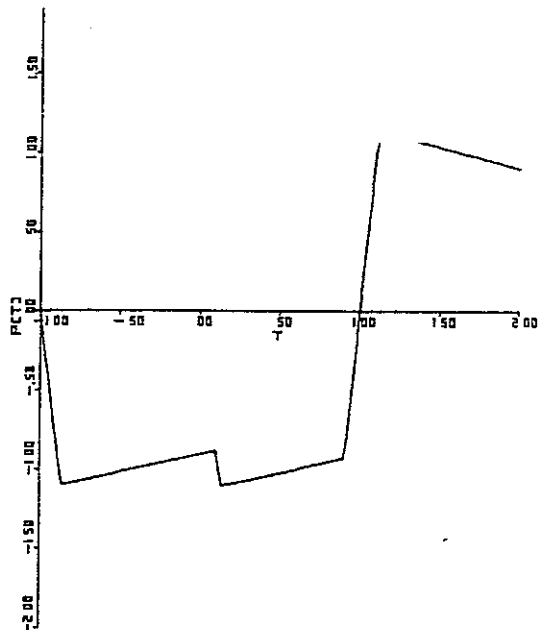Figure 4.3a. | NORMALIZED PULSE SHAPE CHARACTERISTIC |

∘T = 20 NS

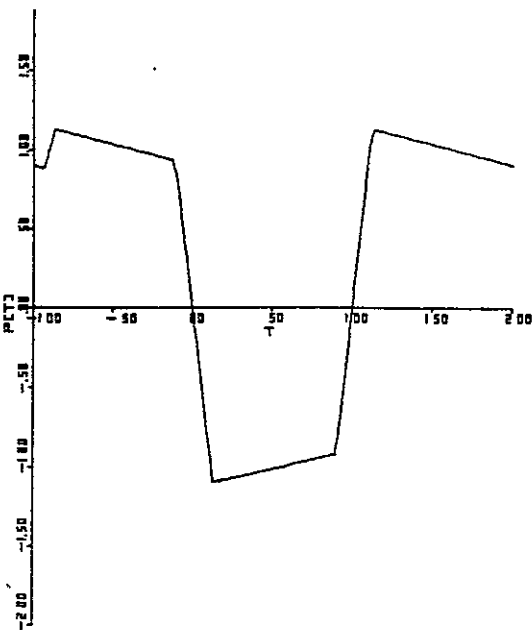∎Rise Time: 1.6 NS
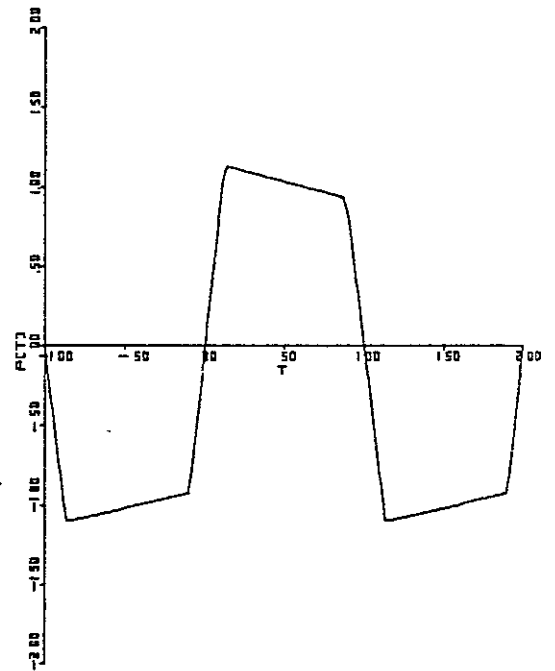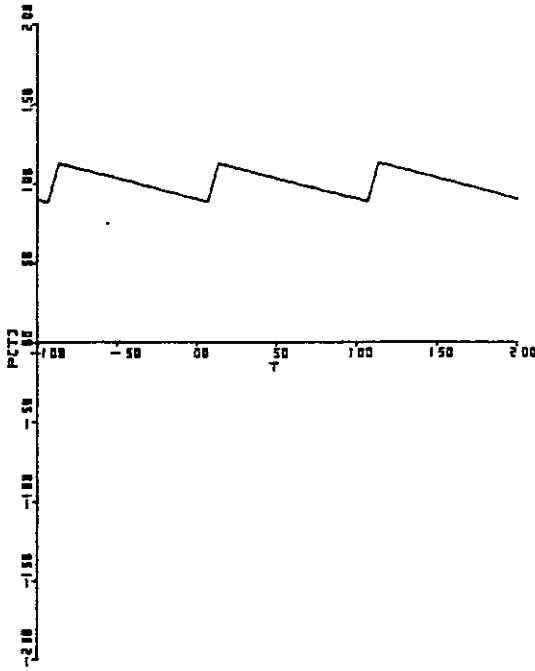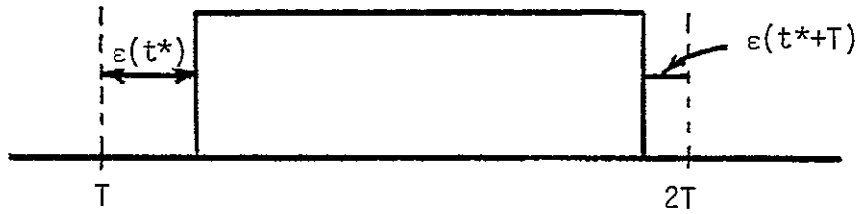(10%to90%)

∎Fall Time: 1.8 NS
(90%to10%)

Figure 4.3b. | TYPICAL INPUT PULSE SHAPES |

We shall assume that $\varepsilon(t*)$ and $\varepsilon(t*+\overline{T})$ are jointly Gaussian correlated random variables and such that

$$\sigma^2 = Var[\varepsilon(t*)] = Var[\varepsilon(t*+\overline{T})] \qquad (1)$$

We now define two new random varibles

$$T_{ck} = \frac{\varepsilon(t*)+\varepsilon(t*+\overline{T})+\overline{T}}{2\overline{T}} \qquad (2)$$

and

$$T_b = \frac{\varepsilon(t*+\overline{T})-\varepsilon(t*)+\overline{T}}{\overline{T}} \qquad (3)$$

It is clear then that the T_{ck} and T_b are two independent Gaussian random variables

$$T_{ck} \sim \mathcal{N}(1/2,\sigma^2_{ck}) \qquad (4)$$

$$T_b \sim \mathcal{N}(1,\sigma^2_b) \qquad (5)$$

we   refer in what follows to

$$\sigma_{ck} = \sqrt{\frac{\sigma^2}{2\overline{T}^2}} \, [1+\gamma] \qquad (6)$$

as clock jitter and

$$\sigma_b = \sqrt{\frac{2\sigma^2}{\overline{T}^2}} \, (1-\gamma) \qquad (7)$$

as bit jitter and where γ is the correlation coefficient between $\varepsilon(t)$ and $\varepsilon(t*+\overline{T})$. Notice that sampling instant of the imperfect pulse entering to the Ku-band transmitter from the attached spacelab payload will be governed by the random variable T_{ck}.

The output of the convolutional encoder is fed into a driver which we assume introduces data asymmetry. The model for data asymmetry we have adopted for our analysis is described in .[1] and is such that a positive going transition occurs early and a negative going transition occurs late relative to the nominal transition time instants. Data asymmetry is then defined as the difference in length between the shortest and longest pulses in the sequence divided by their sum. For our model we get then

$$ \eta = \frac{\overline{T}(1+2\delta)-\overline{T}(1-2\delta)}{\overline{T}(1+2\delta)+\overline{T}(1-2\delta)} = 2\delta \tag{8} $$

where δ represents the fractional (relative to the nominal symbol duration $\overline{T}$) increase in positive pulse length due to a single adjacent negative pulse.

4.3 BER at the Spacelab Ku-Band Transmitter Interface

For this part of the analysis we can concentrate on the mathematical model of Figure 4.4. The input NRZ pulses into the Ku-band transmitter are sampled at random instants of time governed by the random variable t_s where $t_s = \mathcal{N}(\overline{T}, \overline{T}^2\sigma_{ck}^2)$. Since the clock signal is synchronous with the NRZ data, for the purpose of our analysis we can assume that, the NRZ pulses are of perfect duration T. The probability of error at A conditioned on a sampling instant t_s and an input sequence S is
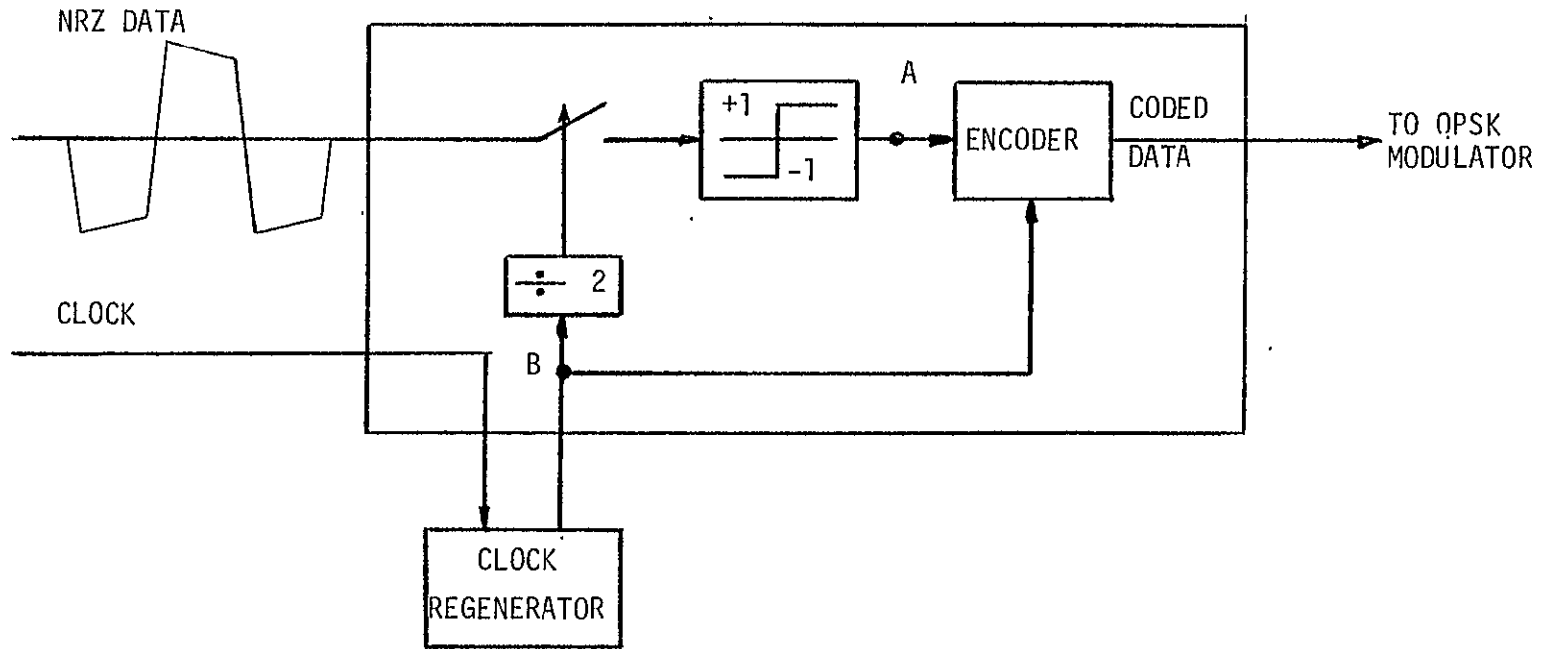
Figure 4.4.   BASEBAND SPACELAB/SHUTTLE INTERFACE

78 0191

$$P_e(t,S) \;=\; \tfrac{1}{2}\,\text{erfc}\left\{\frac{p(t_s/T,S)}{\sqrt{2}\,\sigma_n}\right\} \qquad (9)$$

where σ_n^2 is the power of the noise entering into the Ku-band Shuttle transmitter from the attached spacelab payload $p(t,S)$ is the pulse shape input function which at any given instant of time is a function of at most three consecutive data bits. The relationship between $p(t_s,S)$ and $P(t,S)$ as given in Figure 4.3 is

$$P(\alpha,S) \;=\; \frac{p(\alpha=t/T,S)}{A} \qquad (10)$$

We can obtain the unconditional bit error probability by averaging (9) over all possible sequences S of length three and the random variable t_s, we then have

$$P_e \;=\; \frac{1}{8}\sum_S \frac{1}{2}\int_{-\infty}^{\infty} \text{erfc}\left\{\frac{p(t_s/T,S)}{\sqrt{2}\,\sigma_n}\right\} f(t_s)\,dt_s$$

$$\;=\; \frac{1}{8}\sum_S \frac{1}{2}\int_{-\infty}^{\infty} \text{erfc}\left\{\rho\,\frac{P(T'_{ck},S)}{\sqrt{2}}\right\} f(T'_{ck})\,dT'_{ck} \qquad (11)$$

where ρ^2 is the signal to noise ratio at the interface and given by

$$\rho^2 \;=\; \frac{A^2}{\sigma_n^2} \qquad (12)$$

and $T'_{ck} = \mathcal{R}(1/2,\sigma_{ck}^2/4)$.

When the sampling instant is biased by some T_{bias}, then T'_{ck} has to be replaced in (11) by $T'_{ck}+T_{bias}$, where T_{bias} is also normalized to be between 0 and 1. The relationship in (11) has been programmed and the result of this computation is shown in Figure 4.5.

$$LinCom$$

$E_b/N_0 > 20$ dB

BIT ERROR RATE

±12.5% BIAS

0% BIAS

CLOCK REGENERATOR OUTPUT JITTER (%)

78 2138
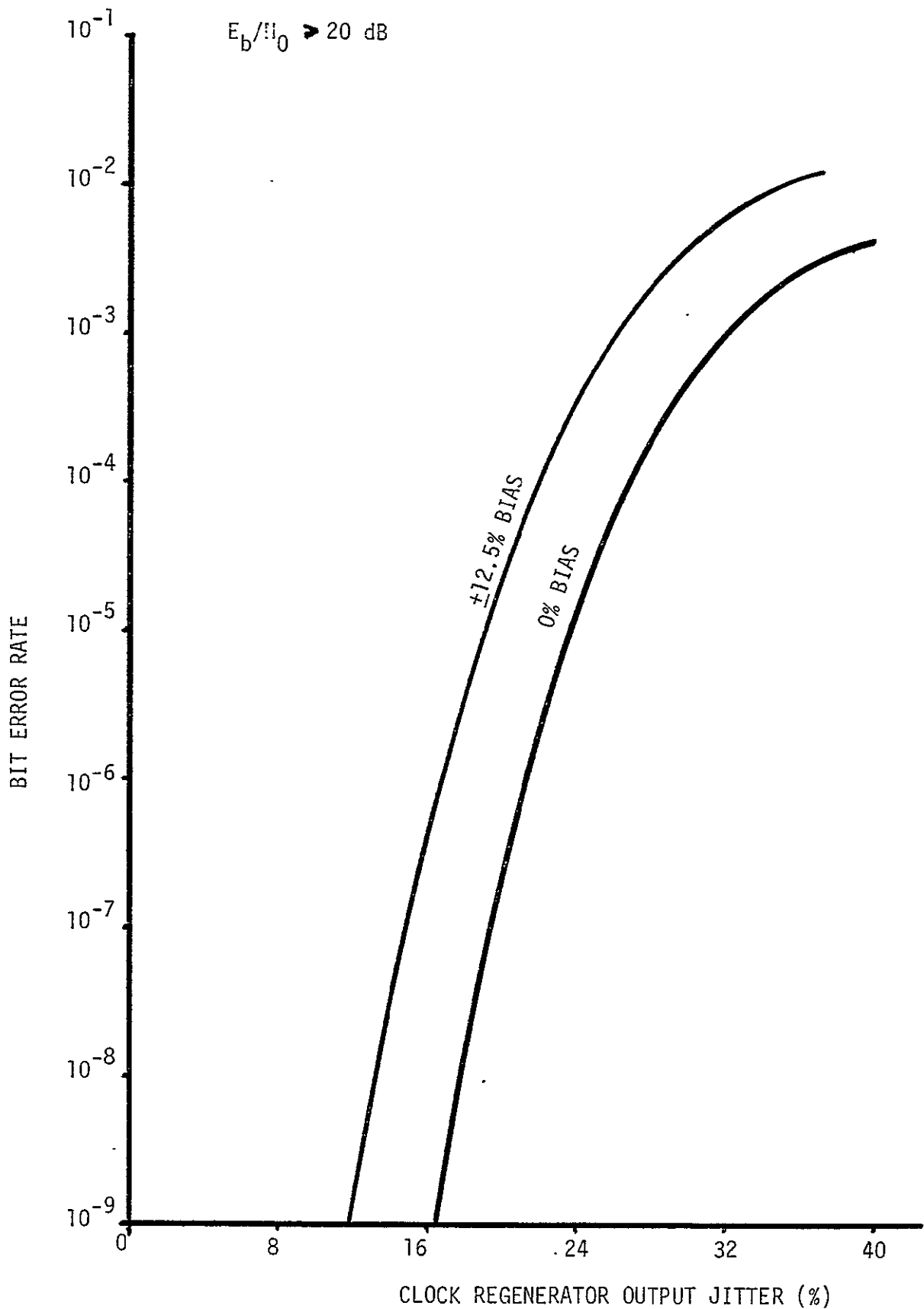
4.4 Coded Link Bit Jitter Performance

We are interested now in the bit jitter performance between points C and D of Figure 41. We shall assume here without any significant loss of accuracy in the final answer that the receiver is implemented as an ideal integrate and dump detector followed by a completely soft Viterbi decoder. We shall also assume that the timing at the receiver is perfect.

Lets assume now that a codeword $\underline{c} = (c_1, c_2, \ldots, c_N)$ where $c_i = \pm 1$ is transmitted out of the Space Shuttle Ku-band transmitter. We model the channel as an ideal AWGN channel, we then have that the decoder input signal

$$\underline{r} = \underline{x}(\underline{c}) + \underline{n} \tag{13}$$

where

$$\underline{r} = (r_1, r_2, \ldots, r_N) \tag{14}$$

$$\underline{x}(\underline{c}) = (x_1(\underline{c}), x_2(\underline{c}), \ldots, x_N(\underline{c})) \tag{15}$$

$$\underline{n} = (n_1, n_2, \ldots, n_N) \tag{16}$$

lets define now for simplicity of notation

$$t_{ij} = \varepsilon[(j-1)\overline{T}] \tag{17}$$

$$t_{fj} = \varepsilon[j\overline{T}] + \overline{T} \tag{18}$$

then it is possible to show after some algebraic manipulation that

$$x_j(\underline{c}) = \frac{\sqrt{\varepsilon_j}}{\overline{T}} \{c_{j-1}(t_{ij}+c_{j-1}^-\delta\overline{T})u(t_{ij}+c_{j-1}\delta\overline{T}) + c_j[(j-1)\overline{T}+t_{fj}+c_j\delta\overline{T}]$$

$$\cdot u(\overline{T}-t_{fj}-c_j\delta T) + c_j j\overline{T}[1-u(\overline{T}-t_{fj}-(j\delta\overline{T})]$$

$$- c_j[(j-1)\overline{T}+t_{ij}+c_{j-1}\delta\overline{T}]u(t_{ij}+c_{j-1}\delta\overline{T}) - c_j(j-1)\overline{T}$$

$$\cdot [1-u(t_{ij}+c_{j-1}\delta\overline{T})] + c_{j+1}(\overline{T}-t_{fj}-c_j\delta\overline{T})u(\overline{T}-t_{fj}-c_j\delta\overline{T})\} \tag{19}$$

If we now define as we did before

$$T_{ck}^{(j)} = (t_{ij}+t_{fj})/2\overline{T} \tag{20}$$

and

$$T_{b}^{(j)} = (t_{fi}-t_{ij})/\overline{T} \tag{21}$$

then from (17),(18),(20) & (21) it is possible to argue that $T_{ck}^{(k)}$ is a slow varying random variable and such that

$$T_{ck}^{(j)} = T_{ck}^{(\ell)} = \tau_{ck} \tag{22}$$

and that $T_{b}^{(j)}$ is a fast varying random variable such that

$$E\{T_b^j T_b^\ell\} = E\{T_b^j\}E\{T_b^\ell\} \quad \text{for } \ell \neq j \tag{23}$$

We then set

$$\tau_{bj} = T_{b}^{(j)} \tag{24}$$

This allows us to rewrite (19) as follows

$$x_j(\underline{c}) = \sqrt{\varepsilon_s}\,(c_{j-1}-c_j)(\tau_{ck}-\tau_{bj}+c_{j-1}\delta)u(\tau_{ck}-\tau_{bj}+c_{j-1}\delta)$$

$$+ c_j(\tau_{ck}+\tau_{bj}+c_j\delta)u(1-\tau_{ck}-\tau_{bj}-c_j\delta) + c_j[1-u(1-\tau_{ck}-\tau_{bj}-c_j\delta)]$$

$$+ c_{j+1}(1-\tau_{ck}-\tau_{bj}-c_j\delta)u(1-\tau_{ck}-\tau_{bj}-c_j\delta)$$

$$= x_j(c_{j-1},c_j,c_{j+1},\tau_{ck},\tau_{bj}) \tag{25}$$

In what follows and in order to avoid any boundary condition problems we let

$$c_0 = c_{N+1} = 1 \tag{26}$$

Lets assume now the decoder picks the codeword $\hat{\underline{c}}$ of the dimension N and $\underline{c}$ is the correct one, then the probability of an error even is

$$P_d(\tau_{ck},\underline{\tau}_b) = \frac{1}{2}\,\text{erfc}\left(\frac{\|\hat{\underline{x}}(\underline{c})-\underline{x}(\underline{c})\|}{2\sqrt{N_0}}\right) \tag{27}$$

where d is the Hamming distance between $\underline{c}$ and $\hat{\underline{c}}$,

$$\underline{\tau}_b = (\tau_{b1},\tau_{b2},\ldots,\tau_{bN}) \tag{28}$$

and $\|\underline{x}(\underline{c})-\underline{x}(\underline{c})\|$ is the Euclidean norm given by

$$\|\underline{x}(\underline{c})-\underline{x}(\underline{c})\|^2 = \sum_{j=1}^{N}[x_j(c_{j-1},c_j,c_{j+1},\tau_{ck},\tau_{bj})-x_j(c_{j-1},c_j,c_{j+1},\tau_{ck},\tau_{bj})]^2 \tag{29}$$

We now let the correct code word be the all 1's code word, then

$$x_j(c_{j-1},c_j,c_{j+1},\tau_{ck},\tau_{bj}) = \sqrt{\varepsilon_s} \tag{30}$$

so that (24) reduces to

$$\|\underline{x}(\underline{1})-\underline{x}(\underline{c})\|^2 = \varepsilon_s \sum_{j=1}^{N} [1-x_j'(\hat{c}_{j-1},c_j,\hat{c}_{j+1},\tau_{ck},\tau_{bj})]^2$$

(31)

We can now rewrite (27) as

$$P_d(\tau_{ck},\underline{\tau}_b) = \frac{1}{2}\,\text{erfc}\left\{\rho_s\frac{1}{2}\sqrt{\sum_{j=1}^{N}[1-x_j'(c_{j-1},c_j,c_{j+1},\tau_{ck},\tau_{bj})]^2}\right\}$$

(32)

In order to obtain the unconditional probability of an error event
we need to average (32) over τ_{ck} and $\underline{\tau}_b$ as

$$P_d = E_{\tau_{ck}}\{E_{\underline{\tau}_b}\{P_d(\tau_{ck},\underline{\tau}_b)|\tau_{ck}\}\}$$

(33)

The conditional expectation in (33) is in general very hard to find
whenever N is larger than three. We notice on the other hand that
the expression inside the square root in (32) is a sum of independent
random variables and for the K=7 rate 1/2 code we are interested in
N is always larger or equal to 18. This allows us to use a central
limit argument to write

$$E_{\underline{\tau}_b}\{P_d(\tau_{ck},\underline{\tau}_b)|\tau_{ck}\} = \int_{-\infty}^{\infty} \frac{e^{-[y-\mu(\tau_{ck})]^2/2\sigma^2(\tau_{ck})}}{\sqrt{2\pi\sigma^2(\tau_{ck})}}\,f(y)dy$$

(34)

where

$$\mu(\tau_{ck}) = \sum_{j=1}^{N} E_{\tau_{bj}}\{[1-x_j'(c_{j-1},c_j,c_{j+1},\tau_{ck},\tau_{bj}]^2\}$$

(35)

$$\sigma^2(\tau_{ck}) = \sum_{j=1}^{N} E_{\tau_{bj}} \{[1-x_j^!(c_{j-1},c_j,c_{j+1},\tau_{ck},\tau_{bj})]^4\}$$

$$- \sum_{j=1}^{N} E_{\tau_{bj}}^2 \{[1-x_j^!(c_{j-1},c_j,c_{j+1},\tau_{ck},\tau_{bj})]^2\} \qquad (36)$$

$$f(y) = \frac{1}{2} \text{erfc} \left\{ \frac{\rho_s}{2} \sqrt{y} \right\} \qquad (37)$$

The bit error can be found from the probability of an error event as given in (33) and the transfer function bound [2]. This approach is very tedious and usually computationally impractical. We can then get a very good approximation to the bit error probability by computing first the probability of an error event for all those paths which are at distance d_{free}*[2] from the correct path. Lets assume there are n such paths, we then find ρ_s^* such that

$$\frac{1}{n} \sum_{i=1}^{n} P_{d_{fi}} = \frac{1}{2} \text{erfc}\{\sqrt{d_f} \; \rho_s^*\} \qquad (38)$$

or in terms of an equivalent bit energy to noise spectral density ratio

$$\rho_b^* = \frac{\sqrt{2} \, \text{erfc}^{-1} \left\{ \frac{2}{n} \sum_{i=1}^{n} P_{d_{fi}} \right\}}{\sqrt{d_f}} \qquad (39)$$

We then set the bit error probability to be the one that corresponds to the decoding of a jitter and data asymmetry free signal transmitted over a channel with an $\mathcal{E}_b/N_0 = \rho_b^*$. This approach has been programmed and the result of this computations are shown in Figures 4.6, 4.7, and 4.8. The clock and bit jitter parameters in these curves are defined with respect to the Shuttle Ku-band transmitter clock regenerator phase detector output and the cycle duration time $\overline{T}$ of the clock signal out of the attached spacelab payload.

*In what follows we let $d_{free}=d_f$.
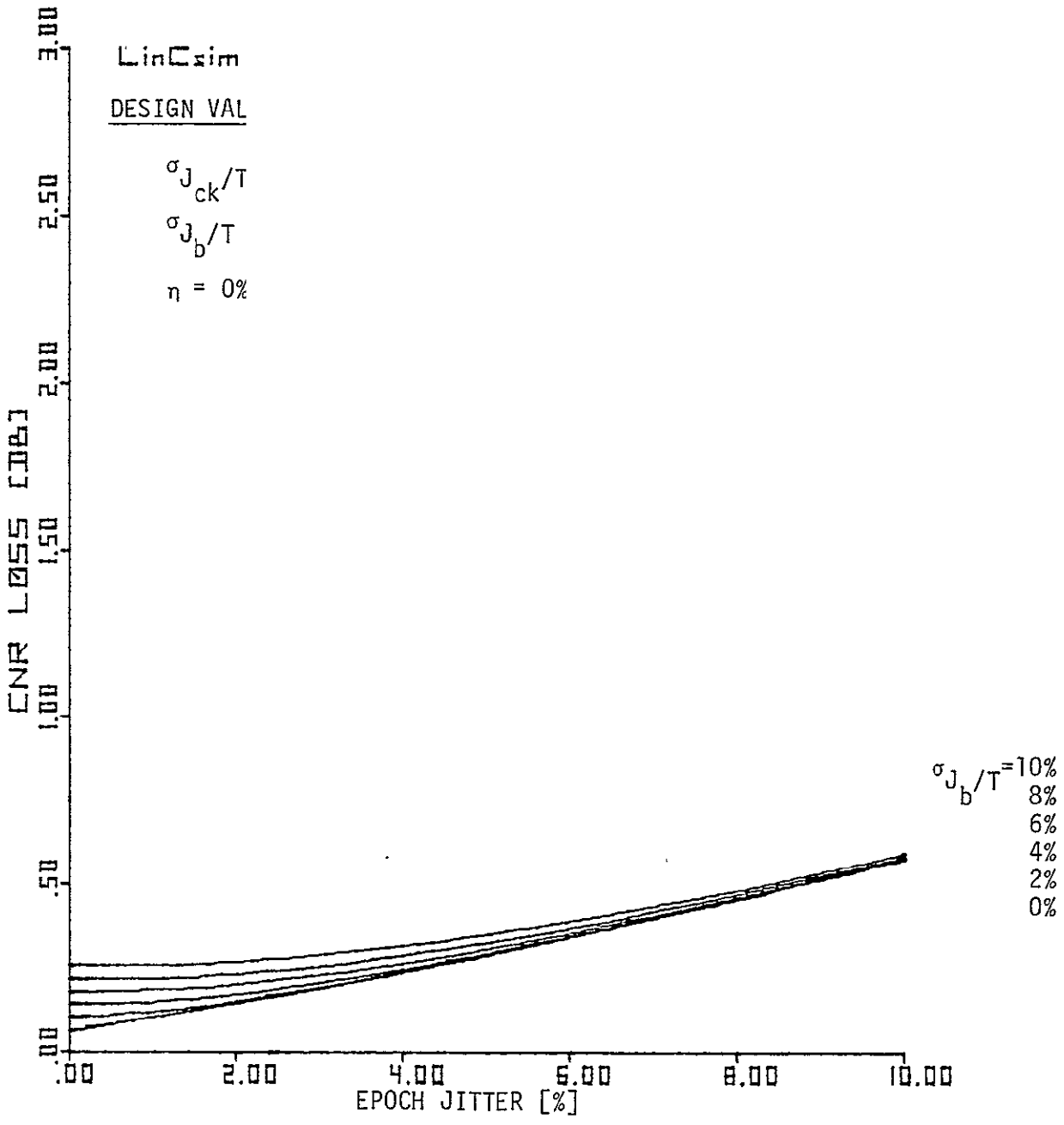
CODED LINK.   CNR LOSS VS CLOCK JITTER FOR FIXED BIT JITTER,
DATA ASYMMETRY: η = 0% AND BER = 10^{-5}.

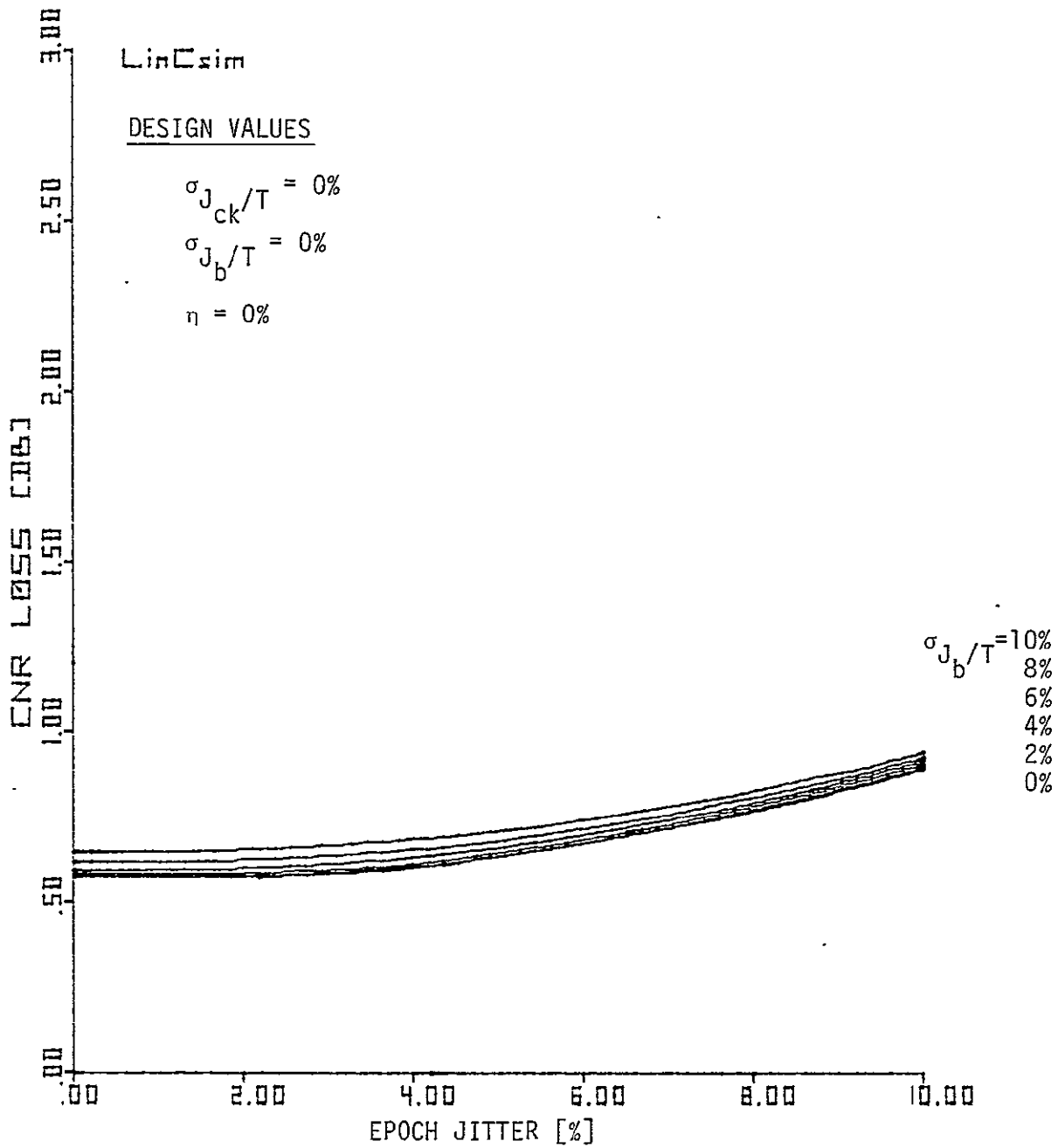Figure 4.6.   Sensitivity Curve for Clock Jitter.

78 0266
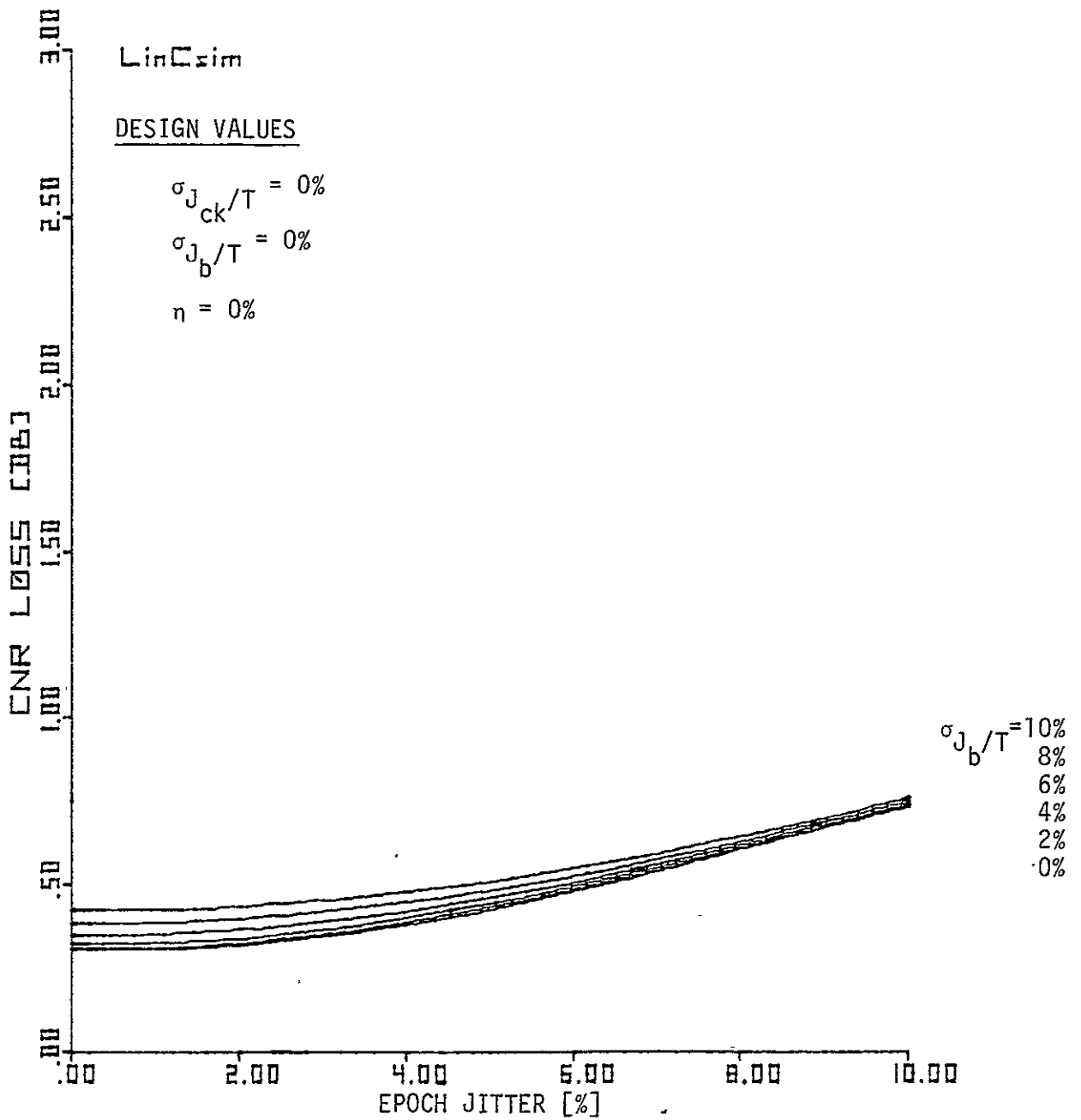
CODED LINK CNR. LOSS VS CLOCK JITTER FOR FIXED BIT JITTER, DATA ASYMMETRY: $\eta = 5\%$ AND BER $= 10^{-5}$.

Figure 4.7. Sensitivity Curve for Clock Jitter.

CODED LINK. CNR LOSS VS CLOCK JITTER FOR FIXED BIT JITTER, DATA ASYMMETRY: $\sigma = 10\%$ AND BER $= 10^{-5}$.

Figure 4.8. Sensitivity Curve for Clock Jitter.

4.5 Summary and Conclusions

We have analyzed here the bit and clock jitter performance of the attached spacelab payload. We have first shown that the effect of an imperfect sampler at the spacelab Ku-band transmitter interface does not impose any measurable loss in performance for rms clock jitter levels less than 10%. On the other hand we have also shown that for a jitter-free link the required E_b/N_0 to maintain a BER of 10^{-5} with 10% of data asymmetry is 4.72 dB. This implies a ΔCNR degradation of 0.52 dB with respect to the 4.2 dB of E_b/N_0 required for an ideal coded channel to achieve a BER of 10^{-5}. In Table 1 we show the additional ΔCNR (with resepct to 4.72 dB) required due to the presence of jitter*.

Table 1.

ΔCNR	Bit Jitter
dB	%
0.1	5.70
0.2	8.01
0.3	9.75
0.4	11.10
0.5	12.48

It is very important to observe that for the levels of the jitter shown in Table 1, the BER at the SL-Ku-band transmitter interface, remains below 10^{-9}. Its effect on the BER at the above mentioned system interface can therefore be ignored.

Appendix

In this appendix we attempt to predict the SL HDM return

*The numbers shown in Table 1 correspond to worst case jitter for both epoch and duration jitter.

link performance based on the clock pulse shape characteristic and the spectrum characteristic shown in Figure 4.2, which has been provided to us by Sid Novosad. From Figure 4.2 we have estimated* that the C/N_0 present at the HRM clock output is approximately

$$C/N_0 = 104 \text{ dB-Hz}.$$

For this level of C/N_0 we have concluded* that the jitter observed in Figure 4.2b originates mostly from thermal effects. If we now assume that the Shuttle clock regenerator loop bandwidth is 10 KHz, it is possible to predict that the jitter at the scrubber output, including non-thermal effects, will be less than 2%. For this jitter level, the overall performance degradation taking into account the 0.52 ΔCNR due to 10% of data asymmetry will be

$$\Delta CNR = \underbrace{0.52 \text{ dB}}_{\substack{\text{Data} \\ \text{Asymmetry}}} + \underbrace{0.01 \text{ dB}}_{\text{Jitter}}$$

$$= 0.53 \text{ dB}$$

---

*Within the accuracy that this picture allows.

REFERENCES

[1] Simon, M. K., Tu, K., and Batson, B., IEEE Transactions on Communications, Vol. COM-26, No. 11, November, 1977.

[2] Viterbi, A. J., and Omura, J. K., Digital Communications and Coding, McGraw-Hill, New York, 1979 (to appear).

[3] Cager, R. H., LaFlame, D. T., and Parode, L. C., "Orbiter Ku-Band Integrated Radar and Communications Subsystem," IEEE Transactions on Communications, Vol. COM-26, No. 11, November, 1977.

5.0 SHUTTLE PAYLOAD BENT-PIPE MODE SUBCARRIER RECOVERY

5.1 Introduction

In the bent-pipe mode of Shuttle payload data transmission, the data are not detected at the Shuttle payload interrogator. They go through the Shuttle repeater, where they are low-pass filtered, hard-limited, and modulated onto the high-power channel of the subcarrier UQPSK modulator. In this section the performance of the Costas loop recovering the subcarrier in the ground station receiver is studied for this case and compared with an implementation which does not include a hard limiter in the bent-pipe link. The results show a slight degradation of the loop performance when a hard-limiter is used. This advantage is offset, however, by the tight power control afforded by the limiter which reduces the effects of interference on the other two data channels.

5.2 Problem Statement

In the detached-payload bent-pipe mode the binary data stream is received by the Shuttle payload interrogator immersed in additive white Gaussian noise. This signal goes through the Shuttle repeater, where it is low-pass filtered and hard-limited. Then it is modulated onto the high-power phase of the 8.5 MHz subcarrier. This is shown in Figure 5.1.

For the analysis of the 8.5 MHz subcarrier recovery, we may assume that the carrier has been recovered perfectly. This leads to the link model of Figure 5.2.

We wish to characterize the phase-recovery performance of the Costas loop. The theory is developed for an arbitrary signal format at the Shuttle repeater output. The results are then applied to
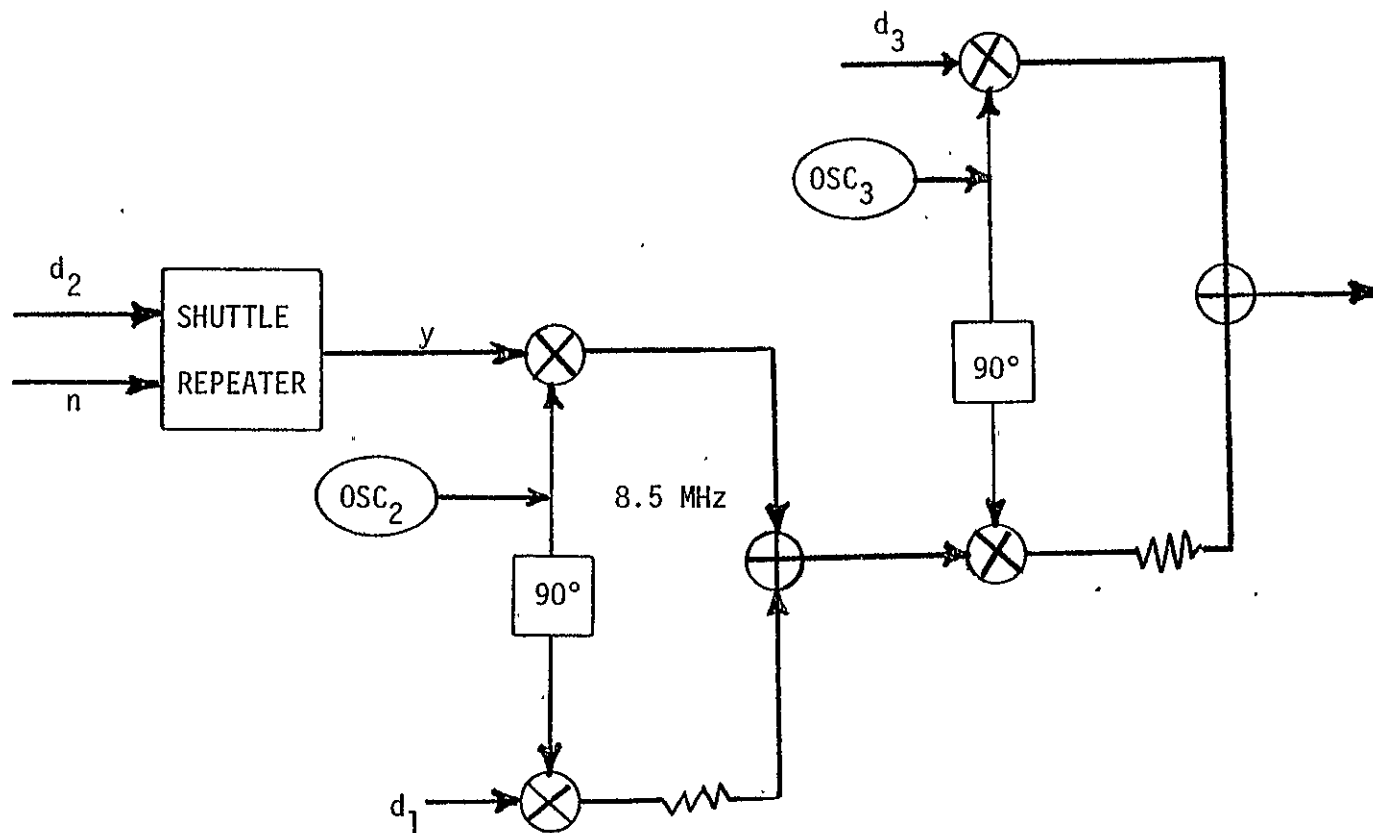
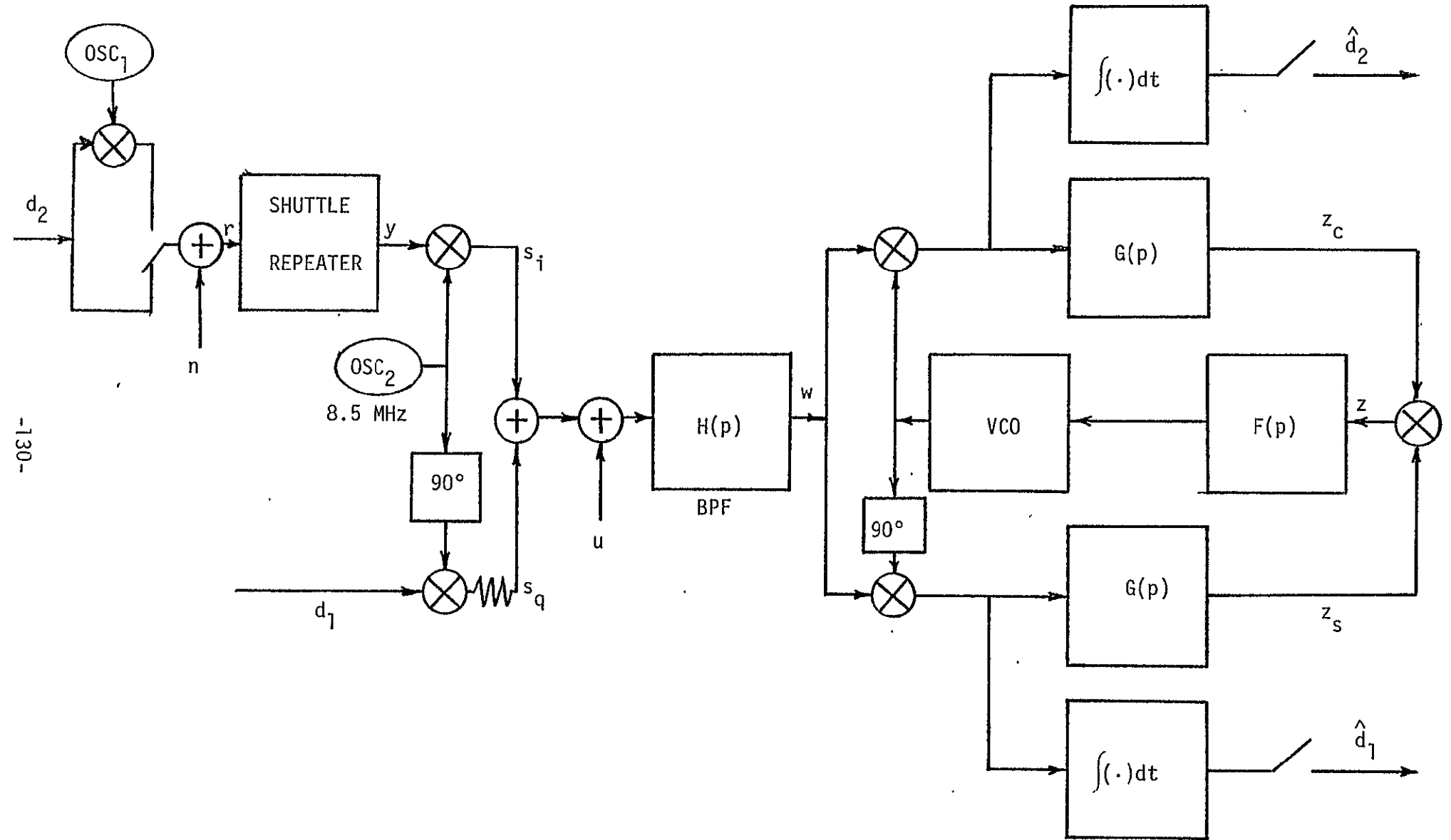Figure 5.1. Three-Channel Transmitter in Bent-Pipe Mode

Figure 5.2. Simplified Link Diagram.

-130-

the case of baseband data with two different implementations for the Shuttle repeater: a hard-limiter preceded by a wide low-pass filter which does not affect the data signal and an arbitrary low-pass filter without hard-limiter.

5.3 Costas Loop Model (Following Reference 1)

The input signal to the Costas loop is the random process (see Fig. 5.2),

$$w(t) = H(p)(s_i(t) + s_q(t) + u(t)) \qquad (1)$$

where $H(p)$ is the ground station receiver filter, $s_i(t)$ is the high-power bent-pipe signal, $s_q(t)$ is the low-power digital voice signal and $u(t)$ is the downlink thermal noise. This signal can be written

$$w(t) = \sqrt{2}a(t) \sin \Phi(t) + \sqrt{2}b(t) \cos \Phi(t) \qquad (2)$$

for some random processes $a(t)$ and $b(t)$, where $\Phi(t) \equiv \omega_2 t + \theta(t)$ and $\theta(t) = \Omega_0 t + \theta_0$ is the input phase to be estimated. Let $\hat{\Phi}(t)$ be the loop estimate of $\Phi(t)$. In the upper arm of the loop, $w(t)$ is multiplied by $\sqrt{2K_1} \cos \hat{\Phi}(t)$, in the lower arm by $\sqrt{2K_1} \sin \hat{\Phi}(t)$. The multiplier units have gain $\sqrt{K_m}$ and are insensitive to the double-frequency terms. Each output passes through a filter corresponding to $G(p)$, yielding the upper-arm signal $z_c(t)$ and the lower-arm signal $z_s(t)$.

$$z_c(t) = \sqrt{K_1 K_m} \; G(p)[a(t) \sin \varphi(t) + b(t)\cos \varphi(t)] \qquad (3)$$

$$z_s(t) = \sqrt{K_1 K_m} \; G(p)[a(t)\cos \varphi(t) - b(t)\sin \varphi(t)] \qquad (4)$$

where $\varphi(t) \equiv \Phi(t) - \hat{\Phi}(t)$ is the loop phase error. The two signals are multiplied together, with unit gain, to produce the dynamic error signal

$$z(t) = z_c(t) z_s(t) \qquad (5)$$

We assume that $\varphi(t)$ varies much more slowly than $a(t)$ and $b(t)$ and that the $G(p)$ filter is sufficiently wide so that

$$z(t) = \{[(G(p)a(t))^2 - (G(p)b(t))^2] \frac{1}{2} \sin(2\varphi(t))$$

$$-[G(p)a(t)G(p)b(t)]\cos(2\varphi(t))\} K_1 K_m \qquad (6)$$

The instantaneous frequency of the VCO output is related to $z(t)$ by

$$\frac{d\hat{\Phi}(t)}{dt} = K_v F(p) z(t) + \omega_2 \qquad (7)$$

where K_v is a gain constant. Hence, the stochastic integro-differential equation of operation of the loop is

$$2 \frac{d\varphi(t)}{dt} = 2\Omega_0 - 2K_v F(p) z(t) \qquad (8)$$

Conditioned on φ, $z(t)$ can be partitioned into a nonrandom part and a zero-mean random process:

$$z(t) = S(\varphi) + n_z(t, \varphi) \qquad (9)$$

where

$$S(\varphi) = E\{z(t)|\varphi\} \qquad (10)$$

$$n_z(t, \varphi) = z(t) - S(\varphi) \qquad (11)$$

This allows us to rewrite (8) as

$$2 \frac{d\varphi(t)}{dt} = 2\Omega_0 - 2K_v F(p) S[\varphi(t)] - 2K_v F(p) n_z(t, \varphi) \qquad (12)$$

This equation describes a non-Markovian diffusion process. However, under suitable conditions (in particular, if the process $n_z(t,\phi)$ is considerably faster than the process $\phi(t)$) it can be approximated by a Markov process and Fokker-Planck techniques can be applied to characterize the stationary distribution of the modulo-2π-reduced phase noise process as well as the cycle-slipping rate. For this analysis the S-curve $S(\phi)$ and the statistics of the equivalent noise process $n_z(t,\phi)$ are needed.

5.4 Costas Loop S-Curve

We will assume that $\Omega_0=0$ and that the baseband equivalent of the $H(p)$ filter is symmetric. We first obtain the input signal to the Costas loop.

We will denote a narrowband signal $a(t)$ with center frequency ω_2 by

$$a(t) = \sqrt{2}\ \text{Re}[a'(t)e^{j\omega_2 t}] \tag{13}$$

where $a'(t)$ is the baseband equivalent to $a(t)$.

Defining the payload signal as

$$s_i(t) = \sqrt{2P_2}\ y(t)\ \sin(\omega_2 t) \tag{14}$$

where $y(t)$ is normalized such that $E\{y^2(t)\} = 1$, we find

$$s_i'(t) = -j\sqrt{P_2}\ y(t) \tag{15}$$

$$x_i'(t) \equiv H'(p)s_i'(t) \tag{16}$$

where $H'(p)$ is the baseband equivalent of $H(p)$.

For the low-power signal we have

$$s_q(t) = -\sqrt{2P_1}\, d_1(t)\cos(\omega_2 t) \qquad (17)$$

$$s_q'(t) = -\sqrt{P_1}\, d_1(t) \qquad (18)$$

$$x_q'(t) \equiv H'(p)s_q'(t) \qquad (19)$$

Now we consider the noise $u(t)$, a narrowband Gaussian process with center frequency ω_2.

$$u(t) = \sqrt{2}u_1(t)\cos(\omega_2 t) - \sqrt{2}u_2(t)\sin(\omega_2 t) \qquad (20)$$

The spectral density of $u(t)$ is

$$S_u(f) = S_{u'}(f-f_2) + S_{u'}(-f-f_2) \qquad (21)$$

for some real function $S_{u'}(f)$, where $f_2 = \omega_2/(2\pi)$. We define

$$R_{u_i}(\tau) = E[u_i(t)u_i(t+\tau)] , \quad i = 1,2 \qquad (22)$$

$$R_{u_{ik}}(\tau) = E[u_i(t)u_k(t+\tau)] , \quad i \neq k \qquad (23)$$

Letting $R_{u'}$ be the inverse Fourier transform of $S_{u'}$ we have

$$R_{u_1} = R_{u_2} = \text{Re } R_{u'} \qquad (24)$$

$$R_{u_{12}} = -R_{u_{21}} = \text{Im } R_{u'} \qquad (25)$$

We assume that $S_{u'}(f)$ is symmetric about 0, so that

$$R_{u_1} = R_{u_2} = R_{u'} \qquad (26)$$

$$R_{u_{12}} = -R_{u_{21}} = 0 \qquad (27)$$

Since we assumed that the H'(p) filter is symmetric then $H'(p)u_1(t)$ and $H'(p)u_2(t)$ are real-valued processes.

Now we go into the Costas loop.

In the upper arm the input signal is multiplied by $\sqrt{2K_1K_m}\cos(\omega_2 t-\varphi)$ and the double-frequency terms are dropped. The same result is obtained if the baseband equivalent of the signal is multiplied by $\sqrt{K_1K_m}\ e^{j\varphi}$ and the real part is taken. In the lower arm of the loop, the input signal is multiplied by $\sqrt{2K_1K_m}\sin(\omega_2 t-\varphi)$ and the double-frequency terms are dropped. This is the same as multiplying the baseband equivalent by $j\sqrt{K_1K_m}\ e^{j\varphi}$ and taking the real part, or multiplying it by $-\sqrt{K_1K_m}\ e^{j\varphi}$ and taking the imaginary part.

Since z_c and z_s are each linearly related to s_i, s_q, and u, we may write

$$z_c(t) \;=\; z_c(t;s_i) + z_c(t;s_q) + z_c(t;u) \qquad (28)$$

$$z_s(t) \;=\; z_s(t;s_i) + z_s(t;s_q) + z_s(t;u) \qquad (29)$$

where, for example, $z_c(t;s_i)$ is $z_c(t)$ when the loop input is just $H(p)s_i(t)$.

For $s_i(t)$ we have

$$z_c(t;s_i) \;=\; G(p)\left[\sqrt{K_1K_m}\ \operatorname{Re}(x_i'(t)e^{j\varphi})\right]$$

$$=\; \sqrt{K_1K_m}\ G(p)[\hat{x}_i'(t)\cos\varphi - \tilde{x}_i'(t)\sin\varphi] \qquad (30)$$

since s_i, s_q, and u are assumed independent and have zero mean.

$$E[z_c(t;s_i)z_s(t;s_i)|\varphi]$$

$$= \frac{K_1 K_m}{2} \, P_2[G(p)G*(p)H'(p)H'*(p)R_y(0)]\sin(2\varphi) \qquad (40)$$

$$E[z_c(t;s_q)z_s(t;s_q)|\varphi]$$

$$= -\frac{K_1 K_m}{2} \, P_1[G(p)G*(p)H'(p)H'*(p)R_{d_1}(0)]\sin(2\varphi) \qquad (41)$$

$$E[z_c(t;u)z_s(t;u)|\varphi] = 0 \qquad (42)$$

since $u_1(t)$, $u_2(t)$ were assumed independent. Therefore,

$$S(\varphi) = \frac{K_1 K_m}{2} \, G(p)G*(p)H'(p)H'*(p)(P_2 R_y(0) - P_1 R_{d_1}(0))\sin(2\varphi)$$
$$(43)$$

5.5 Spectral Density of the Equivalent Noise

Now we will obtain the spectral density of z for fixed φ. We introduce the notation

$$\overline{a}(t) = G(p)H'(p)a(t) \qquad (44)$$

for any signal a(t). Then

$$R_{\overline{a}}(\tau) = G(p)G*(p)H'(p)H'*(p)R_a(\tau) \qquad (45)$$

Let $C = K_1 K_m$. Then we have

$$z_c(t;s_i) = \sqrt{C}\sqrt{P_2} \, \sin(\varphi)\overline{y}(t) \qquad (46)$$

$$z_c(t;s_q) = -\sqrt{C}\sqrt{P_1} \, \cos(\varphi)\overline{d}_1(t) \qquad (47)$$

$$z_c(t;u) = \sqrt{C} \, (\cos(\varphi)\overline{u}_1(t) - \sin(\varphi)\overline{u}_2(t)) \qquad (48)$$

$$z_s(t;s_i) = \sqrt{C}\sqrt{P_2} \, \cos(\varphi)\overline{y}(t) \qquad (49)$$

where $\hat{x}_i^!(t)$ and $\check{x}_i^!(t)$ are real. Since

$$x_i^!(t) = -j\sqrt{P_2}H'(p)y(t) \tag{31}$$

then

$$z_c(t;s_i) = \sqrt{K_1 K_m}\sqrt{P_2}[G(p)H'(p)y(t)]\sin\varphi \tag{32}$$

Similarly,

$$z_s(t;s_i) = -G(p)\left[\sqrt{K_1 K_m}\ \text{Im}(x_i^!(t)e^{j\varphi})\right]$$

$$= -\sqrt{K_1 K_m}\ G(p)[\hat{x}_i^!(t)\sin\varphi + \check{x}_i^!(t)\cos\varphi]$$

$$= \sqrt{K_1 K_m}\sqrt{P_2}[G(p)H'(p)y(t)]\cos\varphi \tag{33}$$

For the $s_q(t)$ effect, we use the fact that

$$x_q(t) = -\sqrt{P_1}\ H'(p)d_1(t) \tag{34}$$

We find that

$$z_c(t;s_q) = -\sqrt{K_1 K_m}\sqrt{P_1}[G(p)H'(p)d_1(t)]\cos\varphi \tag{35}$$

$$z_s(t;s_q) = \sqrt{K_1 K_m}\sqrt{P_1}[G(p)H'(p)d_1(t)]\sin\varphi \tag{36}$$

For the $u(t)$ effect we have

$$z_c(t;u) = \sqrt{K_1 K_m}G(p)\{\text{Re}[H'(p)u_1(t)+jH'(p)u_2(t))e^{j\varphi}]\}$$

$$= \sqrt{K_1 K_m}G(p)[H'(p)u_1(t)\cos\varphi - H'(p)u_2(t)\sin\varphi] \tag{37}$$

$$z_s(t;u) = -\sqrt{K_1 K_m}G(p)[H'(p)u_1(t)\sin\varphi + H'(p)u_2(t)\cos\varphi] \tag{38}$$

Now we can calculate $S(\varphi)$.

$$S(\varphi) \equiv E[z(t)|\varphi] = E[z_c(t)z_s(t)|\varphi]$$

$$= E[z_c(t;s_i)z_s(t;s_i)|\varphi] + E[z_c(t;s_q)z_s(t;s_q)|\varphi]$$

$$+E[z_c(t;u)z_s(t;u)|\varphi] \tag{39}$$

$$z_s(t;s_q) = \sqrt{C\sqrt{P_1}} \sin(\phi)\bar{d}_1(t) \tag{50}$$

$$z_s(t;u) = \sqrt{C}(-\sin(\phi)\bar{u}_1(t)-\cos(\phi)\bar{u}_2(t)) \tag{51}$$

$$S(\phi) \equiv E[z(t)|\phi] = \frac{C}{2}(P_2 \cdot R_{\bar{y}}(0)-P_1 R_{\bar{d}_1}(0))\sin(2\phi) \tag{52}$$

Hence,

$$\frac{1}{C}(z(t) - E[z(t)|\phi])$$

$$= \frac{1}{2}P_2(\bar{y}^2(t)-R_{\bar{y}}(0))\sin(2\phi)- \frac{1}{2}P_1(\bar{d}_1^2(t)-R_{\bar{d}_1}(0))\sin(2\phi)$$

$$- \sqrt{P_1 P_2}\cos(2\phi)\bar{y}(t)\bar{d}_1(t)$$

$$+ \sqrt{P_2}\cos(2\phi)\bar{y}(t)\bar{u}_1(t) - \sqrt{P_2}\sin(2\phi)\bar{y}(t)\bar{u}_2(t)$$

$$+ \sqrt{P_1}\sin(2\phi)\bar{d}_1(t)\bar{u}_1(t) + \sqrt{P_1}\cos(2\phi)\bar{d}_1(t)\bar{u}_2(t)$$

$$- \frac{1}{2}\sin(2\phi)\bar{u}_1^2(t) - \cos(2\phi)\bar{u}_1(t)\bar{u}_2(t)$$

so

$$+ \frac{1}{2}\sin(2\phi)\bar{u}_2^2(t) \tag{53}$$

$$\frac{1}{C^2}R_z(\tau|\phi) \equiv E\{(z(t)-E[z(t)|\phi])(z(t+\tau)-E[z(t+\tau)|\phi])\}$$

$$= \frac{1}{4}P_2^2(E[\bar{y}^2(t)\bar{y}^2(t+\tau)]- R_{\bar{y}}^2(0))\sin^2(2\phi)+\frac{1}{4}P_1^2(E[\bar{d}_1^2(t)\bar{d}_1^2(t+\tau)]$$

$$-R_{\bar{d}_1}^2(0))\sin^2(2\phi))$$

$$+ P_1 P_2 \cos^2(2\phi)R_{\bar{y}}(\tau)R_{\bar{d}_1}(\tau) + P_2 \cos^2(2\phi)R_{\bar{y}}(\tau)R_{\bar{u}_1}(\tau)$$

$$+ P_2 \sin^2(2\phi)R_{\bar{y}}(\tau)R_{\bar{u}_1}(\tau) + P_1 \sin^2(2\phi)R_{\bar{d}_1}(\tau)R_{\bar{u}_1}(\tau)$$

$$+ P_1 \cos^2(2\phi)R_{\bar{d}_1}(\tau)R_{\bar{u}_1}(\tau) + \frac{1}{4}\sin^2(2\phi)E[\bar{u}_1^2(t)\bar{u}_1^2(t+\tau)]$$

$$- \frac{1}{4}\sin^2(2\phi)R_{\bar{u}_1}^2(0) + \cos^2(2\phi)R_{\bar{u}_1}^2(\tau)$$

$$- \frac{1}{4}\sin^2(2\phi)R_{\bar{u}_1}^2(0) + \frac{1}{4}\sin^2(2\phi)E[\bar{u}_1^2(t)\bar{u}_1^2(t+\tau)] \tag{54}$$

This equation for $R_z(\tau|\phi)$ holds because we have assumed $\bar{u}_1(t)$ and $\bar{u}_2(\tau)$ are independent and identically distributed for any choice of t and τ. We must obtain $E[\bar{u}_1^2(t)\bar{u}_1^2(t+\tau)]$. To do this, we define the two random

variables $X = \bar{u}_1(t)$, $Y = \bar{u}_1(t+\tau)$. Then $E[\bar{u}_1^2(t)\bar{u}_1^2(t+\tau)] = E[X^2Y^2]$.

Let $\sigma = \sigma_X = \sigma_Y$, $\rho = \dfrac{E(XY)}{\sigma^2}$. To calculate $E[X^2Y^2]$, we introduce the zero-mean Gaussian random variable

$$W \equiv Y - \rho X . \tag{55}$$

Since $E[XW] = E[X(Y-\rho X)] = 0 = E(X)E(W)$, then X and W are independent. We have

$$\sigma_W^2 \equiv E(W^2) = E[Y^2 - 2\rho XY + \rho^2 X^2] = \sigma^2(1-\rho^2) \tag{56}$$

Then

$$\begin{aligned}
E[X^2Y^2] &= E[X^2(W^2 + 2\rho XW + \rho^2 X^2)] \\[2mm]
&= \sigma^2\sigma_W^2 + \rho^2 E(X^4) \\[2mm]
&= \sigma^4(1-\rho^2) + \rho^2 3\sigma^4 \\[2mm]
&= \sigma^4(1+2\rho^2)
\end{aligned} \tag{57}$$

Thus,

$$\begin{aligned}
E[\bar{u}_1^2(t)\bar{u}_1^2(t+\tau)] &= \sigma^4(1+2\rho^2(\tau)) \\[2mm]
&= R_{\bar{u}_1}^2(0) + 2R_{\bar{u}_1}^2(\tau)
\end{aligned} \tag{58}$$

so

$$\begin{aligned}
\frac{1}{c^2} R_z(\tau|\psi) = \frac{1}{4} \quad & \sin^2(2\psi) \, [P_2^2 R_{\bar{y}2}(\tau) + P_1^2 R_{\bar{d}_1^2}(\tau)] \\[2mm]
& + P_1 P_2 \cos^2(2\psi) R_{\bar{y}}(\tau) R_{\bar{d}_1}(\tau) + P_2 R_{\bar{y}}(\tau) R_{\bar{u}_1}(\tau) \\[2mm]
& + P_1 R_{\bar{d}_1}(\tau) R_{\bar{u}_1}(\tau) + R_{\bar{u}_1}^2(\tau)
\end{aligned} \tag{59}$$

5.6 Nonlinear Costas Loop Theory

We are now in a position to investigate the Costas loop performance.

To keep the notation manageable we will develop the theory for a first-order loop only.

The equation of loop operation (12) can be rewritten for a first-order loop as

$$\frac{d\varphi(t)}{dt} = \Omega_0 - K_V S(\varphi) - K_V \sigma_n(\varphi) n_z(t) \tag{60}$$

where $n_z(t)$ is a unit-variance zero-mean random process. Approximating $n_z(t)$ by a delta-correlated Gaussian process the above equation can be rewritten as an Ito stochastic differential equation

$$d\varphi(t) = \left[\Omega_0 - K_V S(\varphi) + \frac{1}{2} K_V^2 \sigma_n(\varphi) \frac{d\sigma_n(\varphi)}{d\varphi} \right] dt$$

$$- K_V \sigma_n(\varphi) dW(t) \tag{61}$$

where $W(t)$ is a Brownian motion process. Introducing the notation

$$K_1(\varphi) = \Omega_0 - K_V S(\varphi) + \frac{1}{2} K_V^2 \sigma_n(\varphi) \frac{d\sigma_n(\varphi)}{d\varphi} \tag{62}$$
$$\text{(drift coefficient)}$$

$$K_2(\varphi) = - K_V \sigma_n(\varphi) \quad \text{(diffusion coefficient)} \tag{63}$$

the equation takes the form

$$d\varphi(t) = K_1(\varphi)dt + K_2(\varphi)dW(t) \tag{64}$$

and we may use the standard techniques to characterize the stationary behavior of φ. In particular, the p.d.f. of ϕ, the modulo 2π reduced phase error, is given by

$$p(\phi) = \frac{1}{K_2^2(\phi)} \exp[-U_0(\phi)] \cdot [C - 2J \int_{-\pi}^{\phi} \exp U_0(s)ds] \tag{65}$$

where

$$U_0(s) = -\int_{-\pi}^{s} \frac{2K_1(x)}{K_2^2(x)} \, dx \qquad \qquad (66)$$

C is a normalization constant and J is the average rate of cycle slips $N_+ - N_-$. In the absence of loop stress the density function is therefore

$$p(\phi) = \frac{C}{K_2^2(\phi)} \exp[-U_0(\phi)] \; . \qquad (67)$$

5.7 Hard-Limiting Shuttle Repeater

The hard-limiting repeater implementation is illustrated in Figure 5.3a. The low-pass filter before the hard-limiter is assumed to be wide enough to pass the signal undistorted.

Assume that signal + noise before the hard-limiter is

$$r(t) = \sqrt{P} \, d_2(t) + n(t) \qquad (68)$$

and $y(t)$ is signal + noise after the hard-limiter, i.e.,

$$y(t) = \text{sgn } r(t) \qquad (69)$$

From Reference 2 we obtain the correlation function of $y(t)$,

$$R_y(\tau) \equiv E[y(t)y(t+\tau)]$$

$$= E[\text{sgn}(r(t)r(t+\tau))]$$

$$= \text{erf}^2\left(\frac{\sqrt{P}}{\sqrt{2}\sigma_n}\right) R_{d_2}(\tau)$$

$$+ \frac{1}{\pi} \exp\left(\frac{-P}{\sigma_n^2}\right) \sum_{k=1}^{\infty} \left(\frac{R_n(\tau)}{\sigma_n^2}\right)^k \frac{1}{k!} \text{He}_{k-1}^2\left(\frac{\sqrt{P}}{\sigma_n}\right) [(1+R_{d_2}(\tau))$$

$$- (-1)^k (1-R_{d_2}(\tau))] \qquad (70)$$

where $\sigma_n^2 = R_n(0)$, He_k is the kth Hermite polynomial,
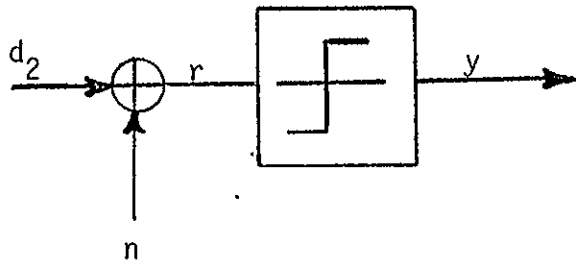
(a)   With Hard-Limiter
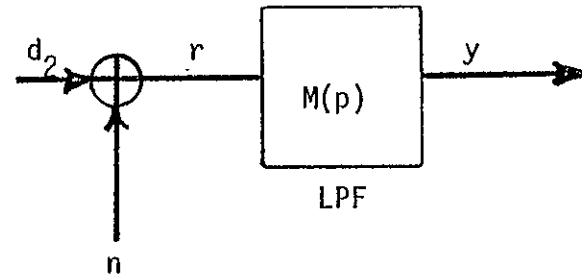
(b) Without Hard-Limiter

Figure 5.3. Two Shuttle Repeater Implementations Studied

'79 0073

$$\text{erf}(x) = \frac{2}{\sqrt{2\pi}}\int_0^{\sqrt{2}x} e^{-u^2/2}du = \frac{2}{\sqrt{\pi}}\int_0^x e^{-u^2}du \qquad (71)$$

$$R_{d_2}(\tau) = \begin{cases} 1-|\tau|/T_2, & |\tau| \le T_2 \\ 0; & |\tau| > T_2 \end{cases} \qquad \text{(NRZ)}$$

$$= \begin{cases} 1 - 3|\tau|/T_2, & |\tau| \le T_2/2 \\ |\tau|/T_2 - 1, & T_2/2 \le |\tau| \le T_2 \quad \text{(BIPHASE)} \\ 0, & |\tau| \ge T_2 \end{cases} \qquad (72)$$

where T_2 is the pulse duration of d_2. If $G(p)H'(p)$ is identity, then the equivalent noise correlation function is particularly simple. We have

$$R_z(\tau|\phi) = C^2[P_1 P_2 \cos^2(2\phi)R_y(\tau)R_{d_1}(\tau) + P_2 R_y(\tau)R_{u_1}(\tau)$$
$$+ P_1 R_{d_1}(\tau)R_{u_1}(\tau) + R_{u_1}^2(\tau)] \qquad (73)$$

The equivalent noise spectral density evaluated at zero frequency is then

$$S_z(0|\phi) = C^2[P_1 P_2 \cos^2(2\phi)\int_{-\infty}^\infty R_y(t)R_{d_1}(t)dt + P_2\int_{-\infty}^\infty R_y(t)R_{u_1}(t)dt$$
$$+ P_1\int_{-\infty}^\infty R_{d_1}(t)R_{u_1}(t)dt + \int_{-\infty}^\infty R_{u_1}^2(t)dt] \qquad (74)$$

where $C = K_1 K_m$, $R_y(t)$ is given in (70), and

$$R_{d_1}(\tau) = \begin{cases} 1 - \frac{3|\tau|}{T_1}, & |\tau| \le T_1/2 \\ \frac{|\tau|}{T_1} - 1, & T_1/2 \le |\tau| \le T_1 \\ 0, & |\tau| \ge T_1 \end{cases} \qquad (75)$$

since channel 1 always uses the biphase data format. We use the estimate that $S_z(f|\phi) = s_z(0|\phi)$ for small f.

5.8 Linear Shuttle Repeater

Now consider the case where the hard-limiter is not used and M(p) is general, illustrated in Figure 5.3b. Then before the LPF we have

$$r(t) = \sqrt{P}d_2(t) + n(t) \tag{76}$$

After it we have

$$y(t) = \frac{1}{\sqrt{R_b(0)+R_v(0)}} b(t) + \frac{1}{\sqrt{R_b(0)+R_v(0)}} v(t) \tag{77}$$

where

$$b(t) = \sqrt{P}M(p)d_2(t) \tag{78}$$

$$v(t) = M(p)n(t) \tag{79}$$

and we have scaled y(t) so that $E[y^2(t)] = 1$. We see that

$$R_b(\tau) = PM(p)M*(p)R_{d_2}(\tau) \tag{80}$$

$$R_v(\tau) = M(p)M*(p)R_n(\tau) \tag{81}$$

Then

$$R_y(\tau) = \frac{1}{R_b(0)+R_v(0)} (R_b(\tau)+R_v(\tau)). \tag{82}$$

$$R_{\bar{y}}(\tau) = \frac{1}{R_b(0)+R_b(0)} (R_{\bar{b}}(\tau) + R_{\bar{v}}(\tau)) . \tag{83}$$

For the statistics of $\bar{y}^2$ we find

$$\bar{y}^2(t) = \frac{1}{R_b(0)+R_v(0)} [\bar{b}^2(t) + 2\bar{b}(t)\bar{v}(t) + \bar{v}^2(t)] \tag{84}$$

$$R_{\bar{y}2}(\tau) = E[\bar{y}^2(t)\bar{y}^2(t+\tau)] - R_{\bar{y}}^2(0)$$

$$= \frac{1}{(R_b(0)+R_v(0))^2} \{E[\bar{b}^2(t)\bar{b}^2(t+\tau)] + 2R_{\bar{b}}(0)R_{\bar{v}}(0)$$

$$+ 4R_{\bar{b}}(\tau)R_{\bar{v}}(\tau) + E[\bar{v}^2(t)\bar{v}^2(t+\tau)] - (R_{\bar{b}}(0)+R_{\bar{v}}(0))^2\}$$

$$= \frac{1}{(R_b(0)+R_v(0))^2} \{E[\bar{b}^2(t)\bar{b}^2(t+\tau)] + 2R_{\bar{b}}(0)R_{\bar{v}}(0)$$

$$+ 4R_{\bar{b}}(\tau)R_{\bar{v}}(\tau) + R_{\bar{v}}^2(0) + 2R_{\bar{v}}^2(\tau) - (R_{\bar{b}}(0)+R_{\bar{v}}(0))^2\}$$

$$= \frac{1}{(R_b(0)+R_v(0))^2} \{E[\bar{b}^2(t)\bar{b}^2(t+\tau)] - R_{\bar{b}}^2(0) + 4R_{\bar{b}}(\tau)R_{\bar{v}}(\tau)$$

$$+ 2R_{\bar{v}}^2(\tau)\} \tag{85}$$

To obtain $E[\bar{b}^2(t)\bar{b}^2(t+\tau)] - R_{\bar{b}}^2(0)$, we note that

$$\bar{b}(t) = \sum_i c_i q(t-iT) \tag{86}$$

where $c_i = \sqrt{P}$ or $-\sqrt{P}$ each with probability $\frac{1}{2}$ and $q(t)$ is the response of the $G(p)H'(p)M(p)$ filter to a ·data pulse (NRZ or bi-phase) of duration $T \equiv T_2$ and absolute height 1.

$$\bar{b}^2(t) = \sum_i \sum_k c_i c_k q(t-iT)q(t-kT)$$

$$= P \sum_i q^2(t-iT) + \sum_i \sum_{k \neq i} c_i c_k q(t-iT)q(t-kT) \tag{87}$$

so

$$R_{\bar{b}2}(\tau) = E[\bar{b}^2(t)\bar{b}^2(t+\tau)] - R_{\bar{b}}^2(0)$$

$$= P^2 \left\langle \sum_i q^2(t-iT) \sum_\ell q^2(t+\tau-\ell T) \right\rangle$$

$$+ \left\langle E\left[\sum_i \sum_{k \neq i} c_i c_k \sum_\ell \sum_{n \neq \ell} c_\ell c_n q(t-iT)q(t-kT)q(t+\tau-\ell T)\right.\right.$$

$$\left.\left. \cdot q(t+\tau-nT)\right]\right\rangle - P^2\left(\left\langle \sum_i q^2(t-iT)\right\rangle\right)^2$$

$$= P^2 \left\langle \sum_i q^2(t-iT) \sum_\ell q^2(t+\tau-\ell T) \right\rangle - P^2 \left\langle \left\langle \sum_i q^2(t-iT) \right\rangle \right\rangle^2$$

$$+ 2P^2 \left\langle \sum_i \sum_{k \neq i} q(t-iT)q(t-kT)q(t+\tau-iT)q(t+\tau-kT) \right\rangle$$

$$= P^2 \left\langle \sum_i q^2(t-iT) \sum_\ell q^2(t+\tau-\ell T) \right\rangle - P^2 \left\langle \left\langle \sum_i q^2(t-iT) \right\rangle \right\rangle^2$$

$$+ 2P^2 \left\langle \left(\sum_i q(t-iT)q(t+\tau-iT) \right)^2 \right\rangle - 2P^2 \left\langle \sum_i q^2(t-iT)q^2(t+\tau-iT) \right\rangle \tag{88}$$

where $\langle \cdot \rangle$ denotes the average over any time interval of length T. A similar expression holds for $R_{\overline{d}_1^2}(\tau)$, with $q(t)$ replaced by the response

of the $G(p)H'(p)$ filter to a biphase pulse of duration T_1.

$$S_z(0|\phi) = C^2 \left\{ \frac{1}{4} \sin^2(2\phi) \left[\left(\frac{P_2}{R_b(0)+R_v(0)} \right)^2 \int_{-\infty}^\infty [R_{\overline{b}^2}(t) + 4R_{\overline{b}}(t)R_{\overline{v}}(t) + 2R_{\overline{v}}^2(t)]dt \right. \right.$$

$$\left. + P_1^2 \int_{-\infty}^\infty R_{\overline{d}_1^2}(t)dt \right]$$

$$+ \frac{P_1 P_2}{R_b(0)+R_v(0)} \cos^2(2\phi) \int_{-\infty}^\infty (R_{\overline{b}}(t)+R_{\overline{v}}(t))R_{\overline{d}_1}(t)dt$$

$$+ \frac{P_2}{R_b(0)+R_v(0)} \int_{-\infty}^\infty (R_{\overline{b}}(t)+R_{\overline{v}}(t))R_{\overline{u}_1}(t)dt$$

$$\left. + P_1 \int_{-\infty}^\infty R_{\overline{d}_1}(t)R_{\overline{u}_1}(t)dt + \int_{-\infty}^\infty R_{\overline{u}_1}^2(t)dt \right\} \tag{89}$$

where $R_b(t)$ and $R_v(t)$ are given in (80) and (81) and $C = K_1 K_m$. We use the estimate that $S_z(f|\phi) = S_z(0|\phi)$ for small f. To evaluate (89) we may use the fact that

$$\int_{-\infty}^{\infty} R_{\overline{w}}(t)R_{\overline{x}}(t)dt = \int_{-\infty}^{\infty} |G(f)H'(f)|^4 S_w(f)S_x(f)df \qquad (90)$$

where w and x are signals and S_w and S_x are the Fourier transforms of R_w and R_x, respectively.

5.9 S-Curve Amplitude Plots

Figures 5.4 through 5.9 are plots of the amplitude S_a of the S-curve.

$$S_a \equiv \frac{2}{K_1 K_m P_2} [S(\varphi)/\sin(2\varphi)]$$

$$= G(p)G^*(p)H'(p)H'^*(p) \left(R_y(0) - \frac{P_1}{P_2} R_{d_1}(0)\right) \qquad (91)$$

It is plotted as a function of Shuttle repeater input E_b/N_0, for channel 2 having NRZ or biphase pulses and rates of R_2 of 2000,192,16Kbps. The channel-1 data rate is 192 Kbps. Recall that the S-curve is independent of the ground station receiver noise. At the top of each figure are curves for the case where the repeater is a hard limiter and at the bottom are curves for the case of a lowpass-filter repeater. Each curve corresponds to a different bandwidth of the combined LPF $G(f)H'(f)$ in units of R_2.

Following are the assumptions made in obtaining the curves. The combined filter $G(f)H'(f)$ is a one-pole Butterworth filter. In the case of HL repeater, the spectrum of this repeater input noise is rectangular with a bandwidth of 1.5 R_2. In the case of LPF repeater, the input white noise and signal are both filtered by a four-pole Butterworth filter of bandwidth 1.5 R_2. In both cases, $P_1/P_2 = .25$.

Figure 5.4. S_a for R_2 = 2000 Kbps, Channel 2 NRZ.
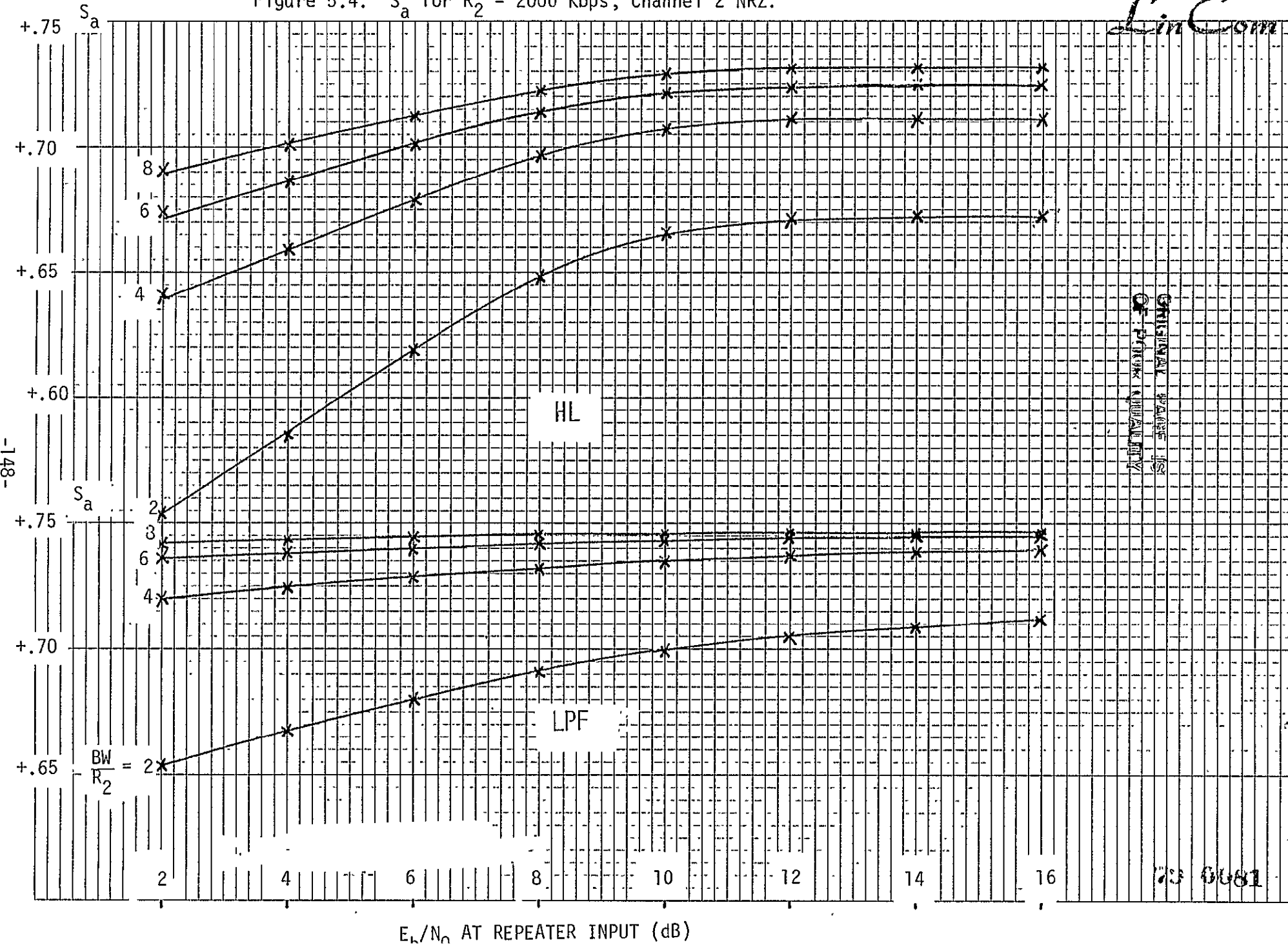
Figure 5.5. S_a for R_2 = 192 Kbps, Channel 2 NRZ.
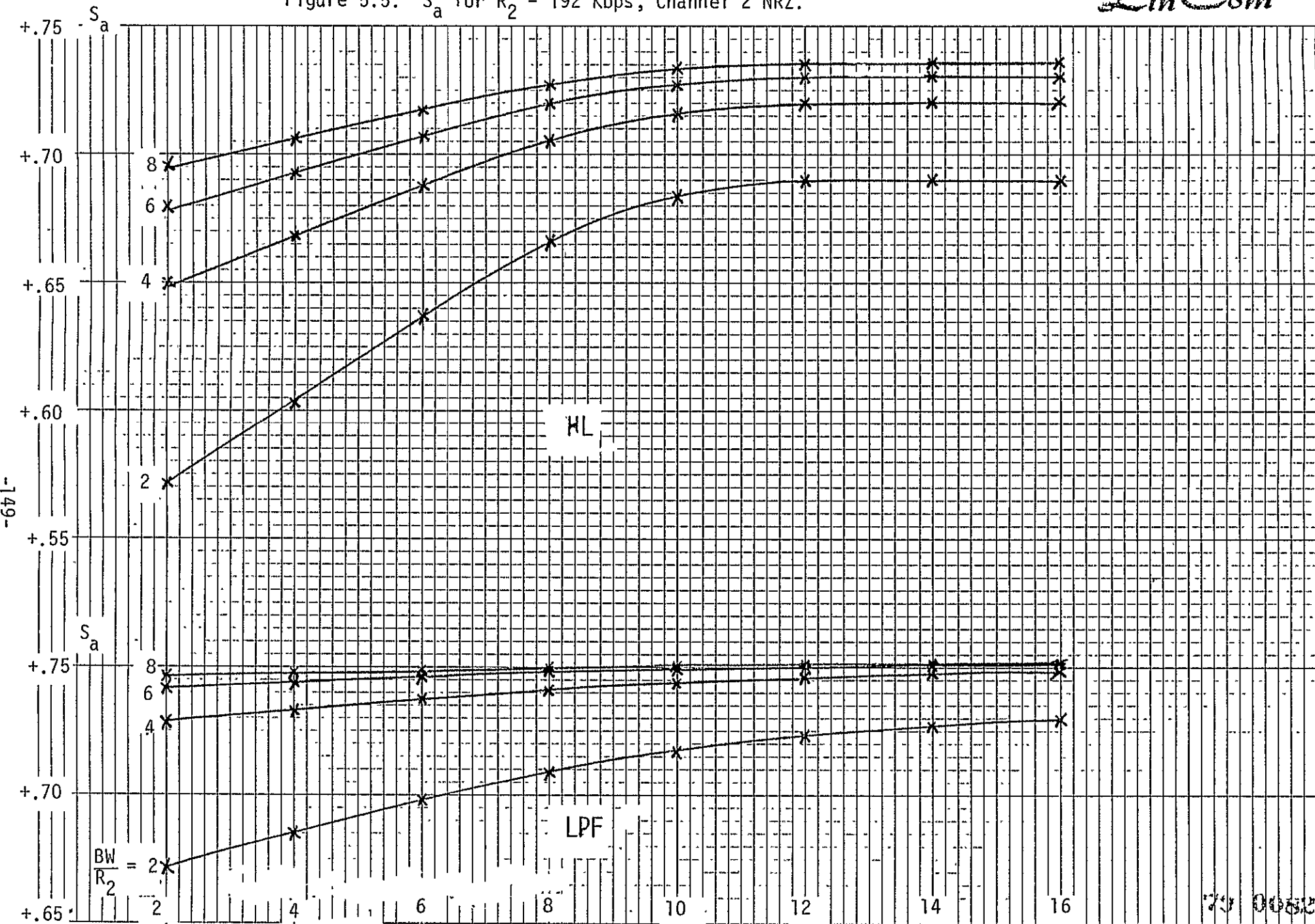
Figure 5.6. S_a for R_2=16 Kbps, Channel 2 NRZ.
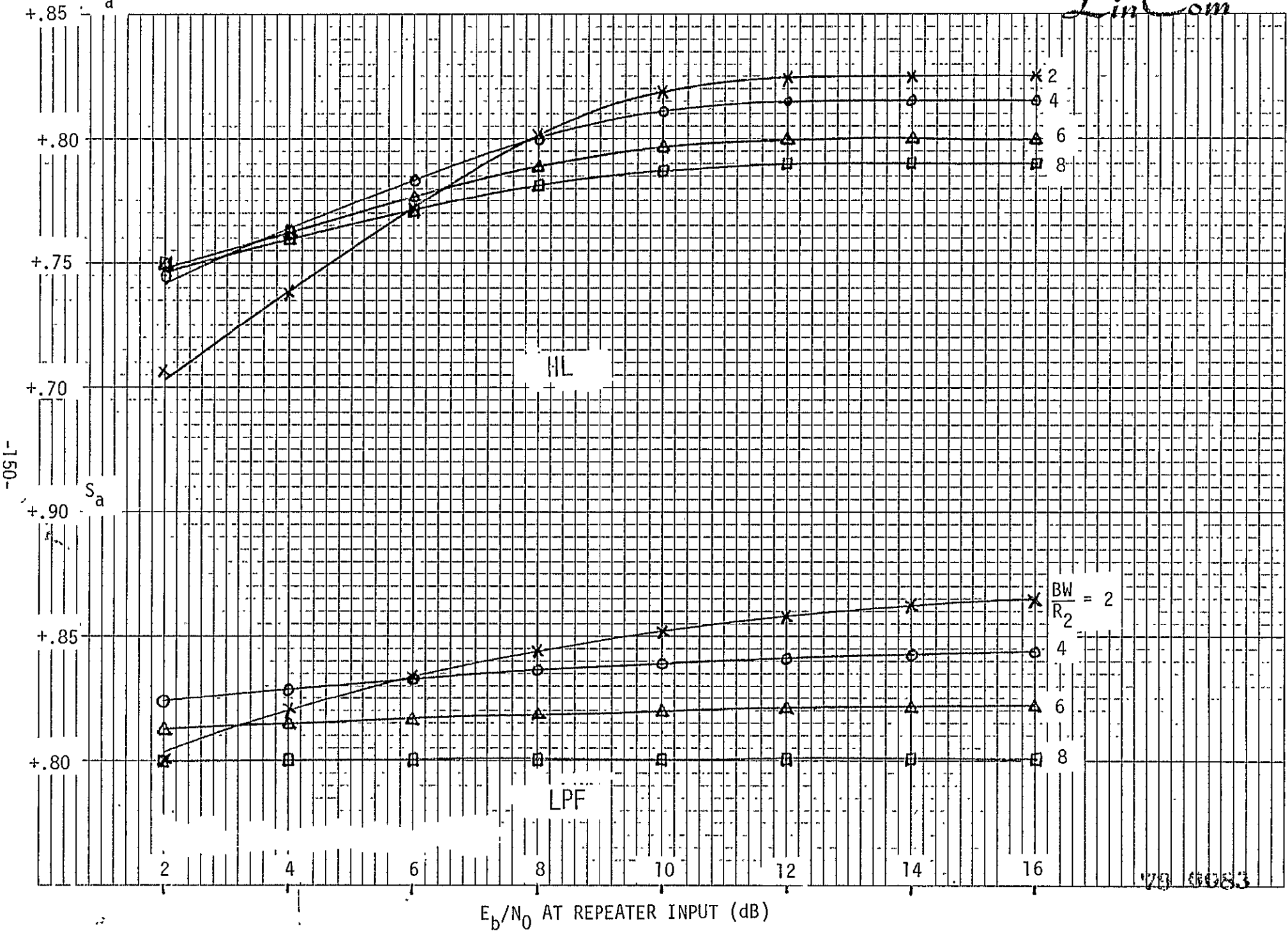
Figure 5.7. S_a for R_2 = 2000 Kbps, Channel 2 Biphase.

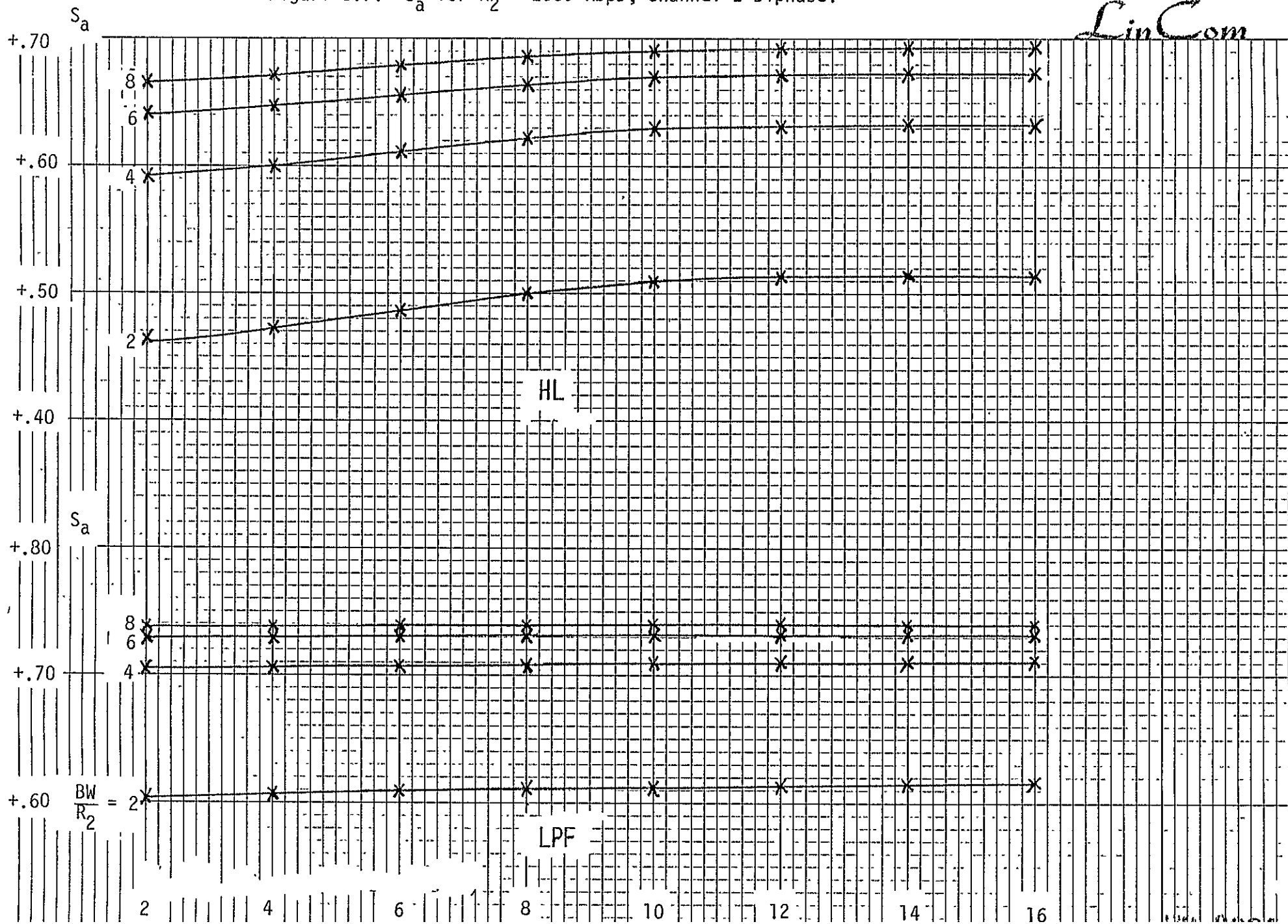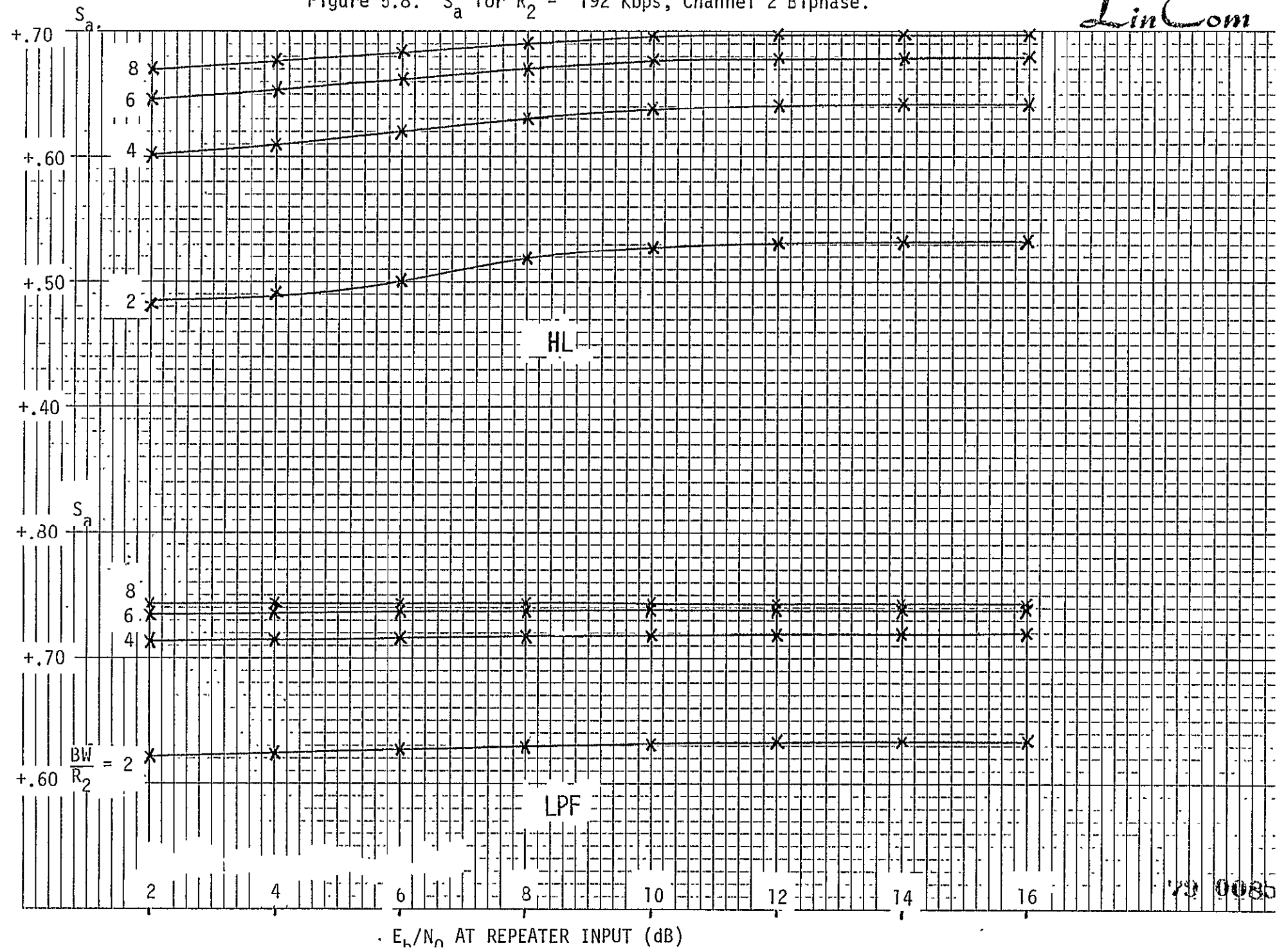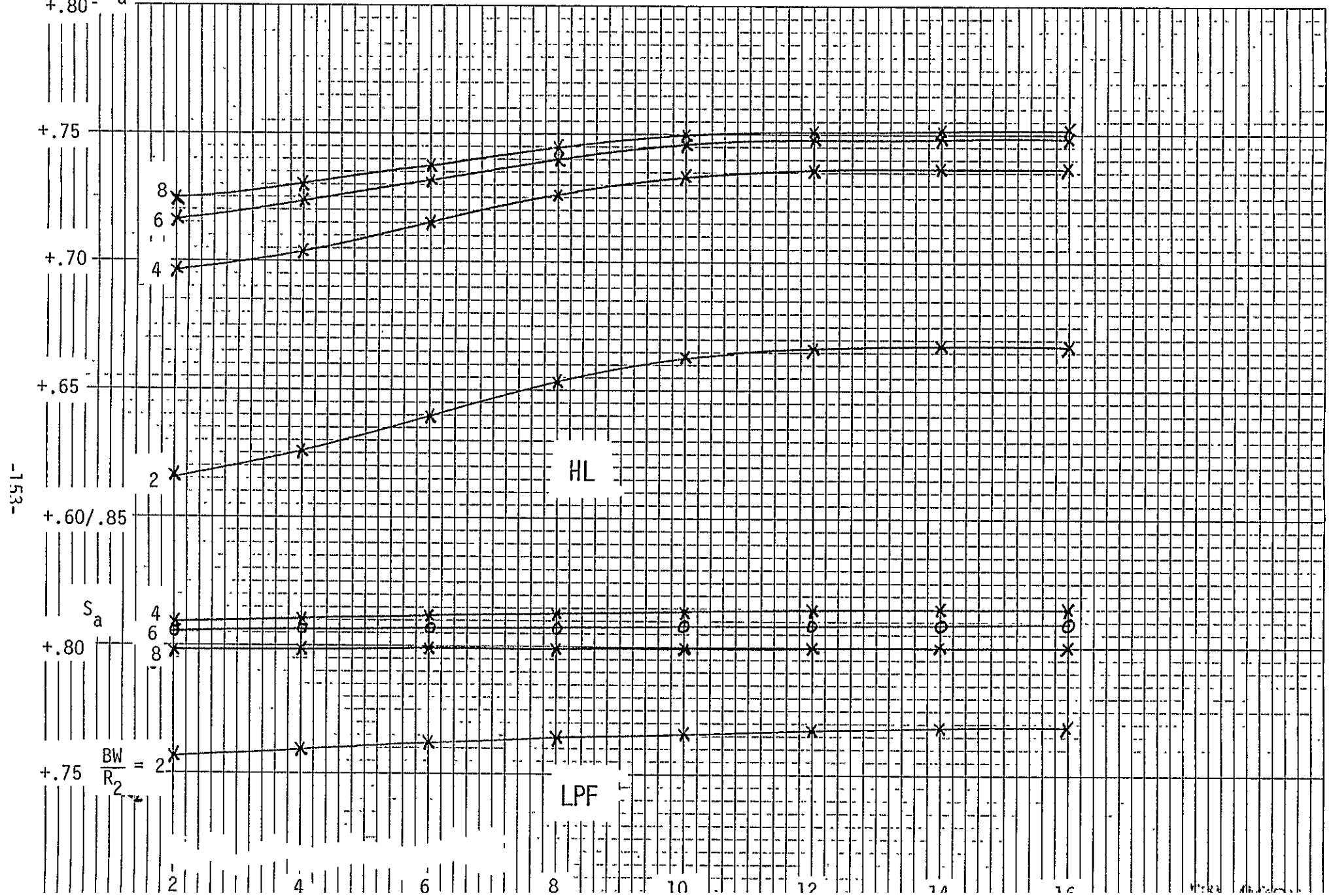Figure 5.8. S_a for $R_2 = 192$ Kbps, Channel 2 Biphase.

Figure 5.9. S_a for $R_2 = 16$ Kbps, Channel 2 Biphase.

5.10 Variance of Loop Phase Error

From Reference 3 we have for loop phase error ϕ,

$$\sigma_\phi^2 \doteq \frac{N_0' B_L}{(S'(0))^2} \qquad (91)$$

where $N_0'/2 = S_z(f=0|\phi=0)$ and B_L is the loop bandwidth, when the bandwidth of the equivalent noise is much wider than B_L. It can be shown that $R_2 S_z(0|0)$ does not depend on R_2 but only on R_1/R_2, if the bandwidth of the $G(f)H'(f)$ filter is taken as a multiple of R_2. We plot

$$\frac{N_0' R_2}{(S'(0))^2} \doteq \frac{\sigma_\phi^2}{B_L/R_2} \qquad (92)$$

in Figures 5.10 through 5.15, using NRZ or biphase pulses and three different data rates for channel 2. Each figure shows results for both repeaters considered. Assumptions made include those noted in the previous section. Additionally, $E_b/N_0 = 10$ dB for s_i and u processes and the spectrum of u is assumed flat over its bandwidth.

5.11 Filter Bandwidth Selection

As shown by equation (43), the Costas loop S-curve contains two terms whose relative magnitudes depend on the UQPSK power split, the payload interrogator bandwidth, the data rates and the IF and arm filter bandwidths in the ground station. In the desired mode of operation the first term, which depends on the channel 2 statistic, is larger than the second term which is determined by the low-rate channel 1. However, if the combined IF and arm filter are too narrow they will reduce the channel 2 power to the point where the second term is larger than the first. In this instance the Costas loop will track the low-

Figure 5.10 $\dfrac{\sigma_\varphi^2}{B_L/R_2}$ $R_2 \doteq 2000$ Kbps, Channel 2 NRZ, $E_b/N_0 = 10$ dB for s_i and u. *LinCom*

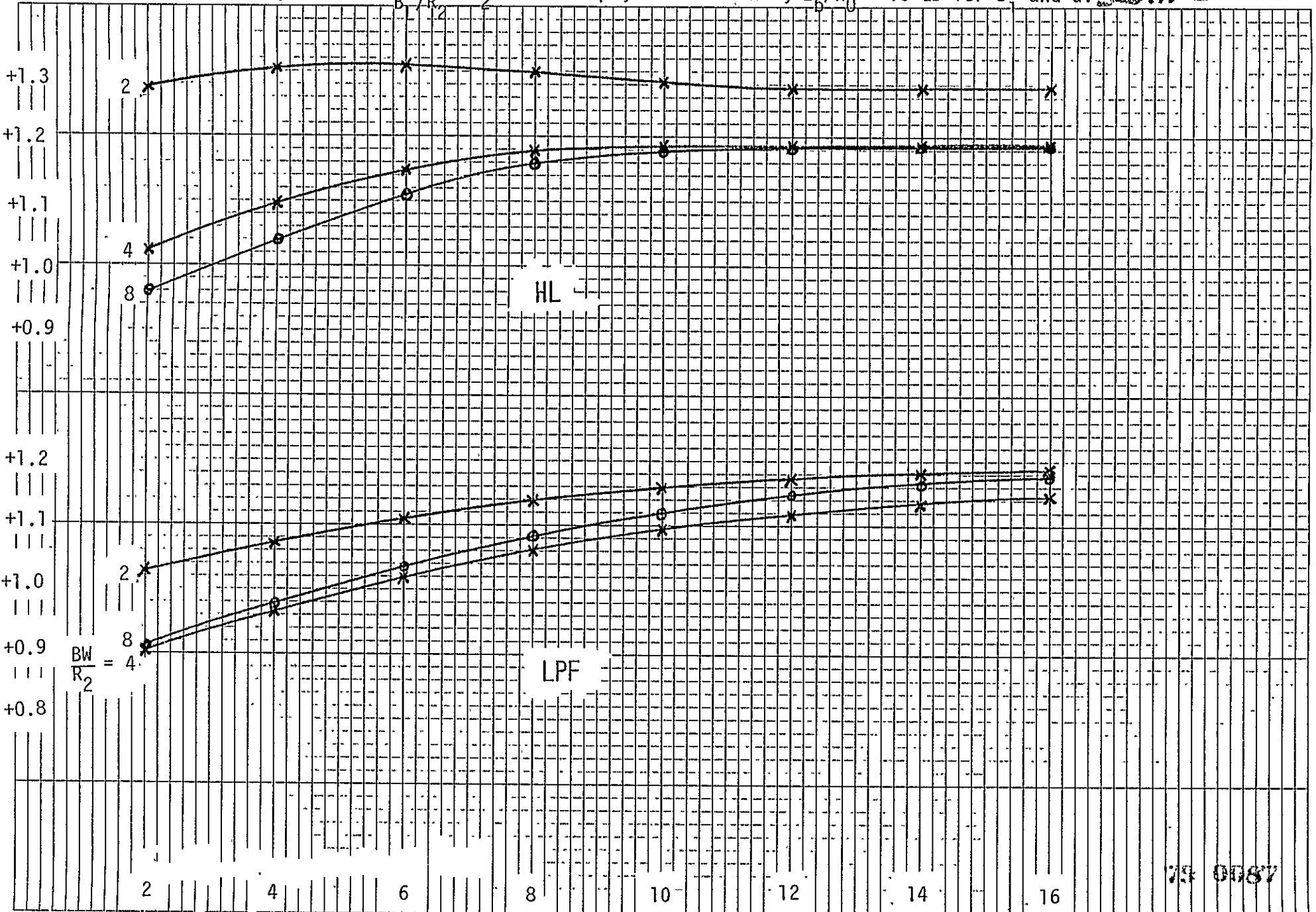HL

LPF

$\dfrac{BW}{R_2} = 4$

-160-

79 0087

Figure 5.11. $\frac{\bar{\omega}}{B_L/R_2}$ for $R_2 = 192$ Kbps, Channel 2 NRZ, $E_b/N_0 = 10$ dB for s_i and u
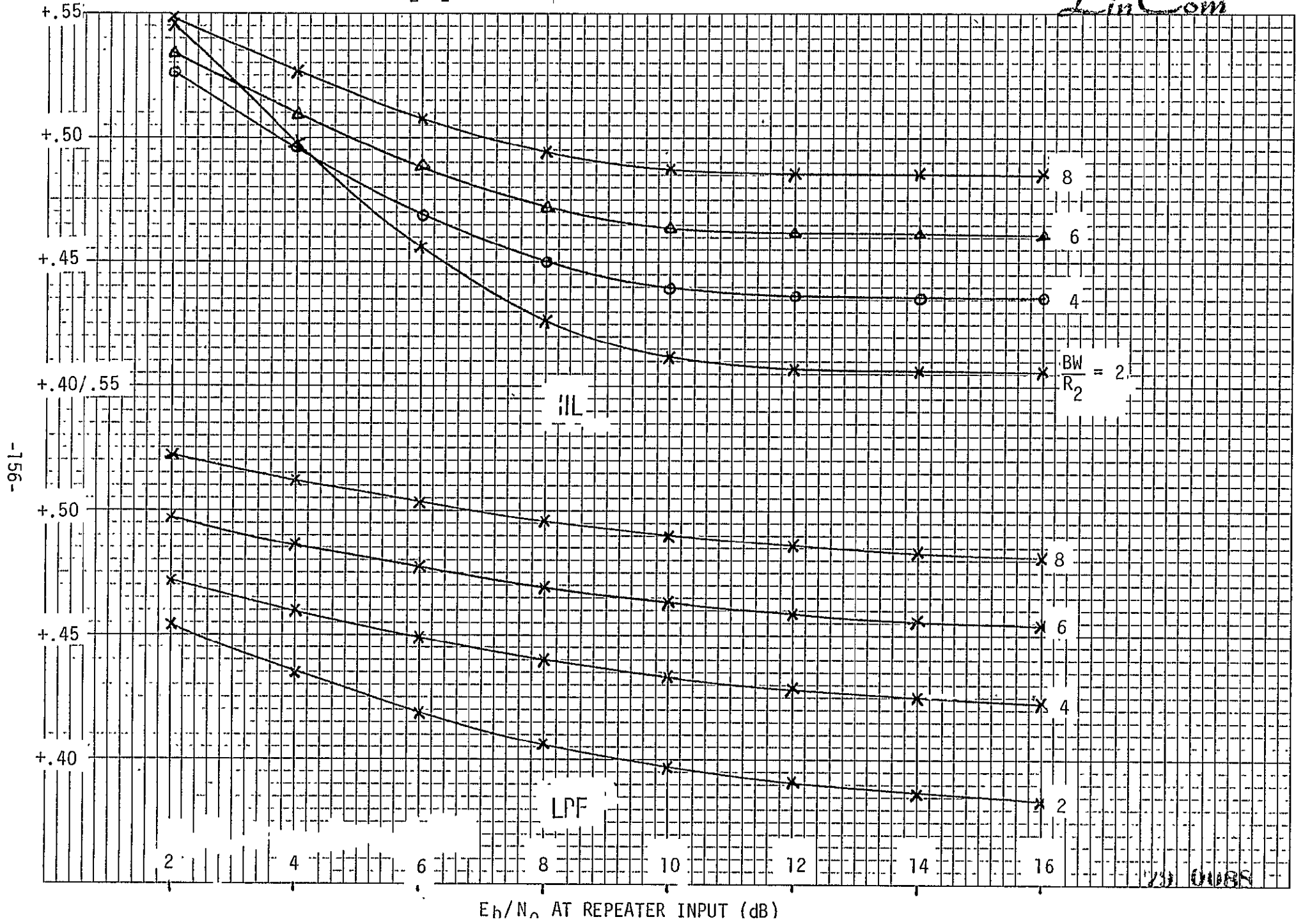
-156-

Figure 5.12. $\dfrac{\sigma_{c\phi}^2}{B_L/R_2}$ for R_2 = 16 Kbps, Channel 2 NRZ, E_b/N_0 = 10 dB for s_i and u

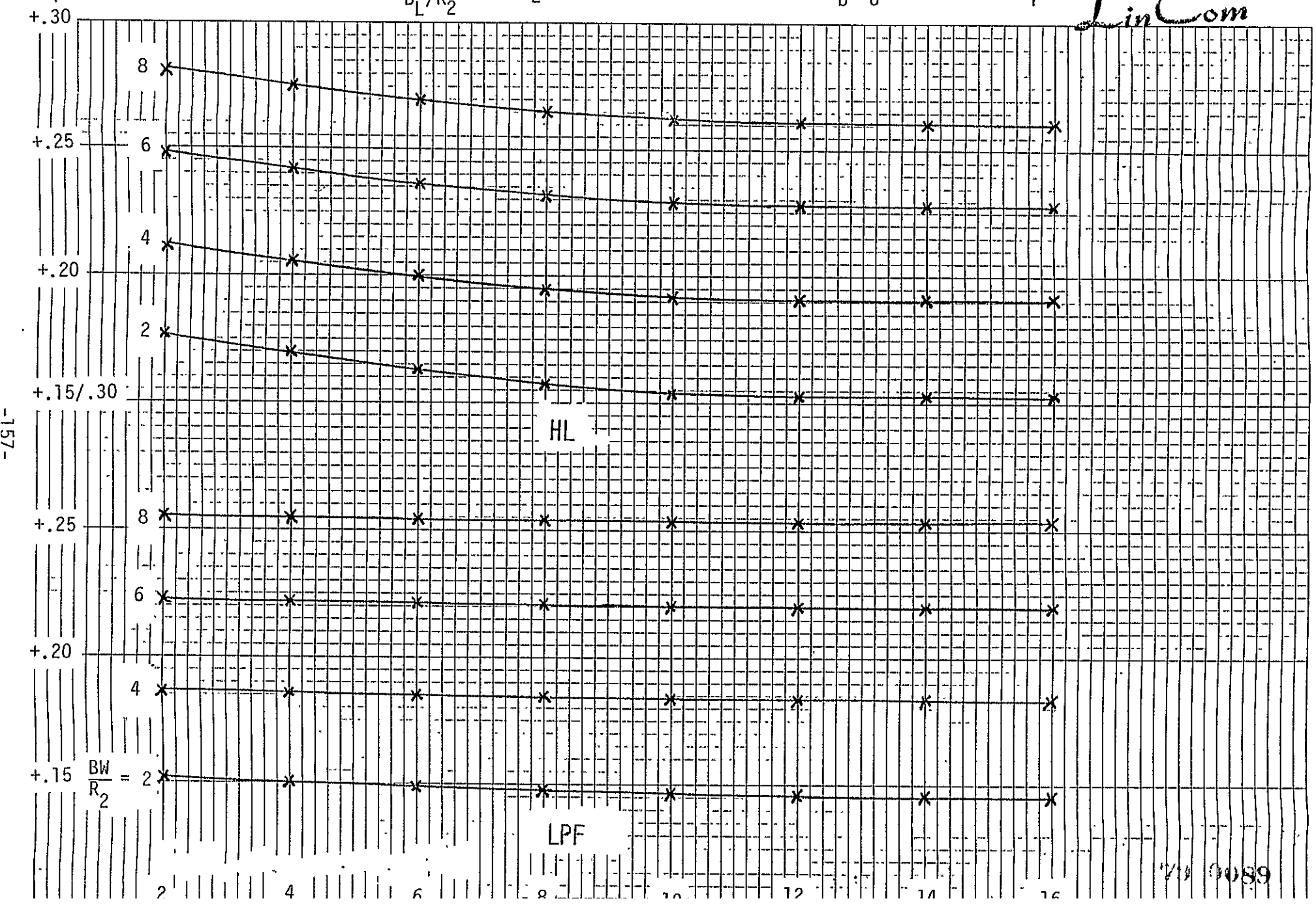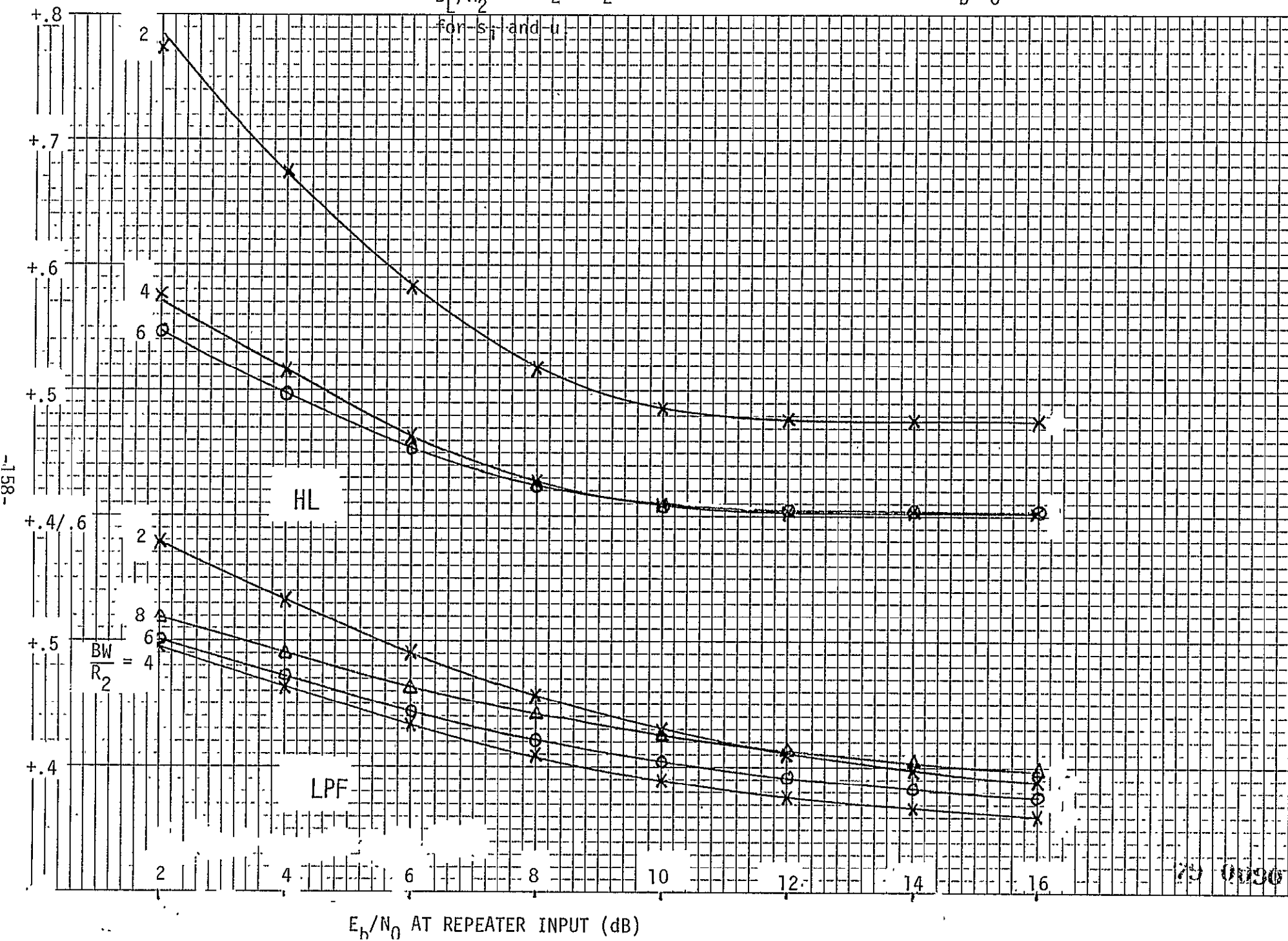Figure 5.13. $\dfrac{\sigma}{B_L/R_2}$ for $R_2' = R_2 = 2000$ Kbps, Channel 2 Biphase, $E_b/N_0 = 10$ dB for s_i and u

E_b/N_0 AT REPEATER INPUT (dB)

Figure 5.14. $\dfrac{\sigma^2_{c\ell}}{B_L/R_2}$ for $R_2 = 192$ Kbps, Channel 2 Biphase, $E_b/N_0 = 10$ dB for s_i and u.

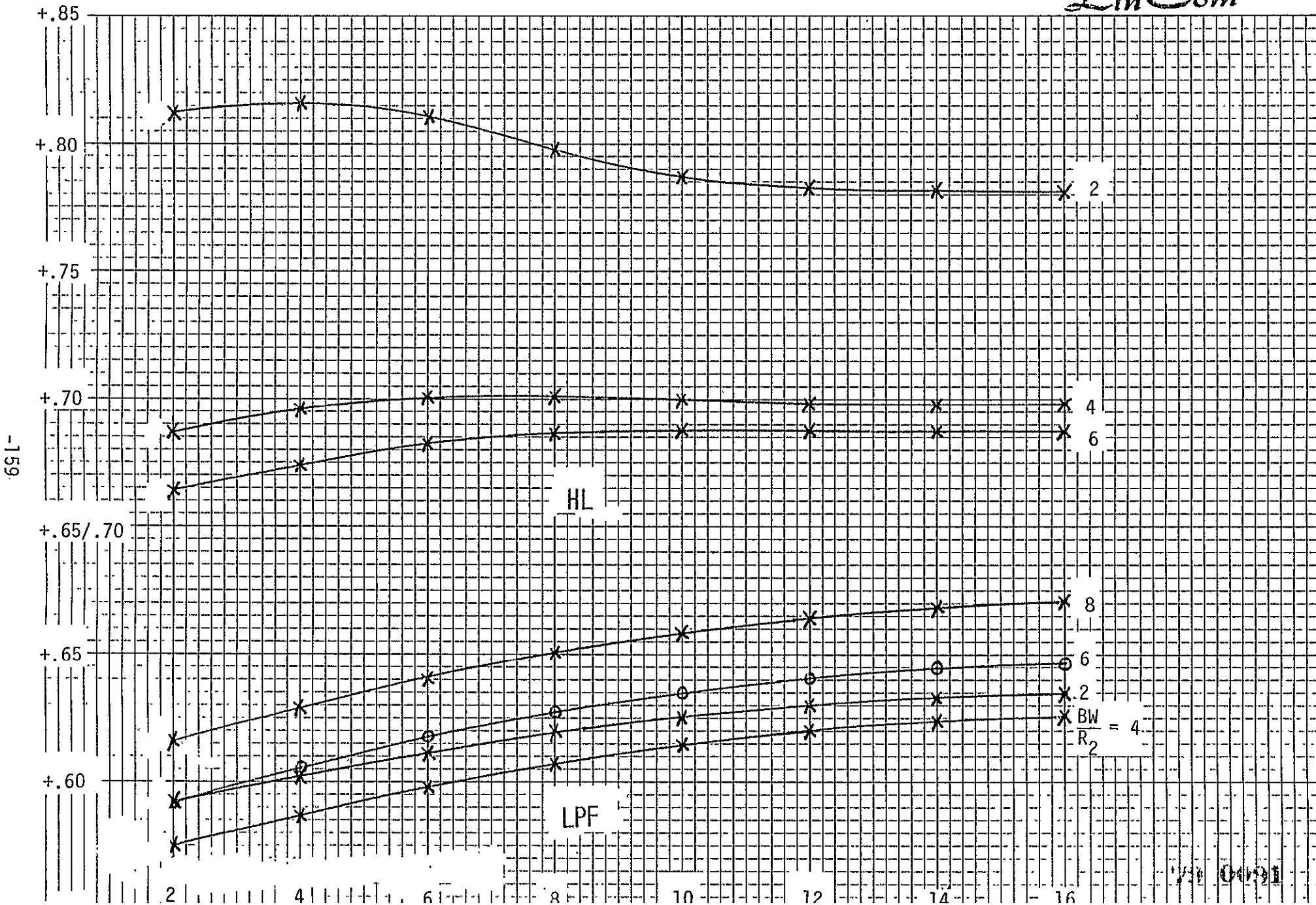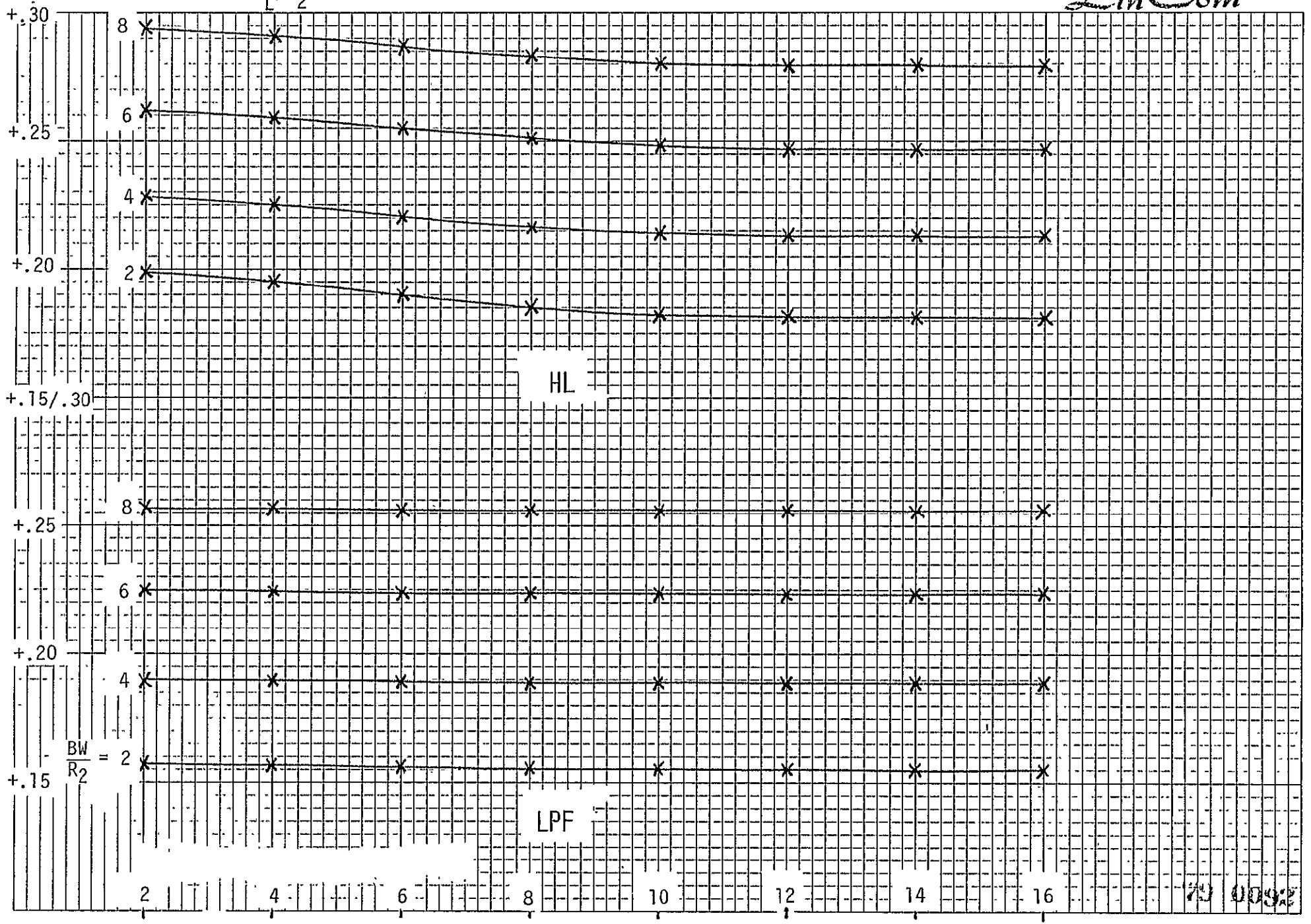Figure 5.15. $\overline{B_L/R_2}$ for R_2 = 16 Kbps, Channel 2 Biphase, E_b/N_0 = 10 dB for s_i and u.

E_i/N_0 AT REPEATER INPUT (dB)

power channel. This problem is particularly serious if the payload

signal drops out and the payload interrogator receives noise only.

Assuming a rectangular spectrum for the noise process n (Fig. 5.2)

the output spectrum is still almost rectangular (Fig. 5.16) with

the same bandwidth. Since the combined IF and arm-filters do not

affect the low-rate channel 1 power we can expect the Costas loop

lock-point to shift by 90 degrees when the arm-filter bandwidth

is less than approximately 1/4 at the payload interrogator bandwidth

for a UQPSK power split of 4:1. In the transition region, i.e.

when the arm filter bandwidth is approximately one quarter of the

interrogator bandwidth, the loop will either track unsatisfactorily

or not at all. These conclusions agree with the findings in [4].

5.12 Conclusions

From the plots, Fig. 5.4 to 5.15 it is clear that the payload

interrogator implementation could be slightly improved, as far as

subcarrier recovery is concerned, by remvoing the hard-limiter. This

is borne out by the fact that the resulting S-curve amplitudes are

higher and less sensitive to the carrier-to-noise ratio at the

payload interrogator. This small improvement comes at the expense

of reduced power control for channel 2 which will result in higher

crosstalk into channel 1.

For the worst-case conditions (lowest data rate on channel 2,

$E_b/N_0 = 10$ dB, i.e. no margin) and for a loop bandwidth of 500 Hz

the expected rms phase error in the detector will be 5 degrees.

If the possibility of losing the payload signal exists the relation-

ship between the payload interrogator bandwidth and the Costas loop

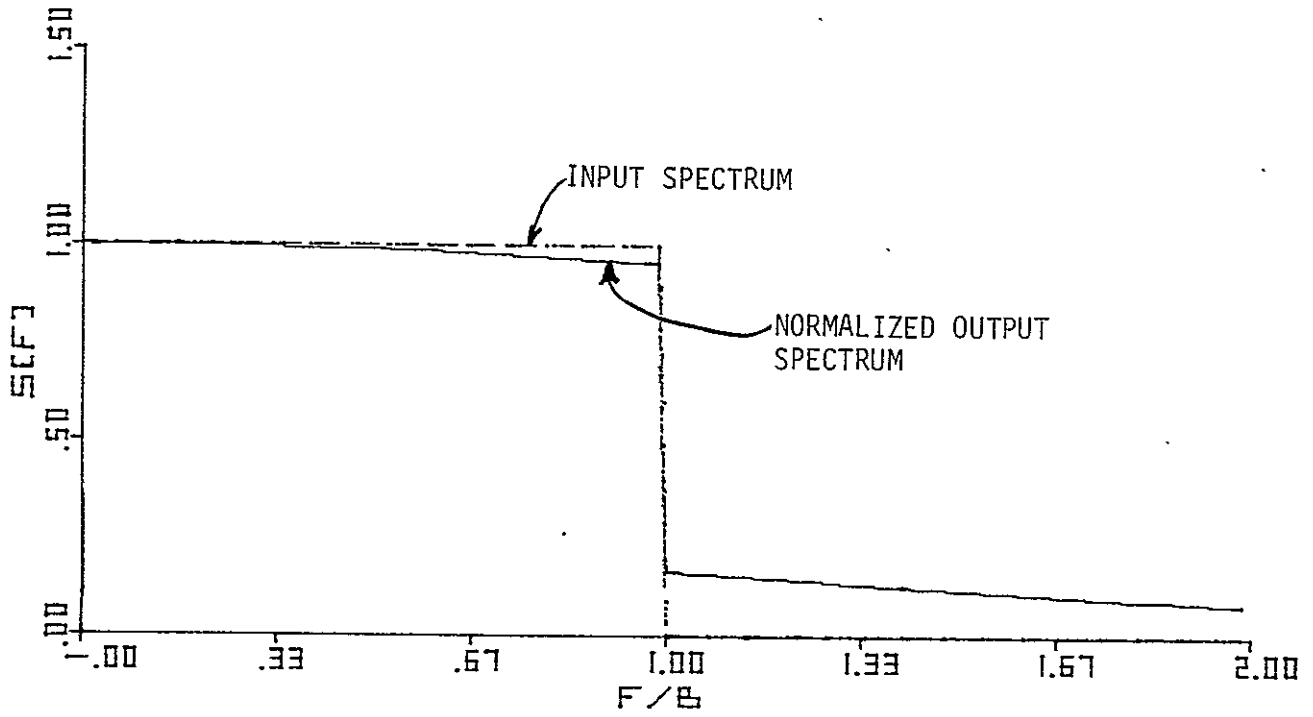arm filter bandwidth has to be selected carefully to avoid tracking

Figure 5.16.   Noise Output Spectrum of Hard-Limiter.

the signal with a 90 degree offset.

NOTE:

In mode 1 of Ku-band return link, the subcarrier is a square wave and not a sine wave as assumed in this analysis. The spectrum of the modulated subcarrier then is like that of the sine-wave subcarrier near 8.5 MHz but has additional harmonics. For the case of the LPF repeater, even when R_2 is as large as 2 Mbps, there is almost no overlapping of various parts of the spectrum because the bandwidth of the LPF is 1.5 R_2, which is less than 4.25 MHz. When the repeater is a HL, there may be more overlapping when R_2 is 2 Mbps. Assuming no overlapping, which is true for practically all values of R_2, then as long as the loop arm multipliers are insensitive to signals above 4.25 MHz, the arm signals z_c and z_s will be the same for square-wave subcarrier as for sine-wave subcarrier if the average power of both channels is multiplied by $\pi^2/8$.

REFERENCES

1. W. C. Lindsey, "Optimum Performance of Costas Type Receivers," Axiomatix Report R7502-1, Feb. 18, 1975.

2. W. C. Lindsey and W. R. Braun, "Tracking and Data Relay Satellite System (TDRSS) Communication Analysis and Modeling Study, Phase I Report," LinCom Corp., prepared under NASA Contract No. NAS 5-23591, October 15, 1976, pp. 93-94.

3. W. R. Braun and W. C. Lindsey, "Carrier Synchronization Techniques for Unbalanced QPSK Signals," prepared under NASA Contract NAS 5-23591, to be published in IEEE Transactions on Communications, September 1978.

4. Shuttle Ku-Band and S-Band Communications Implementation Study, Final Report, Axiomatix Report No. R7902-3, February 28, 1979.